DIGITAL IMAGE PROCESSING TECHNIQUES FOR THE INVESTIGATION OF NONWOVEN STRUCTURES

by

RONG HUA GONG

A Thesis Submitted

to

THE UNIVERSITY OF MANCHESTER

for the Degree of

DOCTOR OF PHILOSOPHY

in the Faculty of Technology

DEPARTMENT OF TEXTILES
UMIST

March 1989

DECLARATION

No portion of the work referred to in the thesis has been submitted in support of an application for another degree or qualification of this or any other university or other institution of learning.

To

My Parents

CURRICULUM VITAE

The author graduated from the Department of Mechanical Engineering, China Textile University, Shanghai, China, obtaining a B.Sc. in Textile Technology in July 1984. He registered for the degree of M.Sc. in the Department of Textiles, UMIST, in October 1985, and transferred to a course leading to a Ph.D. in October 1986.

ACKNOWLEDGEMENTS

I would like to express my gratitude to Dr. Alan Newton, my supervisor, for his guidance and encouragement during this work. I enjoyed the freedom he left me in conducting the research.

I also wish to thank Miss A Mathews, Dr. P J Grigg, Mr. C J Hawkyard and Dr. L W C Miles for their interest in the work and their valuable suggestions.

Special thanks are due to the Worshipful Company of Weavers for their generosity in presenting the Microsight II image analyser, without which this work would not have been possible.

I would also like to acknowledge the indispensable financial support provided by the British Council and the Government of the People's Republic of China.

ABSTRACT

Digital image processing techniques have been used to analyse structural and geometrical properties of nonwoven fabrics. The development of automatic measurement methods for pore size and fibre orientation distribution has been the main focus. The measurement algorithms, together with some preliminary testing results, are discussed in this thesis.

Pore size distribution is a crucial design criterion in many industrial, particularly geotechnical applications of textiles and an important product specification parameter. The orientation of fibres in nonwoven fabrics is one of the determinant factors of the physical behaviour of the fabrics. Reviews of literature have indicated that the existing methods of determination of these two properties are laborious, time consuming and, in some cases, controversial.

The automatic methods described herein enable accurate evaluation of pore sizes and fibre orientation to be achieved far more quickly and economically. The system has the advantage of being fully programmable, thus will be available for other work.

A review of the work was presented to the UMIST Nonwoven Conference, June 1988.

CONTENTS

PART I INTRODUCTION

PART II FABRIC PORE SIZE DISTRIBUTION

PART III FIBRE ORIENTATION DISTRIBUTION

PART IV CONCLUSION

PART 1 INTRODUCTION

CHAPTER 1 INTRODUCTION

1.1 Basic Concepts of Digital Image processing

The technology of digital image processing started in the mid-1960s when computers were first used for the processing of images taken by space probes in the United States of America[1]. It has been a fast growing new technology with an ever widening range of application areas including astronomy, meteorology, geology, agriculture, medicine, forestry, land use studies, planetary science, military applications and industrial applications, both in off-line product analysis and on-line production control. The sheer size of the published literature concerning the techniques and applications of digital image processing precludes a comprehensive review of all the aspects of digital image processing in this thesis. The intention here is therefore only to give a brief account of some basic concepts that are closely related to the present work.

In general, digital image processing is concerned with the manipulation and analysis of images by computers. A typical image processing system will contain three fundamental elements: image acquisition element, image processing element and image display element[1].

Among the many types of image acquisition devices, array sensor, flying-spot scanner and TV camera are the most common three[2]. The image acquisition element performs the conversion of a continuous scene to its equivalent digital form or a digital image which may be regarded as a matrix of numbers. Each point (pixel) in the digital image corresponds to an area in the scene, and a digital value assigned at each point in the digital image is related to some physical measurement, mostly the intensity of light, of that area in the scene.

In generating the digital image from a scene the following decisions have to be made: the spatial sampling frequency (resolution), the intensity sampling frequency (number of grey levels), and the shape of each picture element or the spatial pattern into which the picture is divided (tessellations). Higher resolution, both in spatial domain and intensity domain, makes an image which represents the original scene more faithfully but which requires a larger storage space, longer processing time and normally results in a higher system cost. The tasks of a practical application and the

characteristics of images related to it are the most influential factors in making the trade-off between resolution and system cost in the selection of an image processing system for that application. The most common spatial resolution at the present time is 512 by 512 pixels and this is particularly true for TV camera type digitizers. The number of grey levels is generally 256 due to the traditional design of 8-bit bytes as the addressable units of storage in most digital computer systems. Rectangular, and in particular square tessellations are almost universally utilized by digital image acquisition systems for their simple geometrical property, such as the simplicity of the measure of distance[3].

The digital image obtained by the image acquisition element is processed by the image processing element which is generally composed of one or more computers and their peripherals. The complexity of these devices varies greatly in different applications. For example, the computer used can be as simple as a conventional sequential microcomputer or as advanced as a purposely built multi-processor system. Naturally, the speed and complexity of operation will be increased with a more advanced system. But this is associated with the increase of system cost. The essential task of the image processing element, however complex it may be, is to convert the digital image to its successive substitutes so as to achieve various goals in the following three broad sub-areas[4].

(a). Image enhancement, restoration and reconstruction. Specific tasks include the improvement of degraded (e.g. low-contrast, blurred, noisy) pictures, reconstructing pictures from sets of projections.

(b). Image analysis. Examples are isolation and measurement of image features, detection of objects within pictures, image registration, description and comparison between the resulting description and models that define classes of pictures.

(c). Image coding. The task of this process is to represent a digital image with a minimal number of codes for more efficient communication and storage.

Finally, digital images have to be converted back to analogue forms for viewing by human observers. This is achieved by the image display element. Video monitor is by far the most widely used image display system. But it only provides volatile image display. Film and video products are common hard-copy forms of analogue images.

The process of converting one digital image into another is an operation and the function which defines the operation is an operator. Although there exist some basic operations that have a wide range of applications, image processing still remains a

heavily application-oriented technology. It is not unusual that an operator working most efficiently for one application fails completely to work for another application. Generating of new operators is normally required in the course of finding the best solution for a specific problem.

1.2 Nonwoven Fabrics

"Nonwoven fabrics, usually, are made from fibres, or polymer granules, which are made DIRECTLY into a web. This web is then consolidated by various means, including needling, bonding by adhesives and thermally fusing of the fibres" [5]. This latest definition of nonwoven fabrics by ISO and EDANA differentiates nonwoven fabrics from woven, knitted and other types of traditional textile materials by highlighting the fact that the manufacturing of nonwoven fabrics bypasses the spinning process.

Started in the 1930s, nonwoven technology has now grown into an important integrated part of modern textile industry, instead of replacing the much more lengthy and slower traditional fabric manufacturing processes such as weaving and knitting, which was initially the motivation of the development of nonwoven technology.

As indicated in the definition, the manufacturing of nonwoven fabrics has two major steps, web formation and web consolidation. Typical web formation methods are dry-laying, wet-laying, spun-bonding and melt-blowing. Web consolidation is achieved by interlocking and/or bonding of fibres. Interlocking of fibres in a web is achieved by punching through of barbed needles (needle punching) or water jets (spunlacing). The strength of the structure made by fibre interlocking is mainly due to the surface friction between the entangled fibres. Much stronger materials are made by bonding of fibres. The most widely used two types of bonding processes are chemical bonding and thermal bonding. Chemical bonding refers to the process where adhesive binders in the form of liquid or foam are added to the web through immersing, spraying or printing. In thermal bonding processes, thermoplastic fibres are incorporated into the fibre web. The web is then subjected to heat and pressure to produce bonds at fibre cross points. Thermoplastic powders can also be applied to a web. These powders are then melted under heat and pressure to bond the fibres. These are the very basic techniques involved in the making of nonwoven fabrics, but the actual manufacturing processes of nonwoven fabrics are numerous and continuous effort is being made throughout the world in the development of new processes and new products.

The applications of nonwoven fabrics have been expanding all the time and the list of products is inexhaustible. A few examples of durable nonwoven products are apparel, particularly interlinings; home furnishing, such as draperies, upholstery, mattress padding, carpet backing and wall covering; industrial uses such as filters, insulation and geotextiles. Diaper, sanitary napkins, surgical and industrial masks, bandages, towels and tea bags are several typical disposable nonwoven products. More important than their replacement of many traditional textile items, nonwoven fabrics have opened up a number of major markets, most prominently in geotechnical applications, and thus widened the meaning of textile.

1.3 Aim of the Present Work

Proper application of materials always requires a clear understanding of their structure, and nonwoven fabrics are no exception. The fact that a nonwoven fabric is a fibrous web structure immediately suggests that the arrangement, or the orientation distribution, of the constitutional fibres in the web is an important structure property. This property can be obtained by visual analysis of fabric samples under a microscope, but the process involves manual tracing and

measuring of a large number of individual fibres and therefore is very laborious and time consuming.

The size of pores in a fabric is another major structural parameter, particularly in geotechnical applications, such as filtration. It is in practice impossible to obtain the pore size distribution of a nonwoven fabric by manual measuring of individual pores in the fabric because of the high irregularity of the microstructure of a nonwoven fabric. The pore size property of a nonwoven fabric is therefore normally obtained indirectly, typically by measuring the size of particles that can be sieved through the fabric. Because smaller particles will pass through larger pores, precise fabric pore size distribution can not be obtained by this method.

A common feature of the above problems is that the desired information is "visible" and theoretically obtainable from images of a fabric. Although it is very difficult to obtain the information manually, it is possible to automate the measuring process by taking advantage of the developments in computer technology. It is the aim of the present work to investigate the feasibility of automatic measuring of fibre orientation and pore size distribution in nonwoven fabrics by using computer image processing techniques.

In the next chapter the hardware aspects of the image processing system employed and the overall strategies adopted in the development of computer software will be discussed. The detailed discussion of the algorithms and testing results associated with pore size and fibre orientation measurements will be presented separately in part 2 and part 3, followed finally by a concluding part, part 4.

CHAPTER 2 THE SYSTEM

2.1 Hardware Aspects

The image processing system used in the present work consists of a MicroSightII System produced by Digithurst Ltd, a MonoVar Zoom System from Micro Instruments (Oxford) Ltd and a BBC Microcomputer System. An overview of the system is shown in Fig2-1 and the internal structure is illustrated in Fig2-2.

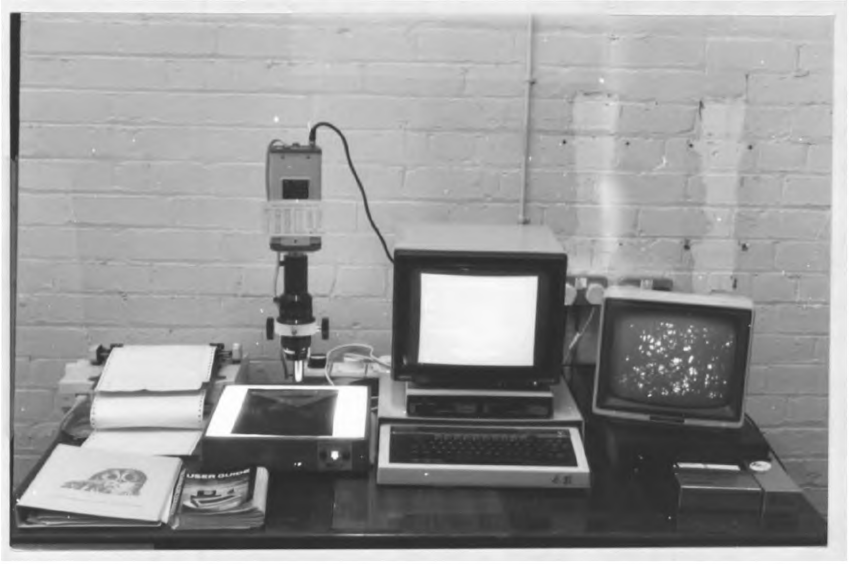

Fig2-1 The MicroSightII Image Processing System

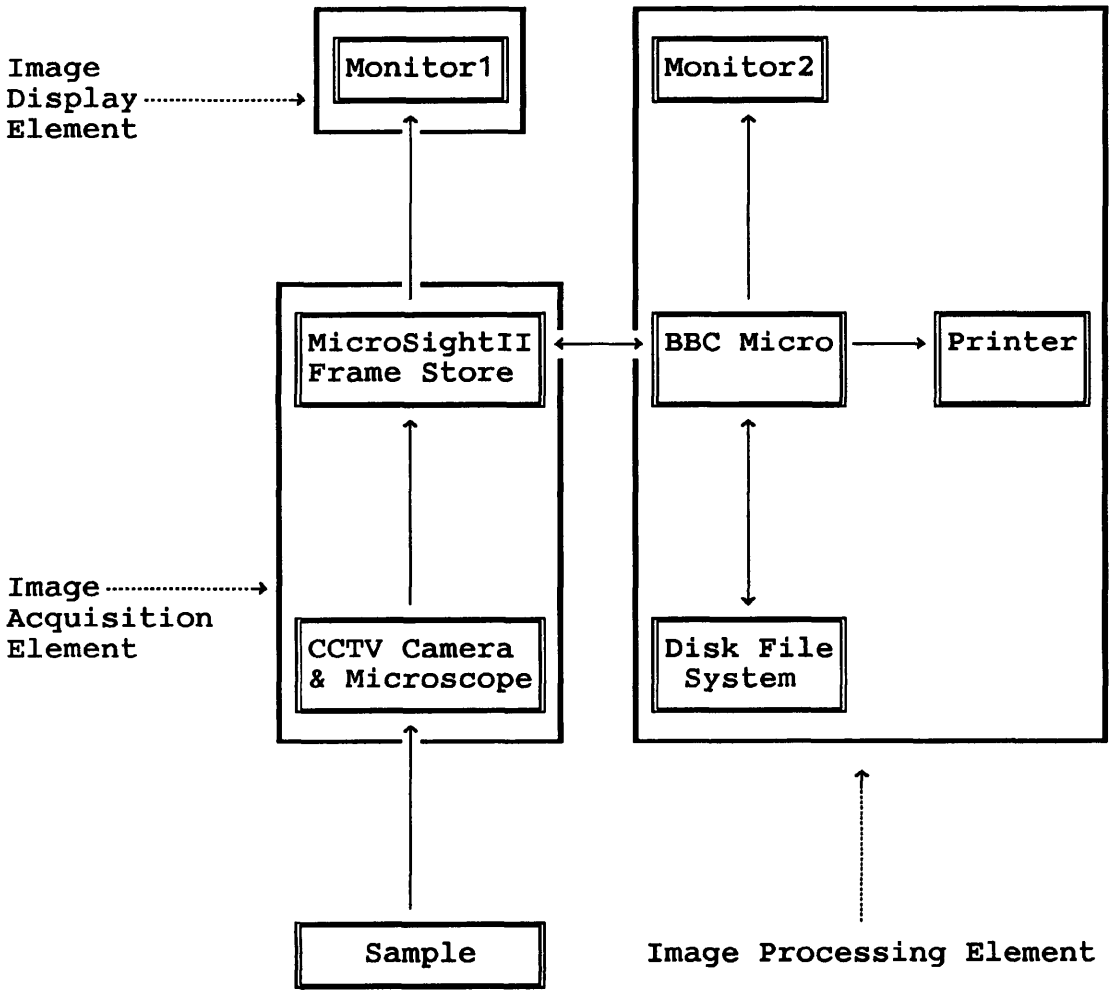

Fig2-2 Block Diagram of the System

The MicroSightII System includes a TV camera (Hitachi CCTV camera, model HV-735K) and the MicroEyeII interface, inside which there are an A/D converter, a D/A converter and a digital store (frame store). The frame store provides a total storage of 512 by 512 pixels with 6 bits (equivalent of 64 grey levels) for each pixel. The system utilizes rectangular tessellations of a width-to-height ratio of 1.5. The TV camera is attached to the Monovar Zoom System which has a zoom range of 0.7 to 4.7. The objective field size ranges from 12.5mm by 8.3mm to 1.86mm by 1.24mm, equivalent to a resolution of 24.4μm per pixel to 3.64μm per pixel, depending on the magnification of the zoom system. Larger or smaller objective field sizes can be obtained by attaching auxiliary lenses to the zoom system or directly to the camera. As indicated in Fig2-2, the above described devices make up the image acquisition element of the whole system.

The image processing element mainly consists of a Model B BBC Microcomputer system which has 32K total RAM storage. The MicroEyeII interface is connected to the BBC Micro via the 1MHz Bus and the User Port of the computer. Also connected to the computer are a CUMANA dual disk drive, a colour video monitor (monitor 2) and an EPSON printer.

Another b/w video monitor (monitor 1) is connected to the MicroEyeII interface. This monitor provides display of the image stored in the frame store and is indicated in Fig2-2 as

image display element.

The arrows in Fig2-2 represent the directions of data communication within different parts of the system. The image of a sample taken by the CCTV camera through the zoom system is sent to the MicroEyeII interface and digitized by the A/D converter within it. The digitized image is stored in the frame store and displayed on monitor 1 after converted back to analogue form by the D/A converter within the MicroEyeII interface. The digital image stored in the frame store is processed through the BBC Micro and the processed image can be sent back to the frame store, overlapping the original data. Every change of data in the frame store is instantly displayed on monitor 1.

Image data may be loaded into the RAM of the microcomputer and displayed on monitor 2. But the size of image that can be stored in the RAM is very small (less than 128 by 128) due to the small RAM storage. Bigger images can be displayed on monitor 2 by directly mapping image data into the RAM part for graphics. Only binary images (or images with pseudo colours) may be displayed on monitor 2. This means grey level thresholding has to be carried out during the mapping process. Grey level thresholding may be single level or multi-level depending on the displaying mode of the computer. When single level thresholding is performed the grey level value of each pixel in the original image is compared with one threshold

value and, pixels having grey levels on different sides of the threshold are mapped into two different colours. In an n-level thresholding (n>0), n threshold values are used to separate the grey level range into n+1 intervals and pixels are mapped into n+1 colours according to which interval their grey levels fall in. It is obvious that increasing the number of threshold values or increasing the number of colours to be displayed will decrease the spatial resolution of the displayed image because the total RAM storage is limited. In two colour modes, for example, an image of 640 by 256 pixels can be displayed while in four colour modes the resolution is reduced by a half to 320 by 256 pixels.

Pseudo colour display is effective for manual analysis of images because human visual systems are much more sensitive to differences in colour than to differences in light intensity. Because of the difference in tessellation, however, the image displayed on monitor 2 is subjected to distortion. The BBC computer also uses rectangular tessellations but the width-to-height ratio is different from that of the MicroEyeII system. In fact this ratio also varies in different display modes. There are three ratios, 1:2 (mode 0), 1:1 (mode 1 and mode 4) and 2:1 (mode 2 and mode 5), but none of these matches the 1.5:1 ratio of the MicroEyeII system. The image displayed on monitor 2 will therefore be relatively compressed either vertically (in mode 2 and mode 5) or horizontally (in mode 0, mode 1 and mode 4).

Because the data storage of the BBC computer graphics is not in the normal two dimensional format, it will be extremely inefficient to process image data with such a structure. Consequently all image processing software has been developed to operate on the image data stored in the frame store. This matter is discussed in more detail in the next section.

Any data stored in the frame store is volatile and not recoverable after a power off. But the image data can be sent to the disk file system for permanent storage onto a floppy disk. Storage of images onto disks is necessary when the original image in the frame store needs to be retained as the original data will be overlapped by the processed image data which is sent back into the frame store. The data stored on a disk can be loaded back into the frame store via the microcomputer.

A hardcopy of the image stored in the frame store is available through the printer. The printer is a dot matrix system and prints rectangular dots with a width-to-height ratio of 1.2:1. This ratio is smaller than the 1.5:1 value of the MicroEyeII system and the print-out picture will be relatively compressed in the horizontal direction. The width of the print-out picture is limited to 480 points. The maximum print-out picture is therefore 480 columns by 512 lines. One further point is that the print-out can only be binary and a single level grey level thresholding is required before printing.

2.2 Software Overview

The system was intended for general purpose image processing applications and the software supplied initially with the unit was very limited and had little practical value for the particular applications with which the present work is concerned. Although software development has mainly been oriented to the needs of the present work, some general purpose software has also been generated in the consideration that they are essential to an image processing system. The developed software can then be classified into two categories:

(a). General purpose software. This type of software is essential to an image processing system and can serve a wide range of applications.

(b). Application-oriented software. This type of software fulfils the special requirements of some particular applications and therefore can only provide meaningful operations on a certain types of images.

A list of all the general purpose software is given in Appendix 1 accompanied by brief descriptions. Except that

which is particularly important to the present work, general purpose software will not be discussed in more detail. The algorithms involved can be easily found in image processing text books [2],[3],[4] and the implementations of those algorithms are mostly straight-forward.

The main aim has been the automatic analysis of nonwoven structures which is mainly concerned with image analysis, one of the three application areas of image processing technology described in section 1.1. Detailed discussion of software and testing results will be presented later in the thesis, but the general strategies adopted in software development are discussed below.

2.2.1 Software Structure

The objective of image analysis in general is to extract from the very large amount of data in an image, that small set of measurements containing the information of interest. The standard strategy to achieve this is to break the whole task into a sequence of smaller, independent steps. The object of each step is to achieve a limited but significant reduction in the amount of data by discarding irrelevant information. The result of each stage is a new representation of the image.

Objects in an image have to be separated from each other and from their background before any measurements of object properties can take place. This strategy is analogous to the way in which human visual systems work, as one sees an object in a scene only because that object is different, thus separable from its surroundings in some manner. An object in a digital image is a group of points that have some similar properties and are contiguous in two or three-dimensional space. The process of isolating a meaningful object or region is termed as image segmentation and is a crucial stage in image analysis. Unfortunately there is neither a standard approach to segmentation nor a general criterion of successful segmentation and, the performance of a segmentation method can only be judged by the utility of the measurements based on the segmented results[2].

Different approaches, namely grey level thresholding and a line operator, have been used respectively to achieve initial segmentation of raw images for the measurement of fabric pore size distribution and for the measurement of fibre orientation distribution. They are dealt with in Chapter 4 and Chapter 7 respectively. Because only two sub-regions within an image need to be considered in both of the above cases, fibres and non-fibres (or pores), the initial segmentation results are represented by binary images. In a binary image there are only two grey levels, each of which represents one of the sub-regions. The sub-region of interest will be termed as

object and the other sub-region as background. Pixels within objects and those within the background will be symbolically represented by 1s and 0s respectively. Further segmentation of objects into individual objects, the simplification of the shapes of individual objects, and the measurement of their properties are all carried out on binary images and, the software written for these purposes will not operate on raw images.

The vast amount of data contained in an image makes it unpractical to write all image processing programs in high-level computer languages. It is far more rational to accomplish intensive computation on bulk image data with low-level languages and achieve the subsequent analysis in high-level languages. The low-level language used is the 6502 machine code and the high-level language is BBC BASIC. The BASIC programs provide operational instructions, simple data processing and result presentations while all image processing operations are carried out by machine code subroutines. All the machine code subroutines were initially written in 6502 Assembly Language and assembled into machine codes by the assembler of the computer. Execution of machine code subroutines are performed by calling them through BASIC programs.

2.2.2 Border Pixel Handling

Operations on images may be classified as point operations, local operations and geometrical operations[2]. A point operation is an operation in which the value of a pixel in the output image depends only on the value of the corresponding pixel in the input image. A simple example is grey level thresholding. In a local operation, however, the output value of a pixel is determined by the input values of pixels within a neighbourhood of that pixel (a window), such as grey level averaging. Geometrical operations are the most complex type of the three categories. Here the output value at a pixel is decided by the input values of some pixels defined by a geometrical transformation. Image rotation and scale changing are two simple examples of geometrical operations.

For point operations, border image pixels can be treated in the same way as inner image pixels. But for local and geometrical operations the situation is complicated by the fact that some of the pixels which are required for the determination of the output value of a border pixel may be outside the image. To overcome this problem a special border pixel handling method is required. Listed below are some common border pixel handling methods[2],[6].

(a). Treating images as cyclically closed. This is not natural as the two pairs of edges of an image are not really connected.

(b). Assuming all pixels outside an image have constant values, e.g. zeros. This is a realistic way to represent the image as all images are extend limited. But it contradicts the fact that the real scene is boundless.

(c). Operating only on a sub-image of the original image. The result given in this way is meaningful for all pixels but the output image is smaller than the input image.

(d). Reducing the window size when the operation approaches the border. This method will produce noticeable edges in the output image.

(e). Extending images by mirror reflecting at the edges. This method eliminates sharp grey level transitions at the edges but the meaning of the output values at border pixels are difficult to interpret.

(f). Giving a complex definition to cover those

pixels involved, both outside and at the borders. This is generally difficult and costly in terms of computation time and memory requirement.

Method (c) has been chosen whenever special border handling is required in the present work. In addition to its simplicity, a slightly smaller output image should have little influence on the final statistical results. For an m by n rectangular operator the output image will be m-1 columns and n-1 lines smaller than the input image. Other types of window can be treated in the same way by defining a minimum rectangle that contains the window. The largest window used is 9 by 9 pixels and the output image from the 512 by 512 input image by this operator is 504 by 504 pixels. That is equivalent to a 1.6% reduction in objective size which is negligible. A further advantage of this border handling method will be revealed in the following section where the data storage strategy is discussed.

2.2.3 Data Storage

It was mentioned earlier in section 2.1 that both the pre-processed and the post-processed image data are stored in the frame store due to storage limitation of the computer. For point operations such as grey level thresholding this does not

cause any problem as the output at a pixel can be stored back at that pixel replacing the original data. The original datum at a pixel is only required to compute the output at the same pixel and once the output is determined the original datum can be deleted. But it is not such a simple case when applying a parallel local operation to an image. By parallel it is meant that the output value at each pixel is determined solely by the input values of those pixels defined by the operator, not affected by any output values. As the operation is local, the original value of a pixel is required both for the computation of the output of itself and that of some other pixels defined by the operator. Unless parallel processors are used the computations of the outputs at different pixels are performed in sequence. The original value of a pixel therefore has to be preserved until the outputs at all of its neighbouring pixels defined by the operator are determined. When the operation is applied only to a sub-image equal to or less than half the full frame store size, the solution to this problem is simple because the frame store can provide storage both for the output and the original data. When the operation is applied to a sub-image larger than half the frame store size, special methods have to be used to solve this problem.

One of the possible solutions is to allocate a buffer within the computer RAM to temporarily hold the output values of pixels whose original values need to be retained for the output computations at other pixels. The content of the buffer

will have to be renewed as the operation moves on from one part of the image to another. For example, when the image size is 512 by 512 pixels and the operator has a window of 3 by 3 pixels, a buffer of 512 bytes (one image column) will be required. This is not a serious drawback in terms of memory requirement but will complicate the implementation of the operator and will require extra processing time due to the handling of the buffer. However, when image border pixels are handled by method (c) as described in 2.2.2 the problem can be solved at no extra cost of either memory or computation time.

Consider applying an m by n operator to a 512 by 512 image and assume it proceeds from top to bottom along every column while moving column by column from left to right. If the top-left corner of the window is P(i,j) and the operation is applied at P(i+a, j+b), where $0 \leq a \leq (m-1)$ and $0 \leq b \leq (n-1)$, the first pixel to be computed will be P(a,b) when P(i,j) is at P(0,0) which is the top-left corner of the image. Computations of outputs at pixels both to the left of P(a,b) and above P(a,b) will require out-of-image values which is not allowed by the border pixel handling method. The operator then proceeds downwards along column a to $(a,1+b)$, ..., $\{a,512-(n-b)\}$, and then moves on to pixel $(1+a,b)$ in column $1+a$, ..., until pixel $\{512-(m-a),512-(n-b)\}$. The operation can not be applied to pixels to the right of $\{512-(m-a),512-(n-b)\}$ and below $\{512-(m-a),512-(n-b)\}$ for the computation of their output values also requires out-of-image values.

The output value at P(a,b) can be stored at P(o,o) without interfering with the output determination of other pixels because P(a,b) is clearly the last pixel whose output is related to the original value of P(o,o). For the same reason P(o,1) can be used for storing the output of P(a,1+b), and P(o,2) for P(a,2+b) and so forth.

In general, the output at P(i+a,j+b) can be stored at P(i,j) with no interference with computations of outputs at other pixels. The only effect is that the output image will be shifted a columns leftwards and b lines upwards relative to the original image and this causes no undesirable influence on the final result. This data storage strategy has been used for the implementation of all parallel local operators.

2.2.4 Connectivity

The connectivity of pixels in a rectangularly tessellated plane has two definitions, namely 8-connectivity and 4-connectivity[7]. Two pixels are 4-connected to each other if and only if they have a common side. As one pixel has 4 sides it will be connected to four and only four pixels. Pixels at image borders are excepted. Pixels are 8-connected if and only if they share at least one corner. By this definition one

pixel, again excluding border pixels, will have 8 and only 8 pixels connected to it.

(a) 4-connective Pixels; (b) 8-connective Pixels

Fig2-3 Pixel Connectivity

Fig2-3 shows two centre pixels with all its 4-connected and 8-connected neighbours. Two functions can be used to express these two definitions. Let $P(x_1,y_1)$ and $Q(x_2,y_2)$ be two pixels in an image and (x_1,y_1), (x_2,y_2) be their two-dimensional coordinates respectively, pixels P and Q are 4-connected if and only if

$$|x_1-x_2| + |y_1-y_2| = 1.$$

They are 8-connected if and only if

$$\max(|x_1-x_2|, |y_1-y_2|)=1.$$

It is obvious that 4-connected pixels are naturally 8-connected, but 8-connectivity does not guarantee 4-connectivity. Both definitions have been used in the present work and it will be noted at the appropriate place which definition is being used there.

2.3 Summary

The system used in the present work possesses the fundamental characteristics of a general image processing system, despite of its various limitations, particularly in computer memory and speed.

The overall software development strategies have been explained. The software has been developed in a combination of high level and low level computer languages, BASIC and 6502 machine code, to achieve both flexibility and speed. To guarantee a fully meaningful output image, operations are applied only to pixels whose output value does not require artificial input values. Because the computer can not provide

adequate data storage space, the processed image data are stored back into the frame store overlapping the original image data. Pixel connectivity in a rectangular tessellation has two definitions, 4-connectivity and 8-connectivity. Different definitions have been used in different applications.

PART II FABRIC PORE SIZE DISTRIBUTION

CHAPTER 3 REVIEW OF LITERATURE

3.1 GEOTEXTILES

Geotextiles are permeable textile materials used as a construction material in conjunction with other construction materials in applications of a civil engineering nature[8]. The technology of geotextiles was mainly built up in the 1970s and thenceforth, although isolated applications of textile materials in civil engineering can be traced back to a much earlier time[9]. In the early days woven fabrics were exclusively used in such applications and geotextiles in general were treated as "novelties limited to non-critical applications"[10]. All of this was changed rapidly by the introduction of nonwoven materials into geotextiles in the early 1970s and by the accumulation of field experience. Geotextiles have now become standard construction materials throughout the world and, are not just being used as advantageous replacements of existing materials but as new materials capable of development for a multitude of potential

applications[11].

In addition to the already very wide range of geotextiles available[8], brand-new products are being developed especially for civil engineering applications. By careful selection of appropriate raw materials and the method and type of construction and finishing, a new product can be produced to satisfy specific requirements of a particular application[11].

In general, geotextiles are much lighter in weight when compared with traditional engineering materials and therefore easier to handle, to store and to install. They have more reliable supply and quality control. Geotextiles also have various other advantages over conventional engineering materials in individual applications. In drainage applications, for example, a single layer of geotextile can perform as a multi-phase graded aggregate filter.

Although geotextiles have numerous applications in civil engineering works, their primary functions can always be identified as including one or more of the following categories[12]:

(a) Separation;

(b) Filtration;

(c) Drainage-in-the-plane;

(d) Reinforcement.

Apparently the engineering and physical properties of geotextiles, such as fabric strength, thickness, pore size and environmental stability, have varying importance in relation to different basic functions. The pore size distribution of a geotextile, for example, is vital to filtration, drainage and separation but trivial to reinforcement.

The designing of an engineering structure which incorporates geotextiles requires the selection of a geotextile whose structural and physical properties satisfy the functional requirements of the application. This can only be achieved if there are appropriate design criteria and quantitative property specifications of geotextiles. Except for some general guidelines, however, up to the present time most geotextile design criteria have been empirical and their applicability controversial. There are even widely different "official" design criteria for similar applications[8]. The measurement methods of most geotextile properties, too, are far from standardized. It is a common practice that the empirical criteria developed by one organization can only be used with the property values of geotextiles obtained through the testing procedures developed by the same organization. The

complications are mainly due to three reasons:

(a) The variability of in-situ conditions;

(b) The diversity of composition and structure of geotextiles;

(c) The differences between laboratory conditions under which geotextiles are tested and the field conditions under which geotextiles are used.

Tests of geotextiles are currently of three varieties: in-isolation testing, in-soil testing and prototype trials[12].

In-isolation tests are carried out under standard laboratory environmental conditions. Most geotextile specification values are obtained by in-isolation tests because of their simplicity and economy advantages. But these testing results are considered to be of little value for design purposes although they may be used as empirical design data as experience is gained in the use of these tests and from measured soil-geotextile system performance. Nevertheless, in-isolation tests can provide the basis for product quality control and product comparison.

In-soil tests are carried out with geotextiles confined

in-soil. In-soil tests are of two categories. When standard soils are used and the tests are carried out under standard laboratory conditions, the results are treated in the same way as those obtained by in-isolation tests and these in-soil tests together with in-isolation tests are referred to as index tests. On the other hand, in-soil tests can also be carried out for design applications by matching the soils used and the conditions of testing to those anticipated on site.

Prototype trials are large scale laboratory tests or field trials. They are used to measure the overall performance of soil-geotextile systems and the resulting data can be directly used in design providing the trial conditions are similar to the field conditions. Complex equipment is required for in-soil tests and prototype trials and because they are very time consuming only a limited number of tests can be performed, and therefore the results have less statistical reliance.

3.2 Measurement of Pore Size Distribution

One of the most important properties of geotextiles is their pore size distribution. It has been claimed that one can have a reasonably clear understanding of the capability of a

particular fabric for geotechnical applications after obtaining its pore size distribution and permittivity value[12]. The correlation of the particle size distribution of the soil with the pore size distribution of the fabric is a necessity in the evaluation of the performance of a geotextile with respect to some of its functions, such as separation, filtration and drainage and in the selection of a geotextile to fulfil the requirements of these applications. When used as filters, for example, the pore sizes of the geotextiles must be large enough to avoid excessive restriction of water flow (clog) but at the same time small enough to avoid excessive particle loss (piping). In fact, all the filter design criteria are based on this principle in spite of their widely differing details[9]. It is therefore necessary to determine the pore size distribution of a fabric before correlating it to the soil particle size distribution.

There is however much controversy over how to measure the pore sizes of geotextiles. Difficulties are mainly caused by the severe irregularity of shape and dimension of pores of geotextiles, particularly that of nonwoven geotextiles. The size of regular rectangular openings in many open woven geotextiles can be measured by direct optical methods. But the determination of the variable dimensions of pores of other types of geotextiles requires special procedures. The following four principal systems are currently used:

(a) Dry sieving.

(b) Wet sieving;

(c) Hydrodynamic filtration;

(d) Image analysing.

The actual techniques employed in the sieving methods (a, b and c) may differ from one laboratory to another [14],[15],[16], but their principles are basically the same. In dry sieving, samples of glass balls or uniform sand particles of known sizes are sieved through a fabric and by plotting the weight of the passed particles against the particle sizes, the apparent opening size distribution of the fabric can be estimated. Wet sieving is similar to dry sieving in procedure, but water is sprayed onto the standard soil which is sieved through the fabric. In hydrodynamic filtration, however, sieving by a standard soil is carried out under alternate flows of water.

It was reported that for the same fabric each one of the above methods will show a different pore size distribution and in particular a different maximum pore size, O_{max}, which can vary as much as a factor of $2^{(14)}$. Furthermore the sieving methods (a, b and c) are all very time consuming.

The image analysing method referred to above was introduced by Rollin and Masounave of Ecole Polytechnic, Montreal, Canada[17]. The fabric to be analysed was first encased in a synthetic resin inert to the fibre material and the resin block containing the fabric sample was then cut to obtain a cross section of the sample. Based on the assumption that this cross section can be represented as a porous medium constituted of a large number of dots, which represent cross sections of fibres, randomly distributed (Fig3-1) and by using probability theories, functions were derived to compute parameters such as the most probable diameter of the porous medium, the mean hole diameter and the maximum diameter of the porous medium. By further assuming the fibre cross area to be zero, the only information required in the computation of these parameters was the number of fibres per unit area of cross section and this was obtained using an image analyser. Their experimental data demonstrated that the above parameters could provide useful information for the prediction of filtration performance of nonwoven geotextiles having a thickness greater than 2mm. It is obvious, however, that these parameters are more related to fabric porosity than to the pore sizes measured by the sieving methods, and therefore are more useful for predicting the percentage of particles of a known diameter that may be retained within a geotextile instead of for predicting the percentage of particles of a known diameter that can pass through the geotextile. Moreover this method is not applicable to thin geotextiles.

Fig3-1

It will be shown in the following chapters that a faster and more economical approach to assessing the pore size distribution of thin and/or compacted geotextiles can be achieved by automatic analysis of surface images of these geotextiles using digital image processing techniques.

CHAPTER 4 PRELIMINARY PROCESSING

Grey level thresholding has been used to segment raw images into binary images for the measurement of pore sizes. The decision is made mainly on two grounds: the simplicity of the algorithm and the object-background nature of the images concerned. Because the segmented images generally contain a considerable amount of noise, other preliminary processing techniques, including a modified shrinking-expanding process and a hole filling process, have been developed to reduce the noise level so that more accurate measurement can be achieved.

4.1 SEGMENTATION

Thresholding is the most common segmentation method of grey level images. If the original image f(x,y) has value range $[G_1,G_2]$ and T_1, T_2, ..., T_n are n different values within (G_1,G_2), then $[G_1,G_2]$ can be divided into n+1 mutually

exclusive subsets: $[G_1,T_1]$, $(T_1,T_2]$, ..., $(T_{n-1},T_n]$, $(T_n,G_2]$. The generalized n-level thresholding operation can be defined as:

$$F(x,y)=\begin{cases} V_o \text{ if } f(x,y) \in [G_1,T_1]; \\ V_i \text{ if } f(x,y) \in (T_i,T_{i+1}], \\ V_n \text{ if } f(x,y) \in (T_n,G_2]. \end{cases} \Big| \; i = 1,\ldots,n-1;$$

Where F(x,y) is the result of the operation and V_o V_1, ..., V_n are values assigned to the relevant subsets. Obviously an n-level thresholding operation can only be successfully applied to an image which has n+1 meaningful sub-regions and each of these sub-regions occupies a unique grey level range. In most cases n equals to 1 and $[G_1,G_2]$ is divided into two subsets, $[G_1,T]$ and $(T,G_2]$, where T is the threshold. The result of a single level thresholding operation is a binary image, or in other words an image with only two grey level values, normally represented by 1 and 0.

A raw image of a thin geotextile fabric contains two sub-regions: the pores (objects) and the fibres (background). If the image is obtained through transmitted illumination the objects will have higher intensities than the background; if the fabric is put on a base which is darker than the fibres and the image is obtained through reflected illumination the situation reverses: the background will be brighter than the

objects. In either cases the two sub-regions are separable by intensity and therefore the image can be segmented by thresholding.

The implementation of the algorithm is very simple as the computation involved is just a comparison process. Difficulty arises, however, in the selection of an optimal threshold. Fig4-1a shows an ideal grey level histogram of an image with two sub-regions. The histogram of an image is a function that gives the frequency of occurrence of each grey level in the image. For an image with a histogram as Fig4-1a, any value between A and B will be an ideal threshold which achieves error-free separation of the two sub-regions. But in reality an image of two sub-regions will have a histogram as either Fig4-1b or Fig4-1c. Fig4-1b is a bimodal histogram which has two peaks and a non-zero valley in between them. The best threshold which minimizes segmentation errors for images with a bimodal histogram is generally the valley bottom, unless more prior information, such as the probability densities of the two subpopulations, is available[2]. But when an image has a unimodal histogram as Fig4-1c, it is very difficult to select a suitable threshold without further knowledge of the image, for example, the expected total area of each sub-region. The unimodal histogram is usually obtained from an image whose sub-regions have widely varying grey levels, or to an image in which the transition between the sub-regions is very smooth.

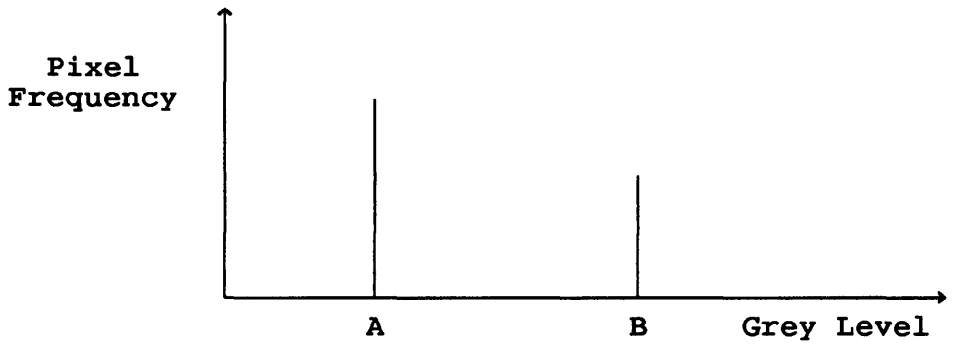

(a) Histogram of a Binary Image

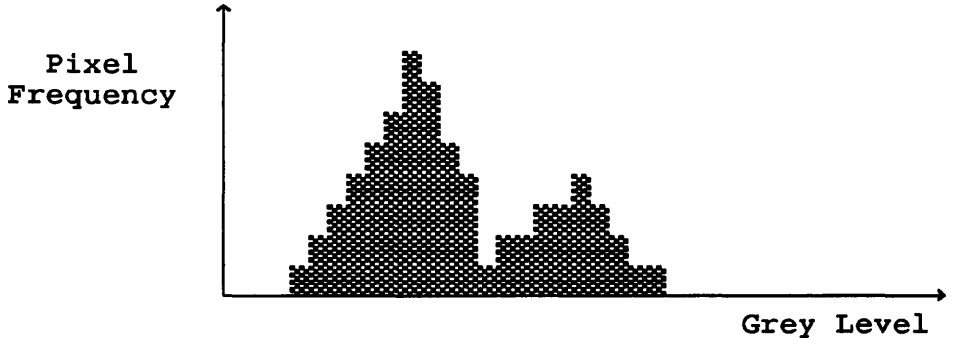

(b) A Bimodal Histogram

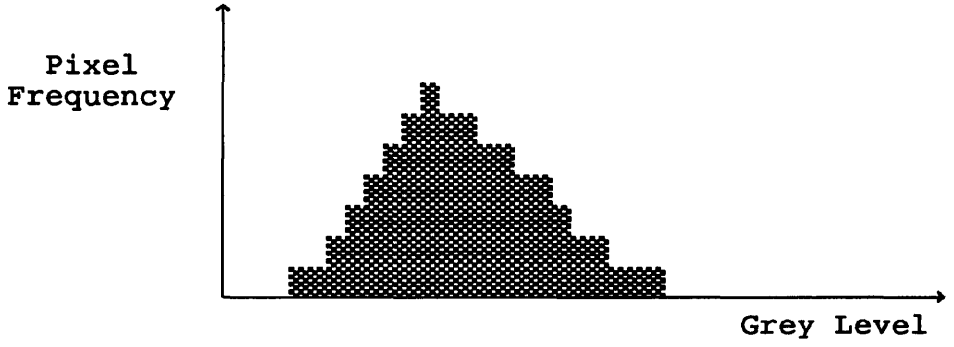

(c) An Unimodal Histogram

Fig4-1 Sample Image Histograms.

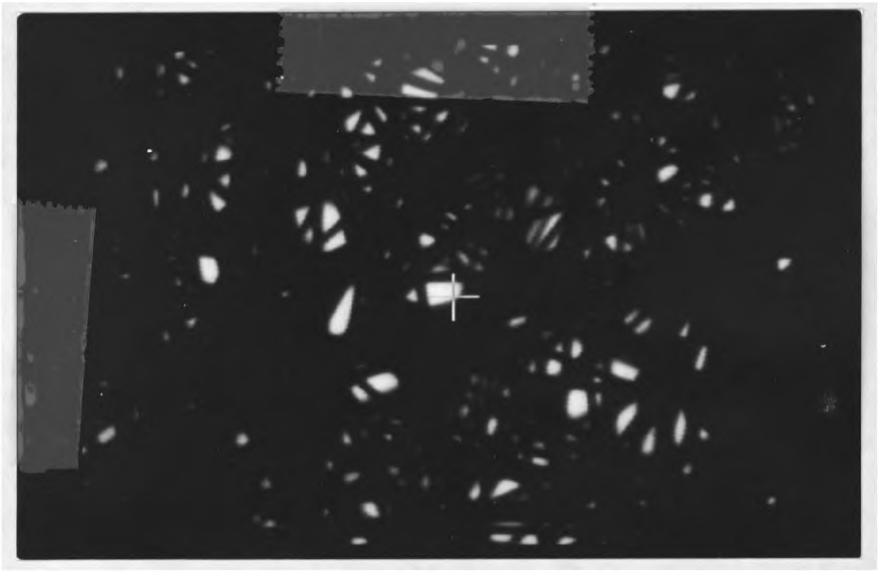

Fig4-2 The Image of a Fabric Sample.

Fig4-2 shows an image of a melt-blown nonwoven fabric. The fabric is originally of black colour and the image was taken under transmitted illumination. Fig4-3 is the corresponding histogram, which is unimodal despite the obvious presence of two sub-regions in the image. This is because the total pore area is very small and therefore the relative frequencies of grey levels in the pore regions have no dominance over that in the transition area. The high and sharp peak at the dark end of the histogram reflects the relatively large and uniform

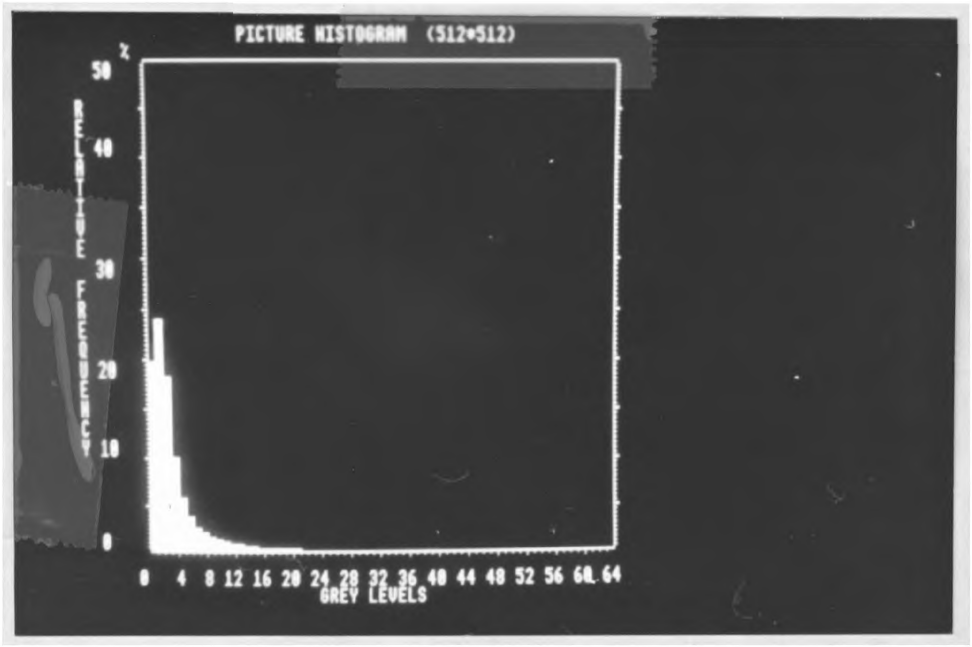

Fig4-3 Histogram of Fig4-2.

background region. From a histogram of this type it is impossible to select an optimal threshold and the analysis of other image features is required. The plot of grey levels across a single line of the image is shown in Fig4-4 which indicates that the image has a good contrast and a threshold can be easily chosen to detect the existence of a pore. But clearly, when the threshold varies, the dimensions of pores in the segmented image will change. A higher threshold will produce smaller pores and a lower threshold will produce larger pores. Because the task is to measure the pore sizes, proper selection of threshold becomes crucial.

There are a number of methods to select an optimal threshold[2], but none of them is applicable here because of the lack of further information about the image. Careful examination of Fig4-4 suggests, however, that the centre points of the transition region can be reasonably regarded as separation points between the objects and the background. This means the MEAN OF THE MAXIMUM AND MINIMUM GREY LEVELS of the image can be selected as the "optimal" threshold. Based on this idea, a MEAN GREY LEVEL THRESHOLDING method has been developed. An additional advantage of this mean grey level thresholding is that the whole segmentation process can be automated. By performing an image scanning, the maximum and minimum grey levels of the image can be obtained and the average value of the maximum and minimum grey levels is then the desired threshold. The segmentation can then be completed

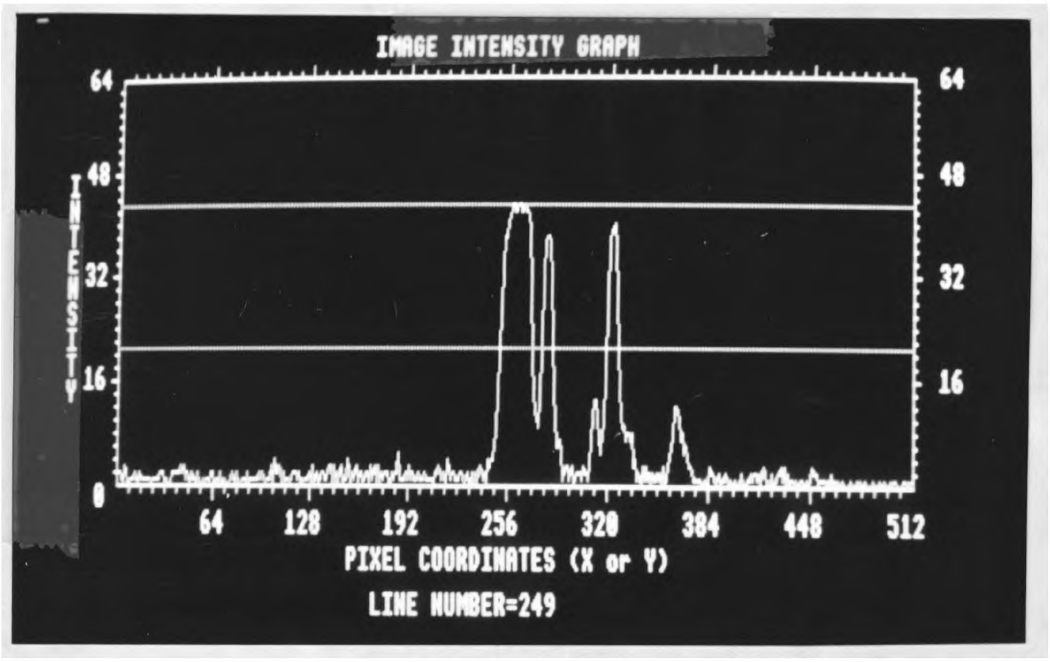

Fig4-4 Intensity Graph of a Single Line of Fig4-2. The Corresponding Line of the Image Is Indicated by a Cross in Fig4-2.

by another scanning of the image. Fig4-5 shows the segmented result of Fig4-2 by the mean grey level thresholding technique.

But it should be noted that the mean grey level thresholding will fail to work with images where the variation range of grey levels within either of the two sub-regions is greater than half the grey level range of the image. It is therefore important that fabric samples are properly treated to produce images in which the fibre regions and the pore regions both have highly uniform grey levels. The most successful treatment found has been dying fabrics to black colour so that all fibres become opaque. Images similar to Fig4-2 in quality can then be obtained by using transmitted illumination and successful image segmentation can be achieved by applying the mean grey level thresholding operation.

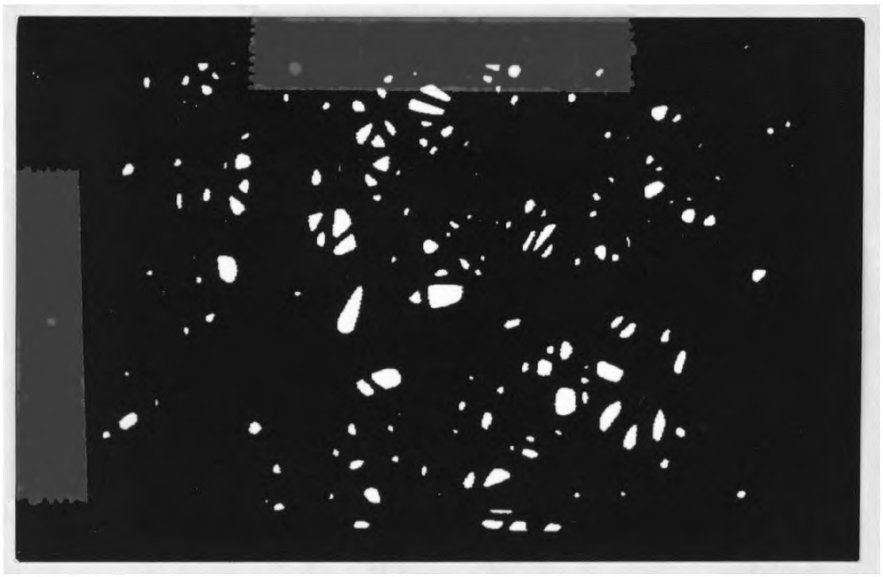

Fig4-5 Segmented Image of Fig4-2 by
Mean Grey Level Thresholding

4.2 Noise Filtering

Image segmentation often results in objects with "hairy" edges and produces other noise such as pinholes and isolated pixels (Fig4-5). This is inevitable as there is no clear cut between grey levels in the object region and in the background region in the raw image. Various methods can be used to reduce the noise. Complete cleaning of pinholes and isolated pixels can be easily achieved by searching and deleting. Smoothing of hairy edges, on the other hand, requires more elaborate algorithms. One method is to approximate the edges with circular arcs and/or straight line segments[18]. But this method is not suitable to the present application because of its complexity and a much simpler algorithm based on the shrinking-expanding principle[2] has been developed.

In a normal shrinking-expanding operation object edge pixels are first deleted by shrinking and all background pixels connected (8-connective) to the remaining object pixels are reverted to object pixels by the subsequent expanding operation. Small objects and thin parts of objects will be wiped out completely by shrinking and consequently cannot be recovered by subsequent expanding. This is the "noise" cleaning mechanism of the shrinking-expanding operation. Fig4-6 shows a simple example.

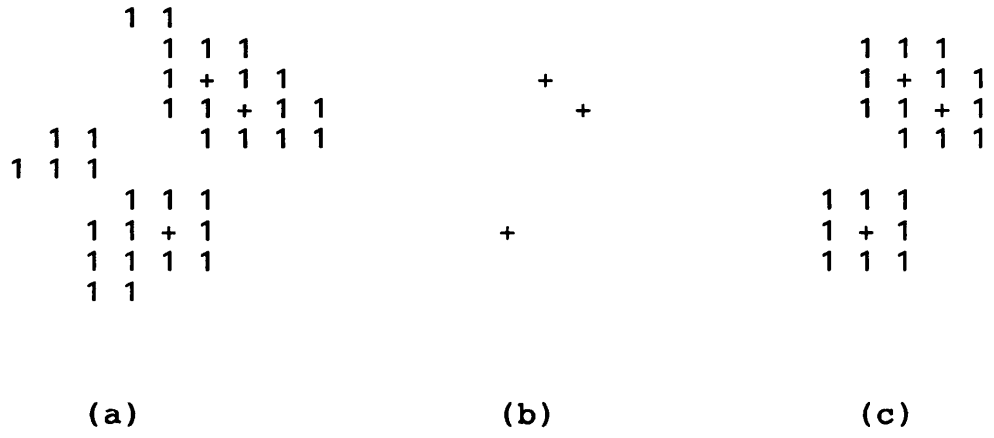

Fig4-6 The Shrinking-Expanding Algorithm.

(a) An Image;

(b) The Image after Shrinking;

(c) The Image after Expanding.

Notation:

Crossed pixels = Inner Pixels That Are Not affected by Shrinking.

The edge pixels of an object are defined as object pixels with one or more of their 8 neighbours being a background pixel. However, this definition has been found to be too sensitive to background noise. This is illustrated in Fig4-7.

```
1 1 1 1
0 1 1 1
1 1 1 0
1 1 1 1
```

Fig4-7 An Object That Will Be Deleted by One Normal Shrinking-Expanding Operation.

The object shown in Fig4-7 will be deleted by one shrinking-expanding operation. But clearly, it will be better that this object is treated as a 4 by 4 square with 2 background noise pixels. The definition of edge pixel is therefore modified to handle these background noises. In the new definition an object pixel is defined as an edge pixel only if TWO or MORE of its 8 neighbours are background pixels. Object pixels with only one of their neighbours being a

background pixel are also regarded as inner pixels and will not be affected by shrinking (Fig4-8). No modification is made at the expanding stage. It should be noted that this modification to the definition of edge pixels is strictly limited to the present section.

As the result of the change of the edge pixel definition, the object shown in Fig4-7 will become the more desirable 4 by 4 square (Fig4-8c). The modified shrinking-expanding algorithm can also clear pinhole noise , which the standard algorithm can not (Fig4-9).

Small objects and thin curves with a widths of two pixels or less will be wiped out by the new algorithm in the same way as by the standard algorithm and the operation can not be used in applications where these small objects and thin curves are significant. In the present application these small or thin objects are regarded as noise and therefore may be deleted. Otherwise these objects are too small to be measured by the present system with reliable accuracy and a greater magnification is required if these small objects are to be measured. Fig4-10 shows the result of applying the operation to Fig4-5. The edge smoothing and noise cleaning effect of the operation is clearly visible.

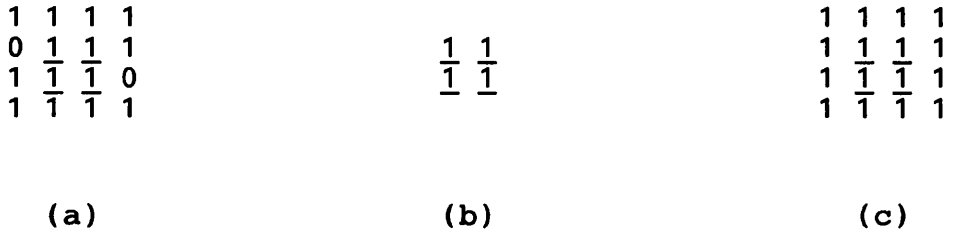

Fig4-8 Modification to the Shrinking-Expanding Algorithm

(a) Same Object As in Fig4-7;

(b) After Modified Shrinking;

(c) After Expanding.

Notation:

Underlined Pixels = Inner Pixels Under Modified Definition.

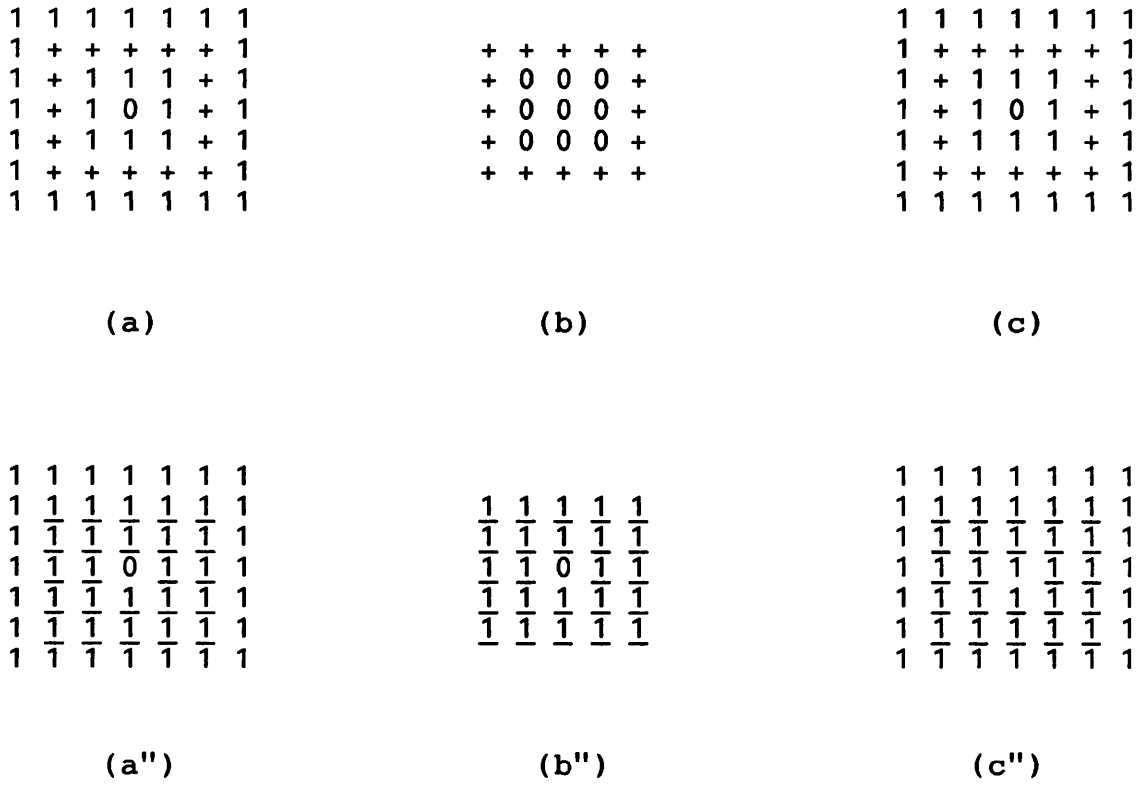

Fig4-9 The Effect of Pinhole Noise: A Comparison between the Normal & Modified Shrinking-Expanding Algorithm.

(a), (a") An Object with a Pinhole;

(b), (b") After Normal & Modified Shrinking Respectively;

(c), (c") After Expanding.

Notations:

Crossed Pixels = Normal Inner Pixels;

Underlined Pixels = Inner Pixels Under Modified Definition.

Fig4-10 Smoothed Image of Fig4-5.

4.3 Deleting of Holes

It has been found that larger holes other than pinholes can also occur in the segmented images. Since objects represent fabric openings, these holes can not exist in reality and their existence are due to noise in the raw images. These large holes have to be deleted for more accurate measuring.

The shrinking-expanding operation can delete pinholes, but it has little effect on larger holes. Because holes are surrounded by object pixels, they can be deleted by a gap filling operation that fills gaps between two object pixels in the same column (or in the same row). But this operation will also fill gaps between any two objects which have common X (or Y) coordinates (Fig4-11a). The operation should therefore be able to distinguish pixels belonging to different objects and should only fill gaps between two pixels belonging to the same object. Object labelling may be used to label every object uniquely, i.e. turn every object into a unique grey level before gap filling. But the number of grey levels available limits the total number of labels to a maximum of 63, which is far from adequate. An object isolation method is consequently used. The outer edge of an object is first followed and

marked. Then all background pixels which lie in between two object pixels of the same column (or the same row) and which are enclosed within the marked edge are inside a hole and can be converted into object pixels. Background pixels which lie in between two marked edge pixels of the same column are inside a concave part of an object, not inside a hole. These pixels should not be changed (Fig4-11b).

Gap filling is accomplished by image scanning. But scanning the entire image for every object is clearly inefficient as most objects are very small compared with the size of the image and a considerable amount of time will be wasted. To restrict the scanning process to the smallest area possible, the top, bottom, left-most and right-most pixels of an object are searched out in the edge following process. These pixels will enable the defining of the upright circumscribed rectangle of the object (Fig4-11c). The scanning process can then be restricted inside this rectangle. Because edge following is the foundation of object size measuring algorithms described in the next chapter a detailed description is given below.

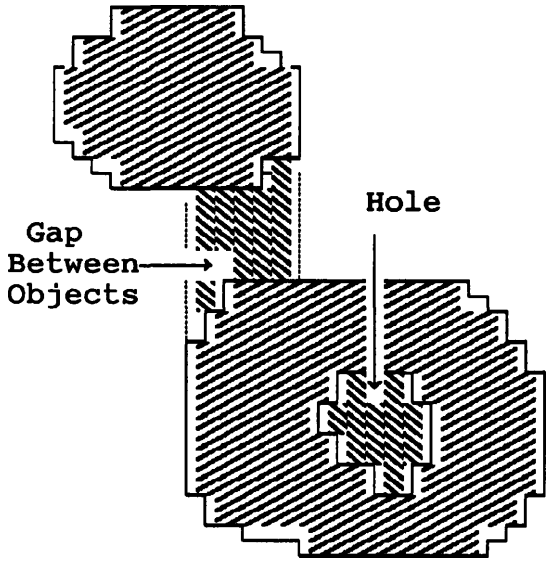

(a) A Gap Filling Operation That Fills Gaps between Object Pixels in the Same Column Will Fill Gaps between Objects As Well As Holes Within Objects;

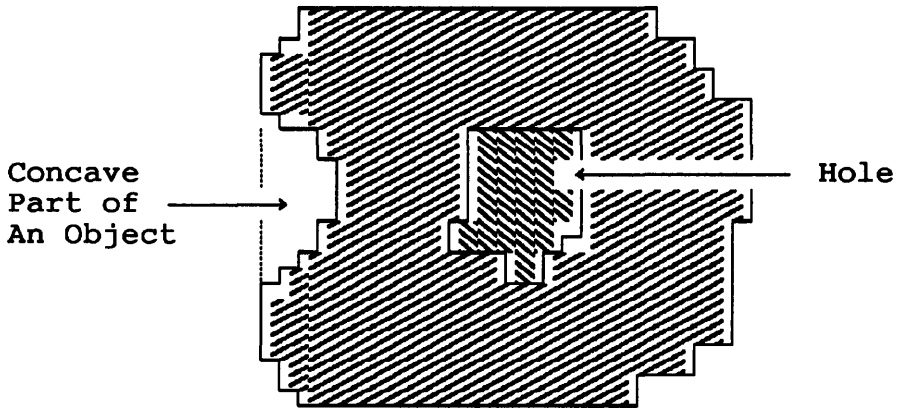

(b) A Gap Filling Operation That Only Fills Gaps between Non-Edge Object Pixels in the Same Column of the Same Object;

(To Be Continued)

(Continued from Last Page)

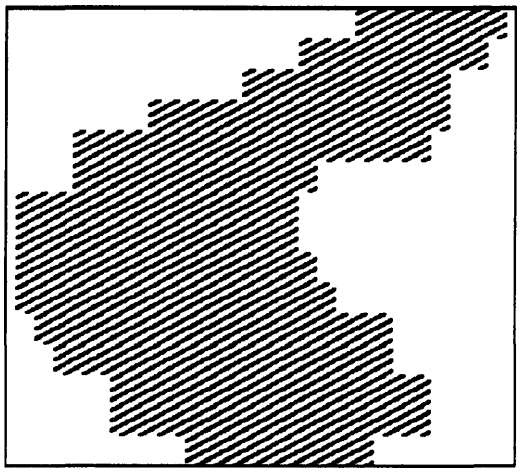

(c) The Upright Circumscribed Rectangle of an Object.

Fig4-11 The Hole Deleting Operation

4.4 Edge Following

4-connectivity has been used for objects in the measurement of pore sizes. The reason for this choice is illustrated in Fig4-12.

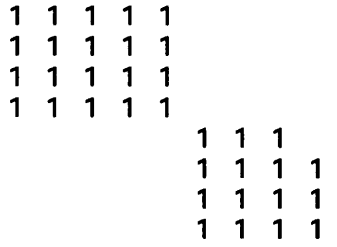

Fig4-12 4-connectivity Is Better for the Segmentation of Block Objects

It is clearly more realistic to treat Fig4-12 as two objects in 4-connectivity than to treat it as one object in 8-connectivity. It should be noted that opposite connectivities have to be used for objects and background to

avoid ambiguity of connectivity[2]. This means when 4-connectivity is used for objects, 8-connectivity has to be used for background, and vice versa. But the length of a thin line, such as the edge of an object, is better measured in 8-connectivity. Fig4-13 shows an example.

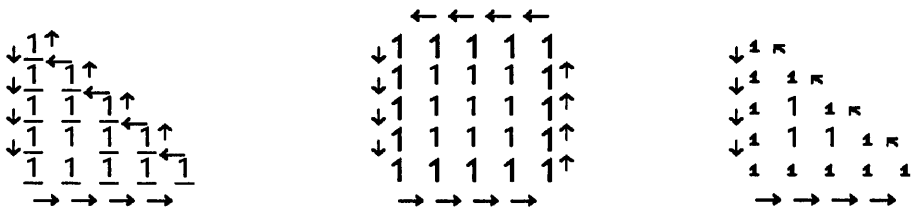

(a) (b) (c)

Fig4-13 Perimeter Ambiguity In 4-connectivity

(a) Perimeter = 8h+8v (in 4-connectivity);
(b) Perimeter = 8h+8v (in 4 & 8-connectivity);
(c) Perimeter = 4h+4v+4d (in 8-connectivity).

Notations:

1), In (a) Underlined Letters Represent the 4-connected Edge Line of the Triangle;

2), In (b) **BOLD** Letters Represent the 4 and 8-connected Edge Lines of the Square;

3), In (c) small Letters Represent the 8-connected Edge Line of the Triangle;

4), The Length of an Edge Line Is Measured in Number of Steps in Three Orientations: Horizontal (h); Vertical (v); Diagonal (d). The Arrows in the Figure Indicate These Steps.

In 4-connectivity the perimeter of the triangle shown in Fig4-13a will be the same as that of the square (Fig4-13b) and this is very misleading. If 8-connectivity is used instead, a more reasonable measure of the edge length can be obtained (Fig4-13c). And because 4-connectivity guarantees 8-connectivity, the 8-connected edge of a 4-connected object always exists. Consequently, a seemingly contradictory scheme of connectivity has been used in this section: 4-connective objects with 8-connective edges on an 8-connective background.

The edge of an object (outer edge is meant throughout this section) is followed counterclockwise. Clockwise following will produce exactly the same result and the steps can be easily derived from those described below. Counterclockwise edge following implies that an object is always on the left of an edge pixel.

Let P_1 be the last edge pixel visited, P_2 the current edge pixel. An EDGE FOLLOWING VECTOR V is defined by P_1 and P_2 and the direction of V is from P_1 to P_2. An imaginary starting vector has to be defined at the starting pixel because the last pixel is a background pixel. The direction of the starting vector is from the last background pixel to the starting pixel. The eight neighbours of P_2 are numbered in counterclockwise order from 0 to 7 (Fig4-14) and so are the eight possible directions of V (Fig4-15). The starting vector is always V_6 since the starting pixel is always the left-most

pixel of an object (viewed from the image) and the object is always on the left of an edge pixel (viewed from the edge following vector) (Fig4-16b).

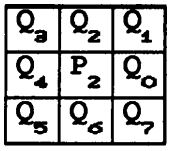

Fig4-14 The 8 Neighbours of an Edge Pixel

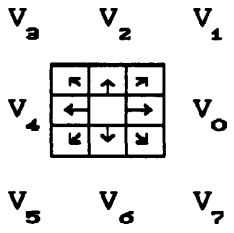

Fig4-15 The 8 Edge Following Vectors

The next edge pixel P_2'' (the new P_2) is among the eight neighbours of P_2 and the first candidate is determined by the direction of the vector or the vector number. Because object

is always on the left of an edge pixel (as edge following process is counterclockwise), when the vector V_i is even numbered (i = 0,2,4,6) the first candidate will be Q_{i-1} (Q_{i-2} is on the right of P_2) and when the vector is odd numbered (i = 1,3,5,7) the first candidate will be Q_{i-2} (Q_{i-3} is on the right of P_2). Let Q_j be the pixel being tested which is initially set to the first candidate, if Q_j is an edge pixel then $P_2'' = Q_j$ and $P_1'' = P_2$. P_1'' and P_2'' will define a new edge following vector. If Q_j is not an edge pixel j is incremented by 1 and the new Q_j is tested and so forth. But if the image contains isolated pixels the process will fail because no P_2'' can be found in the neighbouring pixels of P_2 and the testing will go on forever. To prevent this happening the starting pixel is examined before the testing of its neighbouring pixels. If it is an isolated pixel it is ignored and the process moves on to find a new starting pixel. The coordinates of every new edge pixel are compared with that of the starting pixel and their equality indicates the completion of the edge following process. Fig4-16 shows an object and the complete edge following process.

To minimize the searching time involved in the hole deleting process (section 4.3) and in the object size measuring process (chapter 5), the top, bottom, and right-most pixels of an object are also found in the edge following process so that the upright circumscribed rectangle of the object can be defined. The left-most pixel is readily the starting pixel.

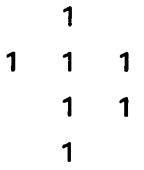

(a) An Object;

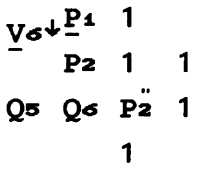

(b) Starting from Left-most Pixel with imaginary V_6 & P_1 (Underlined), $Q_5=0$, $Q_6=0$, $P_2"=Q_7$;

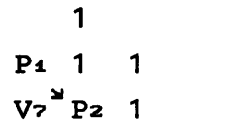

(c) $Q_2=0$, $P_2"=Q_6$;

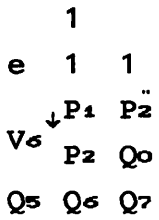

(d) $Q_5=0$, $Q_6=0$, $Q_7=0$ $Q_0=0$, $P_2"=Q_1$;

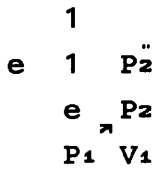

(e) $Q_7=0$, $Q_0=0$ $Q_1=0$, $P_2"=Q_2$;

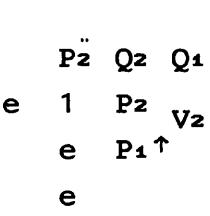

(f) $Q_1=0$, $Q_2=0$, $P_2"=Q_3$;

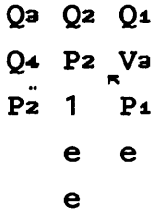

(g) Back to Beginning;

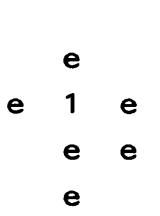

(h) The Final Edge.

Fig4-16 The Edge Following Process (e = Edge Pixel)

4.5 Summary

Image segmentation is necessary in all image analysing applications. Grey level thresholding is the most straight forward approach to image segmentation. The selection of a proper threshold is however not always a simple task and many sophisticated methods are available. It has been shown that the mean of the maximum and minimum grey levels is a reasonable threshold to well contrasted images and this approach has an additional advantage that the threshold can be automatically selected.

Segmented images often contain a considerable amount of noise, most prominently the rough edges and noisy spots both within the objects and the background. A modified shrinking-expanding operation can remove all the isolated pixels and pinholes. It also has a noticeable smoothing effect on the rough edges. Large holes may also occur due to more severe noise in the raw image and a special hole filling operation is required to remove them. Object isolation is necessary in the hole filling process and it is achieved by edge following and labelling. Noise reduction operations will increase the accuracy of measurement but they are not compulsory. If processing time is more important direct measurement can be taken immediately

after segmentation. The edge following and labelling process has been discussed in great detail because it has a fundamental importance in the pore size measuring algorithms presented in the next chapter.

CHAPTER 5 MEASUREMENT OF PORE SIZE DISTRIBUTION

5.1 Definition of Pore Size

An object (only two dimensional space is considered) has many size properties, such as area and perimeter which are in daily use. Complete specification of the size of an object requires not only its size properties but also the description of its shape. Consistent results are obtained if one compares the sizes of objects of the same shape by different size properties. As an example, the same result is obtained when a number of circles are arranged in order of area as when they are arranged in order of perimeter. But this consistency seldom holds for objects of different shapes. For example, the perimeter of a rectangle whose area is smaller than a circle is not necessarily shorter than that of the circle. Usually, only one of the many size properties of an object is of prime importance in a particular application and the object size is specified in terms of the property concerned, regardless of its shape. When several size properties have to be considered

at the same time, it is a common practice to form a new size property by combining together all the properties concerned according to some rules defined by the requirements of the application. A well-known example is in hydrodynamics where the cross sectional size of a tunnel is specified by a diameter which is defined as 4 times the cross sectional area of the flow divided by the wetted perimeter of the tunnel.

Three size properties of fabric openings have been considered important to the functions of geotextiles: area, hydrodynamic diameter and thickness. The hydrodynamic diameter is defined as 4 times the area of a pore divided by the its perimeter; the thickness of a pore is defined as the diameter of its maximum inscribed circle. The area and hydrodynamic diameters of fabric openings are determinant factors of hydraulic properties, such as permeability, of a fabric. The thickness of a pore defines the maximum particle that can pass through the pore and therefore is crucial to filtration and separation applications.

5.2 Measurement of Equivalent Diameter

To make the area of a pore more comparable with the other two

size properties considered, it is converted into an equivalent diameter (D_e) by the following simple function:

$$D_e = 2K \sqrt{1.5A/\pi} \quad \text{.....(5-1),}$$

where K is the vertical objective length of a pixel (pixel width = 1.5 X pixel length) and A is the area of an object in number of pixels. Clearly, D_e equals to the diameter of a circular object with an area of A.

The area of an object in a digital image is the total number of pixels contained in that object. The measuring of area is therefore simply the counting of pixels. The total object area in an image can be easily obtained by scanning the image systematically and counting the total number of object pixels in the image. But the measurement of the area of every individual object requires the scanning and counting process being restricted to one object at a time. As in the hole filling process described in section 4.3, the edge following and marking technique is used to isolate an object from the rest of the image. The area measuring process has the following major steps:

(a). Scan the image column by column from left to right until an object pixel is encountered. Suspend image scanning at this pixel.

(b). Follow and mark the edge of the object. Also search out the top, bottom, left-most and right-most pixels of the object in the course of edge following. These four extreme pixels define the upright circumscribed rectangle of the object.

(c). Scan within the rectangular window and count the number of object pixels enclosed inside the marked edge, including the marked edge pixels. Background pixels inside the edge, i.e. pixels within holes, are not counted. This provides the algorithm the ability to handle situations when holes are not caused by noise, such as when the image contains ring shaped objects. If holes are considered noise, they should be deleted by the hole filling operation. All object pixels, including edge pixels, which have been counted are marked with a new label to avoid the same object being counted again while the image can be retained. When the scanning of the window is completed, the number of object pixels is stored.

(d). Repeat steps (a) to (c) until all the objects in the image have been measured.

(e). Process the stored data and draw the pore size distribution curve.

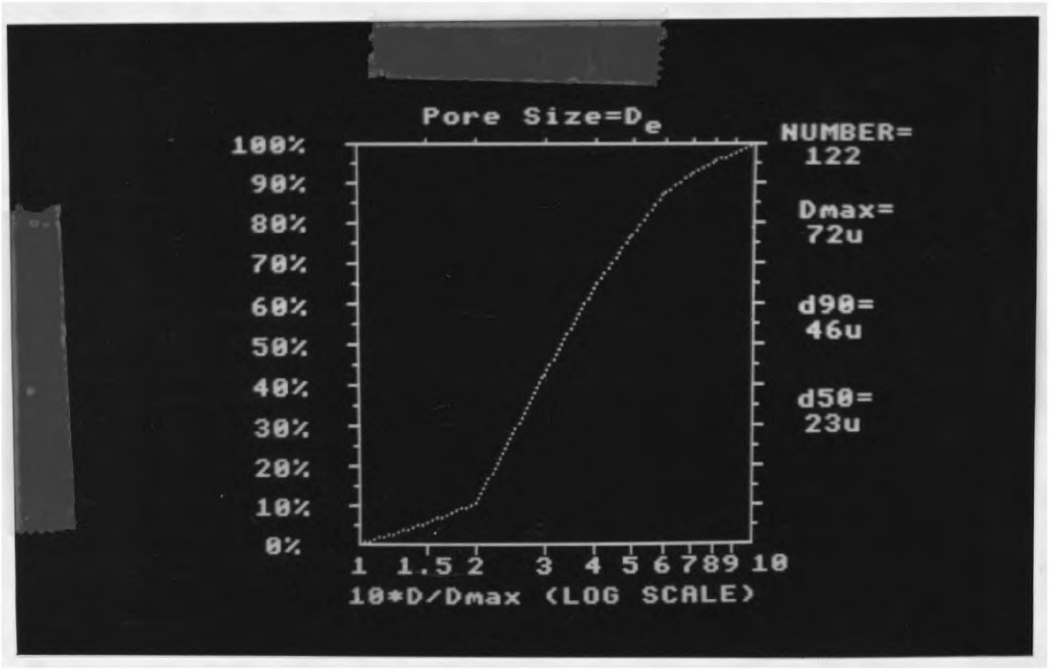

Fig5-1 Pore Size Distribution Measured from Fig4-10 in Terms of Equivalent Diameter D_e,

Denotations:

D_{max} = Maximum Pore Diameter;
D_{90} > Diameters of 90% Pores;
D_{50} > Diameters of 50% Pores.

Fig5-1 shows the result obtained from Fig4-10. The equivalent diameter of a pore is calculated from its area value according to function (5-1). The horizontal axis represents the pore size. The pore size values are plotted relatively to the maximum pore size value D_{max}. The advantage of this approach is that the curve generating process can be normalized. The final curve therefore shows only the distribution of pore sizes and is not affected by the actual pore sizes. The vertical axis represents the accumulated frequency. The maximum pore size value D_{max} and the total number of pores measured are shown in the graph. D_{90} and D_{50} is also calculated and presented in the graph. The meaning of D_{90} is: 90% of the pores are smaller than this value while 10% of the pores are larger than it. D_{50} is simply the median pore size which means 50% of the pores are smaller than it and 50% of the pores are larger than it.

5.3 Measurement of Hydrodynamic Diameter

The measurement of the hydrodynamic diameter of an object requires the measurement of its perimeter in addition to its area. The process of area measurement is identical to that in section 5.2 and the perimeter of an object is measured in the edge following process. Edge following steps are divided into

three groups according to their direction: horizontal, vertical and diagonal. If the length of a vertical step is 1 unit, then the length of a horizontal step is 1.5 units and that of a diagonal step is $\sqrt{1+1.5^2} = \sqrt{3.25}$ units. When the edge of an object is being followed, the total number of steps in each group is counted and the perimeter of the object, P, is calculated according to the following equation:

$$P = K \left[N_v + 1.5N_h + \sqrt{3.25}\, N_d \right] \quad \cdots\cdots\cdots\cdots (5\text{-}2).$$

Where K is the vertical objective length of one pixel and N_v, N_h, N_d are the number of vertical, horizontal and diagonal steps respectively. The perimeter of an object is stored together with its area and, having measured all the objects the data is processed to produce the pore size distribution curve. The hydrodynamic diameter of an object, D_h, is computed through the following equation:

$$D_h = 4X1.5K^2A/P = 6K^2A/P \quad \cdots\cdots\cdots\cdots\cdots\cdots (5\text{-}3).$$

Where K is the vertical objective length of one pixel and A is the area of an object in number of pixels. Fig5-2 shows the hydrodynamic diameter distribution curve of pores in Fig4-10.

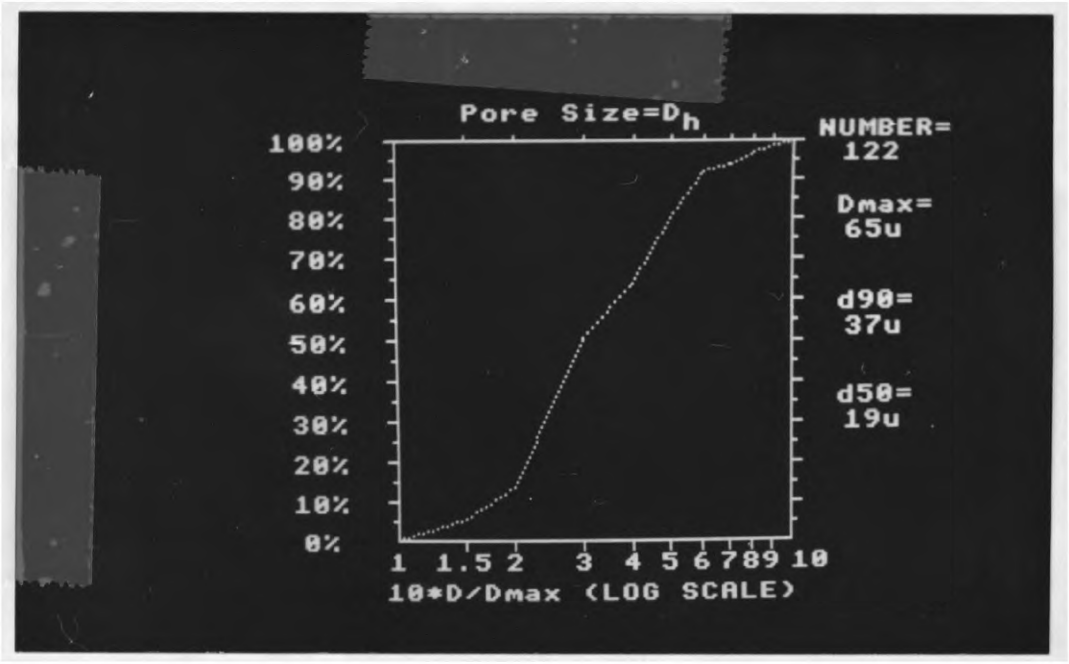

Fig5-2 Pore Size Distribution Measured from Fig4-10 in Terms of Hydrodynamic Diameter D_h.

Denotations:

D_{max} = Maximum Pore Diameter;
D_{90} > Diameters of 90% Pores;
D_{50} > Diameters of 50% Pores.

5.4 Measurement of Thickness

The thickness of an object in a digital image is defined as twice the number of shrinking operations required to delete that object[2]. Shrinking is an operation that removes all edge pixels from an object. Because the operation is omnidirectional the thickness of an object obtained in this way readily equals the diameter of the maximum inscribed circle of that object. Once again the edge following and marking technique is used to restrict the operation to one object at a time and the thickness measuring process is as follows:

(a). Scan the image column by column from left to right. When an object pixel is detected, suspend scanning and follow the edge of the object. Mark all edge pixels with label "e" and find the top, bottom, left-most and right-most pixels of the object so that the upright circumscribed rectangle of the object can be defined. All object pixels 4-connected to the north edge of the object are also marked as edge pixels. The north edge of the object will be two pixels thick in contrast to the one pixel thick south, west and east edges.

(b). Scan inside the rectangle. Delete all the current edge pixels which are marked with "e" and, at the same time, mark all the object pixels which are 4-connected to the current edge pixels with "n". These newly marked pixels will form the next edge of the object after the current edge is deleted. It should be noted that only the outmost edge of an object is guaranteed to be a closed curve. The inner edges can be a collection of single pixels, thin line segments, and smaller closed curves.

(c). Scan inside the rectangle defined in step (a) and mark all "n" pixels with "e". Check the number of deleting operations having been performed. If this number is even, including 0, mark all the object pixels that are 4-connected to the NORTH edge of the object with "e"; otherwise, mark all the object pixels 4-connected to the SOUTH edge of the object with "e".

(d). Repeat (b) and (c) until the object is deleted. Store the number of deleting operations performed.

(e). Repeat steps (a) to (d) until all the objects in the image have been deleted. Process the data to produce the object size distribution curve.

Steps (a) to (d) are illustrated in Fig5-3. The complication of marking object pixels 4-connected to the north and south edge of an object alternately as extra edge pixels in steps (a) and (c) is caused by the rectangular nature of pixels. Suppose the deletion of an object requires M NORMAL shrinking operations, the thickness of the object will be 2M pixels. But it is unknown whether it is in vertical units or horizontal units and because vertical and horizontal units represent different real length, the actual object thickness is still unknown. To overcome this ambiguity, the object is shrunk by three pixels in the vertical direction instead of the normal two pixels in one shrinking operation. Thus if the deletion of an object requires M shrinking operations (the new version) its thickness will either be 2M horizontal units or 3M vertical units. Since the width-to-height ratio of a pixel is 3:2, 2M horizontal units represent the same real length as 3M vertical units and the thickness of the object is then unambiguously defined. The alternation of the thickening of the north and south edges is to ensure the shrinking operation converges to the center of the maximum inscribed circle of the object.

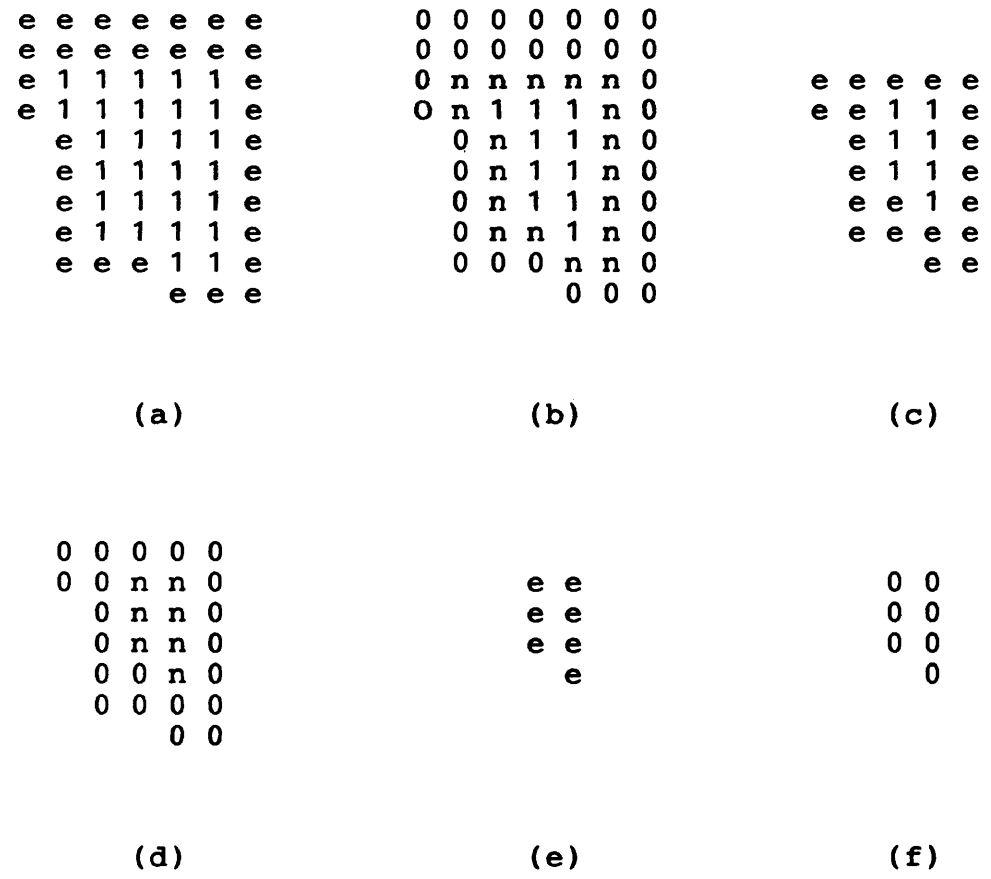

Fig5-3 The Thickness Measurement Algorithm

(a) Labelling the First Edge;

(b) Deleting the First Edge & Labelling the Second Edge;

(c) Labelling the Second Edge Continued;

(d) Deleting the Second Edge & Labelling the Third Edge;

(e) Labelling the Third Edge Continued;

(f) Deleting the Third Edge & the Object is Deleted.
(Object Thickness = 3X2 = 6 Horizontal Pixels)

Denotations:

e = Current Edge; n = Next Edge.

It is clear that all objects having a thickness of odd numbered pixels (in horizontal units) will be measured one pixel bigger. This is due to the fact that the thickness of an object is measured as twice the number of shrinking operations required to wipe it out from the image. Thus if an object is simply one pixel thick it requires one shrinking operation to be deleted and its thickness will be measured as 2x1=2 pixels. A three pixels thick object needs 2 operations and its thickness will be 4 pixels and so on. The error caused by this phenomenon decreases relatively with the increase of object sizes and when the magnification is sufficiently large this error is negligible. In the case that this error is considerable and has to be eliminated, the image can be enlarged by a factor of 2 before measuring so that all objects will have a thickness of even numbered pixels. The thickness of the original object is then just the number of shrinking operations needed to delete the enlarged object. But the precision is gained at the expense of objective area that can be analysed at one time and the measuring time of each frame will also be longer. The objective area of the enlarged image is reduced to only one quarter of that of the normal image. To measure the same objective area will then take at least 4 times as much of time.

In Fig5-4 and Table5-1 the result obtained directly from a 256 by 256 image is compared with the result obtained after the image was enlarged to 512 by 512. The two curves shown in

Fig5-4 display an identical overall trend while the values of D_{max}, D_{90} and D_{50} (Table5-1) show slight disparities. The measured values of D_{max}, D_{90} and D_{50} were all bigger before image enlargement than after, as indeed they should be. The measurement was taken at the highest magnification where one pixel represents 3.64u. The biggest pore had a thickness of 15 pixels and was correctly measured as 55u (15x3.64) after image enlargement. But it was measured 1 pixel thicker before image enlargement as 58u (16x3.64) because it took 8 shrinking operations to delete. These disparities are considered insignificant and all the results presented in the following section were obtained without image enlargement. The pore size distribution of Fig4-10 in terms of thickness is shown in Fig5-5.

Measureing Method	D_{max} (u)	D_{90} (u)	D_{50} (u)
Without Enlargement	58	44	20
With Enlargement	55	38	19

Table5-1 Comparisons Between Pore Size Values Obtained with and without Image Enlargement.

Denotations:

D_{max} = Maximum Pore Diameter;
D_{90} > Diameters of 90% Pores;
D_{50} > Diameters of 50% Pores.

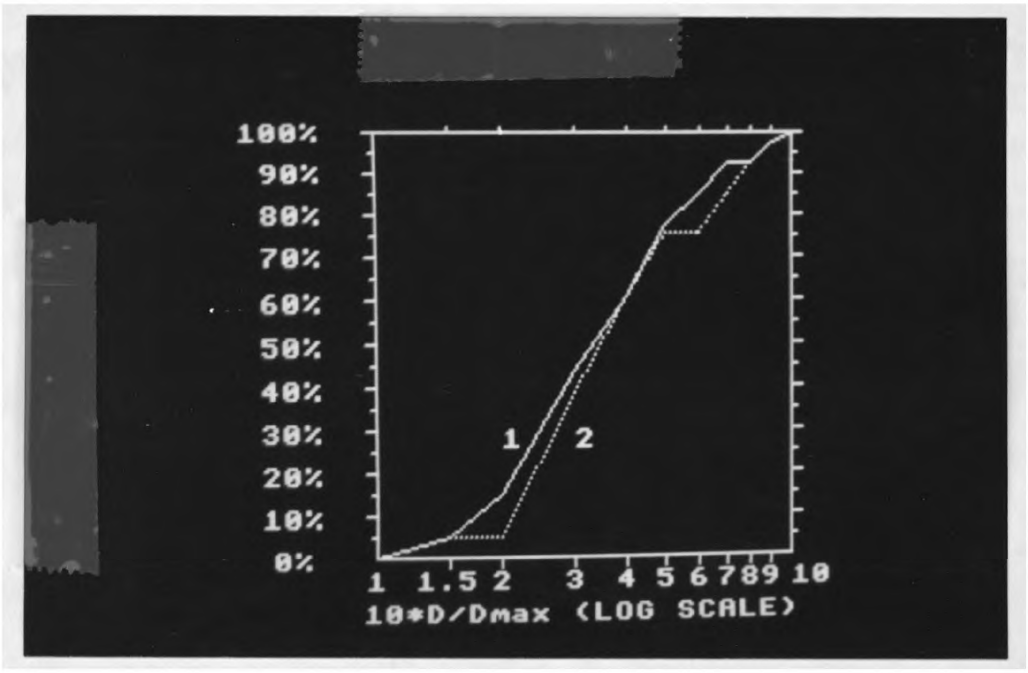

Fig5-4 Comparison of Pore Size Distribution Curves Obtained with and without Image Enlargement.

Denotations:

1 ..... With Enlargement;

2 ..... Without Enlargement;

D_{max} = Maximum Pore Diameter;

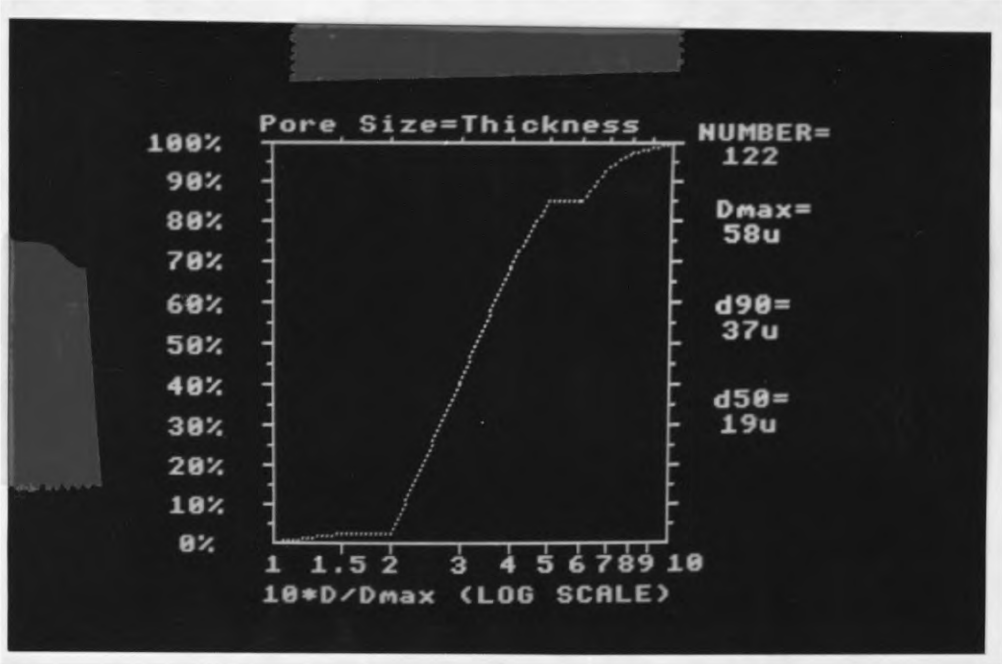

Fig5-5 Pore Size Distribution Measured from Fig4-10 in Terms of Thickness.

Denotations:

D_{max} = Maximum Pore Diameter;
D_{90} > Diameters of 90% Pores;
D_{50} > Diameters of 50% Pores.

5.5 Discussion

5.5.1 Pore Size Definition

From Fig5-1, Fig5-2 and Fig5-5, it can be clearly seen that the pore size distribution graphs obtained according to different pore size definitions differ from one another considerably. This is a plain illustration of the complexity of the shape of pores. Only when all pores are ideally circular will the three results agree with each other. The usefulness of each method can only be decided by the application of its result. As far as filtration is concerned the object thickness approach will be the most appropriate one among the three since the "thickness" of a pore defines the maximum diameter of particles that can pass through the pore.

5.5.2 Objective Area

The high magnification rate required in the analysing of a typical geotextile fabric limits the objective area of one measurement to several square millimeters. Since geotextiles are normally used in quantities of hundreds or thousands of

square meters and the physical properties of geotextiles, particularly of nonwoven fabrics, may vary significantly from one area of such a small size to another, to obtain a result with reasonable reliance, it appears necessary to take a large number of measurements randomly on a sufficiently large area of a fabric. The software that performs the pore size measuring tasks has therefore been written to facilitate multiple measurements. The final pore size distribution can be obtained from the combined data of any required number of measurements.

Three fabrics, two nonwoven and one woven, were examined in a preliminary investigation into the effect of the number of measurements on the final result. The two nonwoven fabrics were polypropylene melt-blown with basic weights of 60 and 80 g/m^2 respectively. The woven fabric was GTF400E made by Exxon Chemical Americas. All three fabrics were dark coloured by the manufacturers and therefore ideal for examination under transmitted illumination. The fabric samples all had an area of approximately 205mm by 255mm. Images of the three fabric samples are shown in Figures 5-6 to 5-8.

A suitable magnification rate has to be chosen before a fabric can be examined. The choice is basically an empirical one and a compromise is generally involved: the image size of pores should be sufficiently large to allow reasonably accurate measurement while the total number of pores in the image

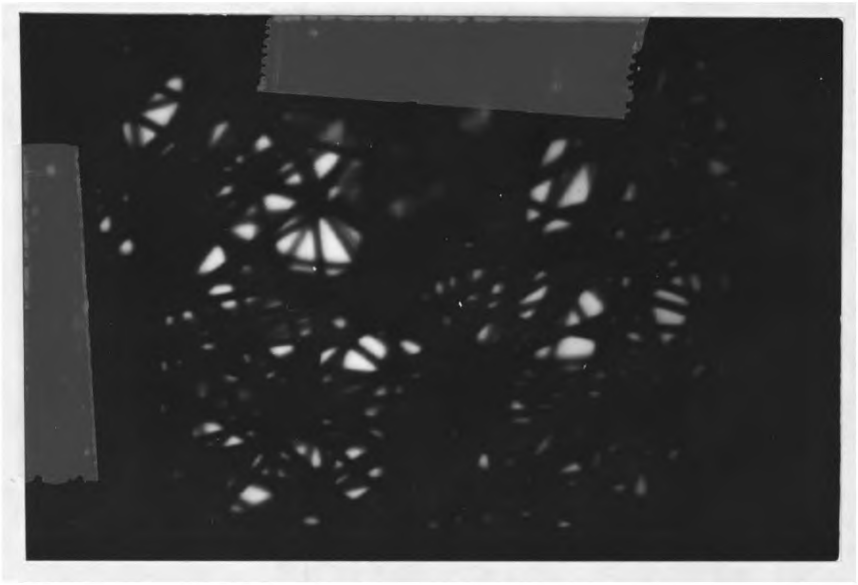

Fig5-6 An Image of a Nonwoven Fabric Sample.
(Meltblown, 60g/m^2, Transmitted Illumination)

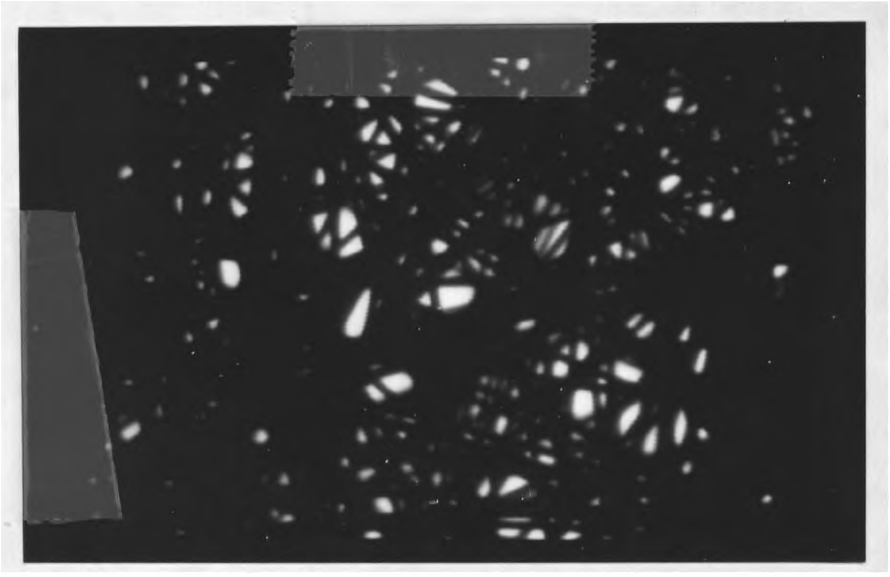

Fig5-7 An Image of a Nonwoven Fabric Sample.
(Meltblown, 80g/m^2, Transmitted Illumination)

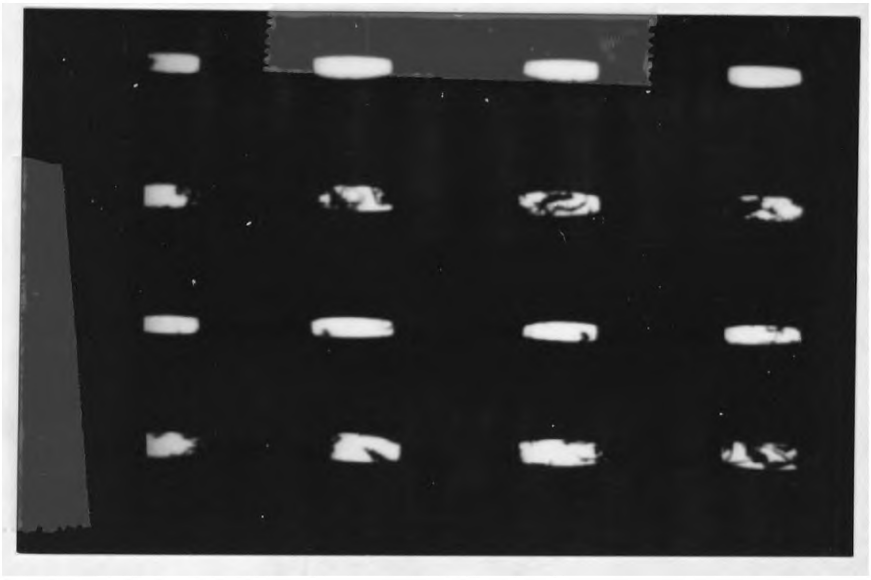

Fig5-8 An Image of a Woven Fabric Sample.
(GTF400E, Transmitted Illumination)

should also be sufficiently large so that reasonable statistical reliance can be placed on the combined results of a small number of measurements or even on the result of a single measurement. The highest magnification rate, marked as scale 13 on the microscope, was chosen for the analysing of the two nonwoven fabrics and a smaller magnification rate, marked as scale 6, was found more suitable for the woven fabric. The total objective area of a single measurement at these two magnification rates are 1.24mm by 1.86mm and 3.45mm by 5.17mm respectively.

Ten measurements were taken for each of the two nonwoven fabrics and five measurements were taken for the woven fabric. The results are presented in Tables 5-2 to 5-4. Each row shows the total number of measurements taken, the total number of pores and the values of D_{max}, D_{∞} and D_{50} after that number of measurements. By the third row of Table5-2, it is shown that 3 measurements had been taken and a total of 369 pores had been detected. The final values of D_{max}, D_{∞} and D_{50} after 3 measurements were 65u, 35u and 21u respectively. Because the ith row (i>1) was obtained by adding one more measurement, the ith measurement, to the (i-1)th row, the total number of pores detected in the ith measurement can be calculated by subtracting the total number of pores shown in the (i-1)th row from that shown in the ith row. In Table5-2, for example, the total number of pores detected in the first measurement was 179, the total number of pores detected in the second

N_m	N_t	$D_{max}(u)$	$D_{90}(u)$	$D_{50}(u)$	i	N_i
1	179	58	37	20	1	179
2	285	65	35	22	2	106
3	369	65	35	21	3	84
4	510	94	35	21	4	141
5	613	94	35	21	5	103
6	755	94	36	22	6	142
7	854	94	35	21	7	99
8	961	94	35	21	8	107
9	1051	94	35	21	9	90
10	1119	94	35	21	10	68

Denotations:

N_m = Total Number of Measurements;
N_t = Total Number of Pores after N_m Measurements;
N_i = Number of Pores in the ith Measurement;
D_{max} = Maximum Pore Diameter;
D_{90} > Diameters of 90% Pores;
D_{50} > Diameters of 50% Pores.

Table 5-2 Effects of the Total Number of Measurements on the Fabric Pore Size Information.

(Fabric: 60g/m^2 Meltblown;
Objective Field Size per Measurement: 1.24×1.86mm)

N_m	N_t	$D_{max}(u)$	$D_{90}(u)$	$D_{50}(u)$	i	N_i
1	44	43	35	16	1	44
2	95	58	37	18	2	51
3	196	58	35	18	3	101
4	229	58	36	18	4	33
5	316	58	35	18	5	87
6	449	58	36	19	6	133
7	544	58	37	19	7	95
8	643	58	36	19	8	99
9	728	58	36	19	9	85
10	822	58	36	19	10	94

Denotations:

N_m = Total Number of Measurements;
N_t = Total Number of Pores after N_m Measurements;
N_i = Number of Pores in the ith Measurement;
D_{max} = Maximum Pore Diameter;
D_{90} > Diameters of 90% Pores;
D_{50} > Diameters of 50% Pores.

Table 5-3 Effects of the Total Number of Measurements on the Fabric Pore Size Information.

(Fabric: 80g/m^2 Meltblown;
Objective Field Size per Measurement: 1.24x1.86mm)

N_m	N_t	$D_{max}(u)$	$D_{90}(u)$	$D_{50}(u)$	i	N_i
1	23	222	208	164	1	23
2	45	222	205	151	2	21
3	64	222	206	161	3	19
4	85	222	203	160	4	21
5	103	222	206	161	5	18

Denotations:

N_m = Total Number of Measurements;
N_t = Total Number of Pores after N_m Measurements;
N_i = Number of Pores in the ith Measurement;
D_{max} = Maximum Pore Diameter;
D_{90} > Diameters of 90% Pores;
D_{50} > Diameters of 50% Pores.

Table 5-4 Effects of the Total Number of Measurements on the Fabric Pore Size Information.

(Fabric: GTF400E, Woven;
Objective Field Size per Measurement: 3.45×5.17mm)

measurement was 285-179 = 106, and so on. These values have been calculated and shown in the tables. The final pore size distribution curves for the three fabrics are presented in Fig5-9. For the two nonwoven fabrics, the distribution curves represent the results after ten measurements and for the woven fabric, the curve represents the result after five measurements.

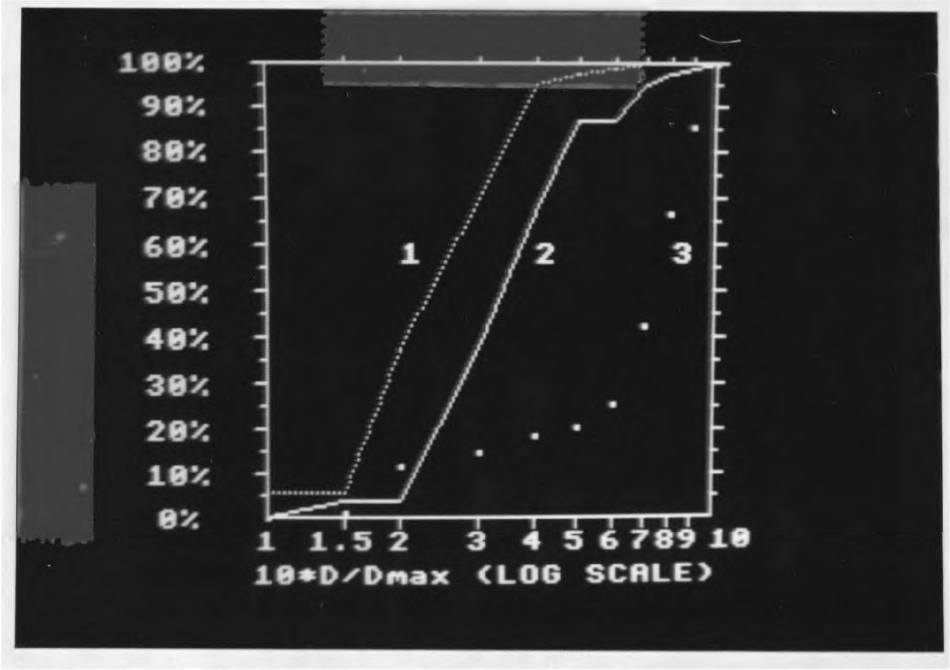

Fig5-9 Comparisons between the Pore Size Distributions of Three Fabric Samples (Pore Size = Thickness).

1..... Meltblown (60g/m^2);
2..... Meltblown (80g/m^2);
3..... Woven (GTF400E).

It is clear from these results that a total number of less than 10 measurements is sufficient to obtain a result with good statistical reliance. In fact, it appears from all the three sets of results that a single measurement may be enough to indicate the pore size property of a fabric. Only the values of D_{max} show substantial variations as the number of measurements increases whilst D_{90} and D_{50} are very stable. However, this does not suggest the fabrics all have a uniform structure as the number of pores detected in different areas of the two nonwoven fabrics differ considerably.

Despite their difference in basic weight, the D_{90} and D_{50} values of the two nonwoven fabrics are surprisingly similar and their pore size distribution curves are almost parallel to each other. These facts are attributed to the structure similarity of the two nonwoven fabrics. Although the thinner fabric has a larger D_{max}, its thinness is more characteristically indicated by a greater average number of pores detected per measurement. This demonstrates that specific opening area is also an important fabric structure property.

As expected, the woven fabric has a much steeper pore size distribution curve and has a similar number of pores detected in different areas of the fabric, which display the fact that woven fabrics have relatively regular mesh openings evenly distributed over the surface of the fabric.

5.5.3 Comparisons Between Image Analysing and Sieving Techniques

Experimental comparisons between the image analysing method and the conventional sieving method have not been carried out. However, because there are fundamental differences between them, compatibility between the pore size information obtained through these methods can not always be expected.

In the image analysing method light is used as a medium which travels straight whilst in the sieving method glass balls are used which can travel along curved passages. The thicker and more porous the fabric, the more these curved passages and the less applicable the image analysing method. Considering a thick fabric that is opaque, if it is porous enough particles like glass balls will still be able to pass through. In fact an estimation made by Wittmann[19] showed that the increase of fabric thickness only causes slight decrease in fabric apparent opening sizes if the fabric porosity is kept constant. Therefore the surface image analysing method will only be applicable to thin and/or compacted fabrics. For thick and porous fabrics a cross sectional analysing method like that developed by Rollin et al will be more appropriate. It is interesting to notice that cross sectional analysis is better

suited to thick fabrics, as pointed out by Rollin[17] and surface analysis and cross sectional analysis seem to be complementary of each other.

Another difference between the image analysing method and the sieving method is that smaller glass balls will pass through larger pores in the sieving method while each pore is only counted once in the image analysing method. Thus when measured by the sieving technique the relative frequencies of smaller sized pores will appear to be higher than they actually are and the lower part of the pore size distribution curve is expected to be steeper than that obtained by the image analysing method. For the same reason it will be very difficult to apply the sieving method to fabrics with large range of pore sizes and those pores smaller than 1/4 of the maximum pore can not be measured effectively. This can be clearly seen from almost all pore size distribution curves measured by sieving method for nonwoven fabrics. Although those relatively very small pores may be unimportant to their geotextile application[20], a large range of pore sizes should be characteristic to most nonwoven fabrics.

5.6 SUMMARY

Three pore size definitions have been considered: area, hydrodynamic diameter and thickness. The measuring algorithms of pore sizes in terms of these definitions have been described. Which of these three definition should be used in a practical application will depend on the actual requirements of that application. For filtration and separation applications, thickness is the most applicable definition. The hydrodynamic definition is more suited to applications where fabric permeability is important, such as in drainage systems.

The surface image analysing method is only applicable to thin and compacted fabrics. Cross sectional analysing techniques are necessary to assess the characteristics of openings in thick and porous structures.

Although the objective area of one measurement is very limited, several measurements randomly taken at different areas of a fabric should provide the pore size distribution property of the fabric with sufficient reliance. A quick assessment of the pore size distribution property of a fabric can be achieved by a single measurement. Testing results demonstrated that similar fabric structures have characteristically similar pore size distribution curves. The

specific opening area has been proven an important fabric structure parameter. The ability to measure this parameter is an additional advantage of image analysing techniques to their overwhelming speed and economic advantages compared with the conventional sieving techniques.

PART III FIBRE ORIENTATION DISTRIBUTION

CHAPTER 6 REVIEW OF LITERATURE

6.1 Mechanical Properties of Nonwovens

There has been intensive research into the mechanical properties of nonwoven fabrics. One of the main intentions has been to predict the mechanical properties of nonwoven structures by relating it to some variables which can be controlled during the manufacturing process. It is believed that this will enable the production of a fabric with desired physical properties by arranging processes and materials accordingly.

As early as in 1960, a fibre web theory was adopted by Petterson[21],[22] to predict the stress-strain behaviour of nonwovens. The theory assumes: (i), all the fibres lie straight between bonded points; (ii), the bonding strength exceeds the fibre rupture strength; and (iii), the fabric is uniform from point to point. So the s-s behaviour of the fabric is a function of two parameters, the fibre orientation

distribution and the fibre s-s curve. Good agreement was observed between the theoretically predicted and experimentally obtained s-s behaviour of a short straight-fibre, wet-laid nonwoven fabric. To apply this theory to a more common nonwoven fabric is difficult since the fibre segments between bonds are generally not straight and the bonding strength is not necessarily stronger than fibre rupture strength.

Stevenson[23] then modified the fibre web theory by introducing a fibre curl parameter. The s-s curve of a binder bonded web structure consequently become a function of four parameters. In addition to the fibre orientation distribution and the fibre s-s curve, two more parameters were involved: the fibre curl factor and the Poisson's ratio of the web. His study of three nonwoven fabrics made of different web types clearly indicated the noticeable effect of the fibre curl on the s-s property of a nonwoven fabric.

The fibre web theory is based on force analysis within a network structure. A far better method was developed by Newton[24] who analysed the energy changes within a network under deformation. The energy method is more flexible and useful because it allows the insertion of additional parameters and requires less knowledge of the way a fabric deforms under stress. Thus it was possible to dispense with smaller assumptions made in force analysis. The major

assumptions made in the energy method were similar to those made in the force analysing method. Fabric was regarded as being made up of two dimensional sheets and the network was considered to be continuous; fibre segments were thought to be linked together by unbreakable rigid bonds; the deformation of the network was assumed to be affine. The fundamental concept in the energy theory is to calculate the fabric stress by equating the total energy taken up by the fabric to the summation of energy stored up in individual fibres. The final function for calculating fabric stress under a given strain was similar to that derived through force analysis.

Ozsanlav[25] later replaced the assumption of unbreakable rigid bonds with a more realistic assumption of deformable bonds. Binders were assumed to be concentrated at fibre crossing points and each bond was assumed to be linking the same number of fibre segments which were equal in length. After these amendments he applied the energy theory to several nonwoven fabrics and confirmed that both fibre and binder components in a fabric contributed to the deformation of the fabric. He also found that the failure of adhesive bonded nonwoven fabrics was caused by the rupture of the binder component.

The energy method was also found applicable to networks composed of filaments by Chun Kwok Wai[26] in a study into the mechanical behaviour of spun-bonded fabrics. Good agreement

between theoretically predicted and experimentally measured fabric s-s curves was observed among fabrics with strong bonds, and the best agreement was found when a fabric reached its maximum rupture strength by having adequate binder content. This was attributed to the exclusion of the effect of binders in the theory used in his study.

More recently computer simulation techniques were used by several researchers to study the mechanical properties of nonwoven fabrics.

Britton and Sampson[27],[28],[29] simulated the mechanical properties of nonwoven fabrics with a model consisting a collection of straight lines of uniform length. These lines were randomly laid down with respect to position and orientation. Of all the intersections of these lines, a predetermined fraction were assumed to be bonds. These bonds have a strength distribution determined according to that of the fabric being modelled. This model was interpreted as an analog of a randomly laid, area-bonded (as opposite to print bonded) nonwoven fabric composing of straight stable fibres. They studied this model by applying a sequence of small displacements to it to simulate the deformation of a fabric under the same strain. The new position of each bond was decided by relaxing the displaced fabric to its strained equilibrium configuration. Since the random distribution of bonds caused some bonds to occur in clusters, a cluster

analysis method was used in the relaxation process. The comparison between the s-s properties of the model fabric and that of a real fabric was not carried out, nevertheless the feasibility of predicting mechanical properties of nonwoven fabrics by computer modelling was clearly demonstrated.

Another computer model was described by Grimdstaff and Hansen[30]. In their model bonds were arranged in a row and column pattern to simulate a print-bonded fabric. A random number of fibres were then distributed in 8 directions from each bond. The fibres were bonded at both ends and were not allowed to bypass bonds. Parameters such as bond layout, fabric density, fibre orientation and curl, fibre and binder tensile properties were included in the model. These parameters were adjusted to model a real fabric. The model fabric was extended in predetermined steps to the desired elongation and the alignments of bonds in the direction perpendicular to that of extension were not changed. This latter point implied the web elongation was assumed to be uniform over the entire sample length (or width when the extension was applied in the cross direction of the sample). They compared the measured s-s curves of four real fabrics with those obtained from their corresponding computer model. The experimental s-s curve and the computed s-s curve showed good agreement for two of the four modelled fabrics.

Other important physical properties such as flexibility which

was a dominant factor in determining the hand of a fabric[31] also attracted wide attentions. One example was Sengupata[32] who investigated the bending flexibility of adhesive bonded nonwoven fabrics and examined the effect of fibre orientation on the bending anisotropy. It was shown in his work that the more the fibre lying in a direction, the greater the flexural rigidity of the fabric in the corresponding direction.

6.2 Measurement of Fibre Orientation Distribution

It has been clearly shown in the preceding section that the fibre orientation distribution in a web plays a crucial role in determining the physical behaviour of the fabric and it is necessary to obtain an accurate measure of the fibre orientation in the web in any quantitative analysis of the anisotropic properties of nonwovens. This measurement has to the present time been limited to a simple direct method.

Stevenson[23] measured the angle of fibres individually on a projection microscope. This method was later extended by others[24],[25],[26] using a Scanning Electron Microscope (SEM) to make the measurement easier. Grimdstaff and Hansen[30] also estimated the fibre orientation information from microscopical photographs of the fabric being modelled.

The tediousness of these manual methods has stimulated continuous efforts of many people to find a more efficient method.

Stevenson[23] suggested that the fibre orientation in a given direction must be accompanied by a fairly high molecular orientation in the same direction, hence it might be possible to obtain the fibre orientation distribution from the directional phenomena of dichroism and birefringence. Before turning back to direct visual measurement he tried a method based on the above theory, but little was achieved.

Chaudhray[33] and Judge[34] made investigations on a "liquid drop method". The principle of this method is that the migration rate in each direction of a network system depends on the relative geometrical characteristic of each capillary system within the network and the capillary system in a nonwoven web structure mainly depends on the fibre orientation. It is therefore possible to obtain the fibre orientation distribution by analysing the shape and dimension of the migration after applying a drop of an appropriate liquid to the fabric sample. In practice, however, their work succeeded only in showing the structure pattern of the web. Quantitative analysis failed because the final shape and dimension of migration were affected not only by the fibre orientation but also by liquid type, binder content and fibre type.

Judge[34] also investigated an optical method based on the principle described earlier by Orchard[35]. The principle can be stated as following: the direction of the light reflected by a single fibre depends upon the angle between the fibre axis and the incident beam. If a web is illuminated with a parallel beam of light then only those fibres which are perpendicular to the plane of incidence on the web will reflect the light in a direction perpendicular to their axes. Here the plane of incidence on the web is defined as the plane containing the direction of a single ray and the web normal. Thus the total intensity of the light reflected in a direction will be proportional to the total length of fibres perpendicular to the plane of incidence. The same discussion applies to refracted light. An apparatus was constructed according to the above principle to detect the refracted light. The apparatus was used by Orchard to measure the fibre orientation information of samples of wool, cotton and viscous rayon webs, but the results were only qualitatively reasonable. Judge detected the reflected light, and obtained the same conclusion: only qualitative analysis was possible.

Chudleigh[36] recently studied the formation of fibre images by single fibres and fibre assemblies. It was shown in his study that selected features of the image, such as fibre boundaries, fibre orientation and fibre colour, can be enhanced or suppressed by suitable masking of the light

source. He suggested that this optical processing technique can be used in conjunction with image processing methods to measure fibre dimensional properties and fibre orientation information.

In the following chapters an automatic method of measuring fibre orientation distribution within nonwoven webs using image processing techniques will be presented. The raw image is simplified successively by image segmentation, noise reduction and a series of thinning operations. Fibres are finally reduced to thin curves which have a single point cross section. The computer then automatically traces along these curves, measures their angles and lengths and finally produces the fibre orientation distribution information of the fabric being analysed.

CHAPTER 7 LINE OPERATOR

7.1 INTRODUCTION

As in the achievement of automatic measurement of pore sizes, image segmentation has to be the first step in achieving the automatic measurement of fibre orientation. However, the solution to the segmentation problem for the measurement of fibre orientation is more difficult. Pores in a fabric are always separated by fibres but fibres can be in close contact with each other. In the extreme, no fibres will be distinguishable in an image formed from a thick fabric under transmitted illumination. Using reflected illumination, it is possible to focus only at the surface layer of a thick fabric. However, images obtained in this way generally have very low signal-to-noise ratios due to such causes as:

(a), the local variation of illumination;

(b), the variation of optical properties along a

single fibre;

(c), the high noise level caused by those out-of-focused fibres.

Fig7-1 shows a digitized image of a fabric. The image was digitized from a photograph taken by Sengupta[32] on the Scanning Electron Microscope (SEM). The clear object-background distinction which appeared in images obtained through transmitted illumination (see Figures 5-6 to 5-8) does not exist in images such as Fig7-1. Consequently, the simple grey level thresholding algorithm used to segment images for the measurement of pore sizes does not offer satisfactory segmentation results here (Fig7-2), and a more elaborated algorithm, the line operator developed by Dixon[37], has been used.

Fig7-1 Digitized Image of a Fabric Sample.

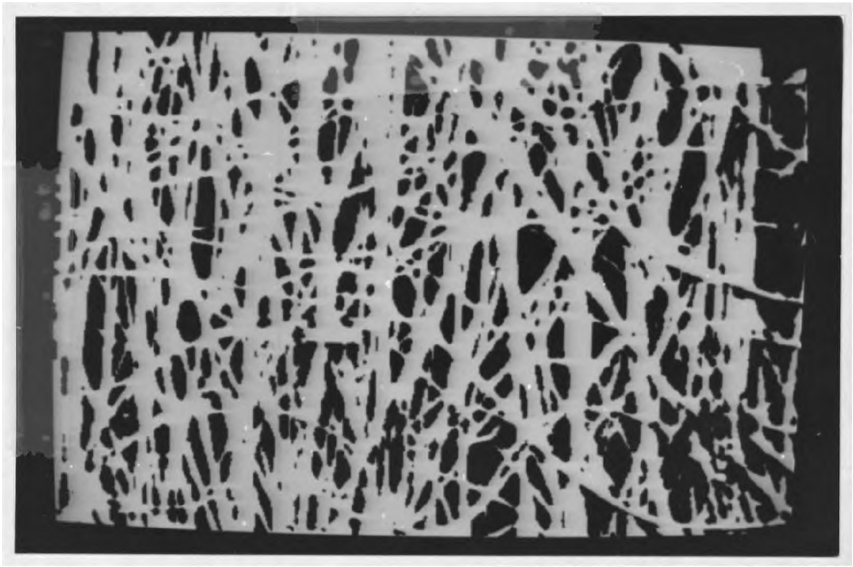

Fig7-2 Segmented Image of Fig7-1 by Thresholding.

7.2 Definition

Although the low signal-to-noise ratio makes the point based grey level thresholding unworkable, the visibility of fibres within an image suggests that contextual information could be used to reduce the effects of noise. This concept is the fundamental principle of the line operator which utilizes the linear spatial correlation of grey levels along a fibre.

Since the direction of a line is initially unknown, the first step of the line operator will be to find the possible direction of the line. This is achieved by computing the mean grey levels along vectors at a number of orientations about a point. It is reasonable to take the orientation of the vector with highest mean (for whiter lines on darker background) as the direction of the line. A measure of local line contrast can then be found by taking the difference between this mean and the mean of the surrounding region. At points in the background the mean grey level of the selected vector should approximate the local regional grey level. Therefore, signals from lines should be preferentially enhanced over background noises.

After comparing different sizes of the surrounding region in which the local mean is computed, it was found by Dixon that a 5 by 5 neighbourhood gave the best speed/performance compromises. Fig7-3 shows the two region sampling elements together with the 8 corresponding vectors. The diagonal region sampling element in Fig7-3 was used to compute the region mean for diagonal vectors (vector 2 and vector 6).

To define the line operator "O", let L_i be the mean grey level of the vector i, R_s and R_d be the mean grey level of the square and diagonal regions respectively, then

$$O = L_j - R \quad \cdots\cdots (7\text{-}1),$$

where

$$L_j = \mathrm{Max}(L_i), \qquad i \in [0, 7];$$

$$R = \begin{cases} R_s & \text{if } j \neq 2, 6, \\ R_d & \text{if } j = 2, 6. \end{cases}$$

Function 7-1 is for positive contrast lines. When dealing with negative contrasted images where lines are darker than background the minimum L_i will have to be sought instead of the maximum L_i and taking the difference $R-L_j$ will then provide a similar function. Alternatively, the image contrast may be reversed before applying the operation. Contrast

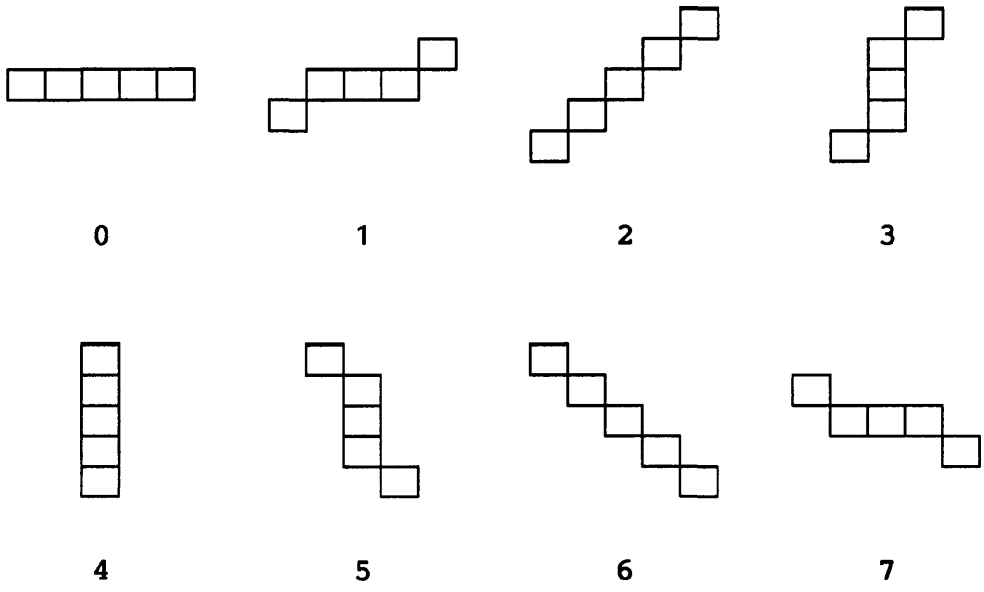

(a) Line Sampling Elements (Vectors);

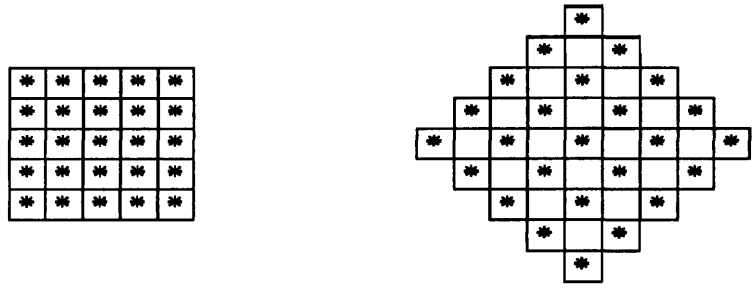

(b) Region Sampling Elements.

Fig7-3 The Line Operator[37].

reversing is simply achieved by replacing the grey level at every pixel with the difference between the maximum grey level and the original grey level at that pixel.

Comparisons between the line operator and other local operators such as "Chen Gradient" and "Roberts Gradient" which are for extracting edges of objects in a grey level image was made by Dixon. The line operator was found to have a better performance in segmenting line objects.

7.3 Discussion

As is shown in Fig7-3, in the initial definition of the line operator there are two region sampling elements, square and diagonal, for the computation of local contrasts of non-diagonal and diagonal vectors respectively. However, it has been found that operating with the diagonal region sampling element for all vectors gives a segmenting result with much lower noise level. Fig7-4 shows the binary image after applying the original line operator to Fig7-1. Fig7-5 is the result of operating with the diagonal region sampling element for all vectors. The performance improvement of the modified line operator over the original line operator is clearly demonstrated by Fig7-4 and Fig7-5. The most possible

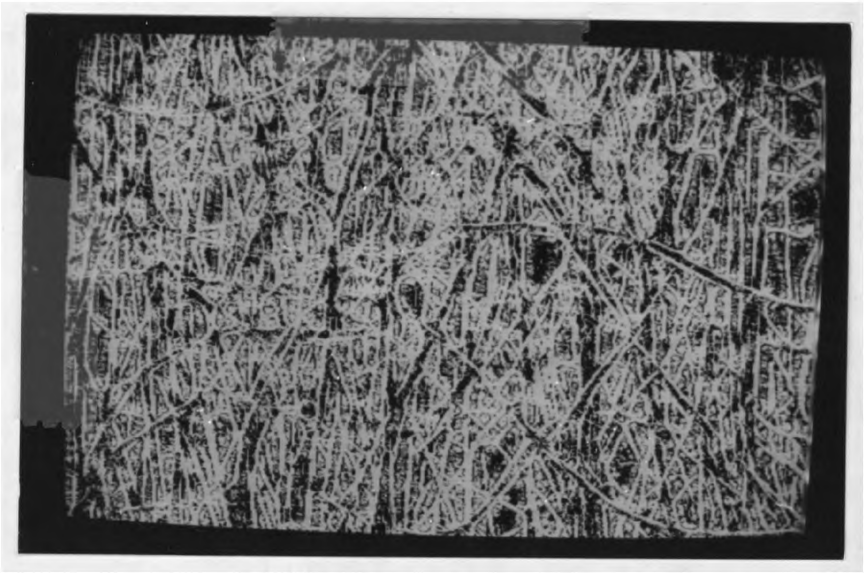

Fig7-4 Segmented Image of Fig7-1 by the Original Line Operator.

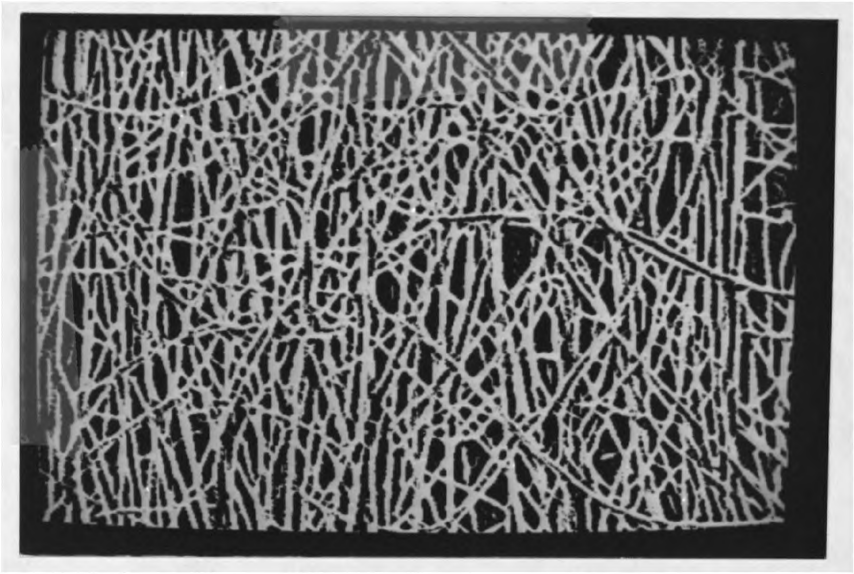

Fig7-5 Segmented Image of Fig7-1 by the Modified Line Operator.

explanation of this phenomenon is that the diagonal region sampling element has a larger area coverage. A simplified case shown in Fig7-6 illustrates this point.

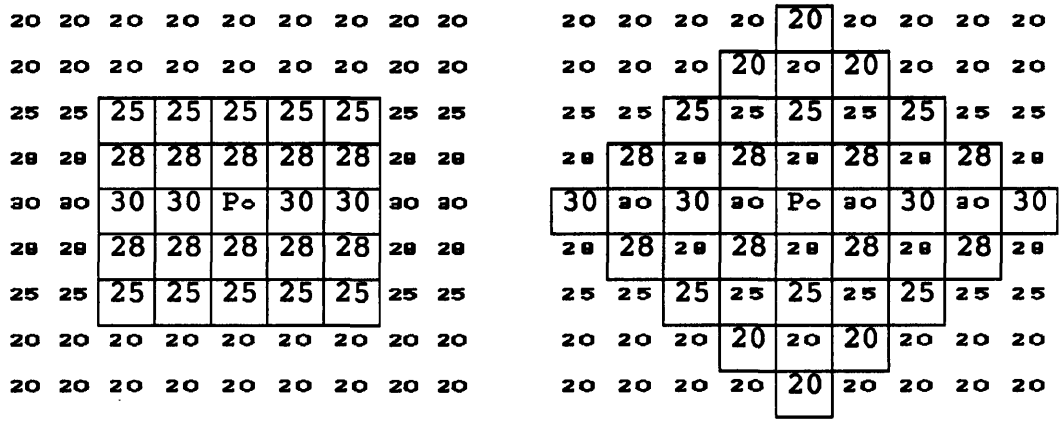

(a) Square (b) Diagonal

Fig7-6 Comparison Between the Two Region Sampling Elements

In Fig7-6, a fibre lies horizontally across the image and the background has an intensity of grey level 20. The brightness of the fibre deceases from centre to its edges. The centre of the fibre has the highest grey level value of 30. Assuming the operator is currently operating at point P_o, then vector 0

which coincides with the axis of the fibre has the highest mean grey level of 30, or $L_o = 30$. The mean of the square region sampling element is

$$R_s = (25x10+28x10+30x5)/25 = 27.2$$

and the mean of the diagonal region sampling element is

$$R_d = (20x6+25x6+28x8+30x5)/25 = 25.76.$$

Then according to Equation 7-1,

$$O = L_o - R_s = 30-27.2 = 2.8.$$

However, if R_d is used instead of R_s then

$$O = L_o - R_d = 30-25.76 = 4.24.$$

A higher response is obtained in the latter case.

A further advantage of using only one region sampling element is that the implementation of the line operator can be reduced to the computation of the same regional mean for all vectors and it is no longer necessary to choose a different region sampling element for different vectors.

It appears from the above discussion that a bigger region

sampling element will give a better performance. But this is only true if the execution time is not important and the increase of local noise level, such as the variation in optical property, associated with the increase of the region sampling element does not reduce the local contrast at the same rate. More specifically, a 7 by 7 neighbourhood will involve 49 pixels in the computation of its mean while a 5 by 5 region only involves approximately half that number of pixels (25 pixels). The diagonal region of 5 by 5 pixels, however, covers approximately the same area as a 7 by 7 square region does [$(5\sqrt{2})^2 = 50 \simeq 7^2 = 49$] while the number of pixels involved is kept at 25. Also, if the region sampling element is too large, two or more fibres may simultaneously be present within the region. This signal interference will cause a reduction of signal-to-noise ratio and may eventually lead to the failure of the operator. On the other hand, if the region sampling element is too small it may be contained within a fibre. When this happens the local contrast detected will be similar to that when the region sampling element is within the background and the line operator will thus become an edge detector and will only respond at edges of fibres.

Therefore, the fibre width in an image, which is dependent on the objective fibre width and the magnification rate selected, is a crucial factor in choosing a suitable size of region sampling element. It is however very difficult to obtain a precise correlation between the image width of fibres and the

suitable size of the region sampling element because the grey level across the width of a fibre varies. The centre part of a fibre is generally brighter than the edges of the fibre, thus even if the region sampling element is formally contained within the fibre the line operator may still be able to give a positive response at the center of the fibre. It is also realized from this point that the width of a fibre in the segmented image does not reliably represent the original fibre width. Fortunately, fibre width is not concerned in the measurement of fibre orientation which only takes into account the length and orientation of fibre segments.

The size of the region sampling element needs to be increased only if the average fibre width becomes so large that when the region sampling element falls within a fibre, grey levels within the region sampling element become relatively constant in all directions. There are two alternatives to the increase of the region sampling element size when the fibres are too thick. One alternative is to reduce the fibre width in the image by shrinking the image by an appropriate factor. Another alternative is to use the line operator as an edge detector and providing all fibres have a similar width, all fibres will be split into two parallel parts. This causes no undesirable effect on the final measurement except doubling the measuring time.

For the present application, satisfactory image segmentation

has been achieved by the 5 by 5 line operator with a diagonal region sampling element.

7.4 Summary

Grey level thresholding is inadequate for segmenting images in the measurement of fibre orientation distribution and a line operator that utilizes the linear spatial correlation of grey levels along a fibre and that operates locally in a 5 by 5 neighbourhood surrounding a pixel has been used. In the original definition, two region sampling elements, one square and one diagonal, were used for different line sampling elements. It has been found, however, that using the diagonal region sampling element for all the line sampling elements not only simplifies the algorithm, but also greatly improves the performance of the operator.

CHAPTER 8 ORIENTATION MEASUREMENT

8.1 INTRODUCTION

After segmentation, the raw grey level image is reduced to a binary image. Fibres are represented by line objects of the same grey level against a unified black background. But it is still difficult to measure the orientation of fibres at this stage because the fibre width varies from place to place. Further simplification of the image is necessary.

The first approach attempted was edge extraction. The large length-to-width ratio of fibres suggested that the orientation and length of fibre edge lines be used as substitutes of those of fibres. In practice this approach was found only appropriate for an image that satisfies the following two conditions:

(a) The width of all fibres in the image is not less than three pixels. This ensures that two approximately parallel and detached edge lines may be extracted for every fibre so that the length of

fibre may be obtained by halving the final measurement.

(b) The total number of fibres in the image is small so that fibre crossings do not seriously reduce the effective length-to-width ratio of fibres. The effective fibre length-to-width ratio is defined as the ratio of fibre segment length between two crossing points to the fibre width. When the number of fibres increases, the distance between fibre crossing points decreases and the edge lines of fibres tend to form an increasing number of smaller closed curves. These small closed curves represent pores rather than fibres.

The extraction of object edge lines in a binary image is a simple task, but the two conditions discussed above were found to be too strict for the images analysed.

Fibre centre lines are ideal representatives of fibres, but direct searching of fibre center lines is difficult because of the variation of fibre cross section, the unknown state of fibre orientation and the frequent occurrence of fibre crossings. An indirect approach to center line extraction has subsequently been adopted. This is the thinning algorithm to be discussed in 8.3. A noise filtering operation is applied to images prior to thinning and it is described first.

8.2 Edge Smoothing

The shrinking and expanding noise filtering method used in the measurement of pore sizes treats thin lines as noise and deletes them. This is an undesirable feature for the measurement of fibre orientation as thin objects become the primary interest. A new edge smoothing algorithm has been implemented which clears isolated points, deletes pinholes, smooths object edges, but preserves thin lines.

Fig8-1 shows the 4 basic templates used. There are a total of 16 templates, 8 in each group. But the other 12 are readily obtained by rotating the 4 basic templates 90° successively. In the operation, every pixel is checked first to see whether it is an object pixel or a background pixel. For an object pixel, its surrounding 3 by 3 neighbourhood is compared with the 8 templates in group A in succession. If a match is found this pixel is deleted; otherwise it is unchanged. For a background pixel, its surrounding 3 by 3 neighbourhood is compared with the 8 templates in group B. If a match is found this pixel is converted into an object pixel; otherwise it is left unchanged. It is obvious that pixels lying within thin lines do not have a neighbourhood that matches any of the 16 templates shown in Fig8-1 and therefore will not be affected

0	1	1
0	1	1
0	0	0

(a)

1	1	1
0	1	0
0	0	0

(b)

Group A

1	0	0
1	0	0
1	1	1

(c)

0	0	0
1	0	1
1	1	1

(d)

Group B

Fig8-1 Edge Smoothing Templates

by the operation. The image shown in Fig8-2 is obtained from Fig7-5 by applying the above operation. The edges of objects are visibly smoother and there is also a clear reduction of other types of noise such as isolated points.

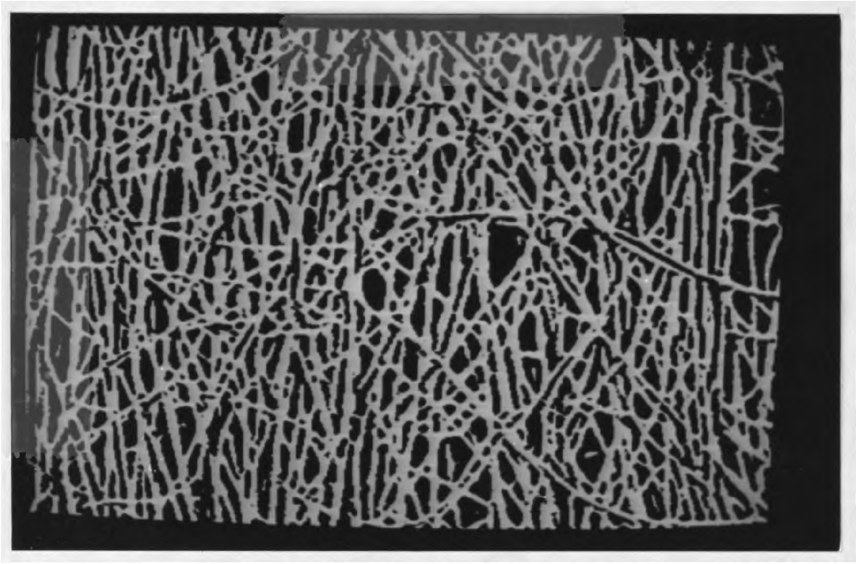

Fig8-2 Smoothed Image of Fig7-5 by Template Matching.

8.3 Thinning

Thinning is an irreversible operation that seeks to reduce a region to minimal cross sectional width[2]. A conventional thinning operation removes from the image edge pixels on one side of an object repeatedly, north, south, west and east in turn, providing the removal of these edge pixels does not affect the image connectivity. To preserve the length information of objects, 4-connective end pixels should also be kept. A 4-connective end pixel is one that has only one 4-connected neighbour, such as the centre pixel in Fig8-3.

0	0	0
0	1	0
0	1	1

Fig8-3 An Arc End Pixel in 4-Connectivity
(Centre Pixel)

Skeletonizing an image by the conventional thinning operation is a slow process because it only removes edge points on one side of an object in one operation. A more serious drawback of the conventional thinning operation is that it often produces spiky skeletons, especially when objects have many end points or when end points arise prematurely in the course of the thinning process. These spiky skeletons are prone to cause erroneous length and orientation information about the original objects. This point is illustrated in Fig8-4.

To overcome the above problems in the conventional thinning operation, a new vector-thinning algorithm has been developed. Edge pixels on all sides of an object are removed in a single operation and most spike branches are broken off from the main skeletons. The operation is completed in two stages. In the first stage objects are thinned to figures whose cross sections are not more than two pixels. These figures are then skeletonized in the second stage.

In Fig8-5a, the eight neighbours of pixel P_o are divided into four groups (or four vectors). The operation is applied to object pixels only. That means the centre pixel of a vector, P_o, is always an object pixel and the following discussion will be focused ONLY on the OTHER TWO COMPONENT PIXELS of the vector. The value of a vector is defined as ZERO if its other two component pixels belong to the same subregion, object or background. To differentiate a zero vector with two object

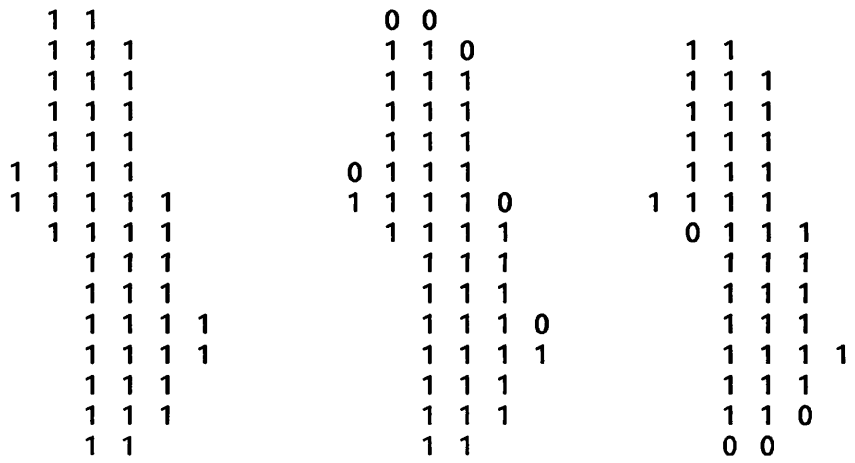

(a) An Object; (b) Thinning from North; (c) from South;

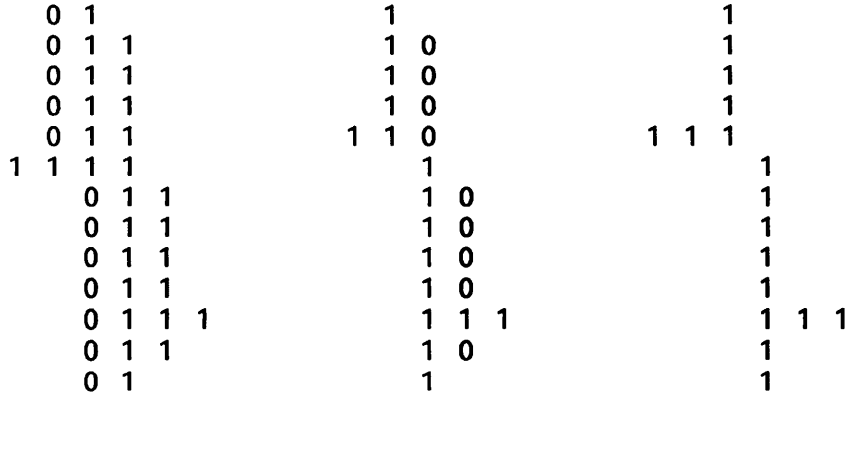

(d) from West; (e) from East; (f) the Final Skeleton.

Fig8-4 The Noise Sensitivity of Conventional Thinning.

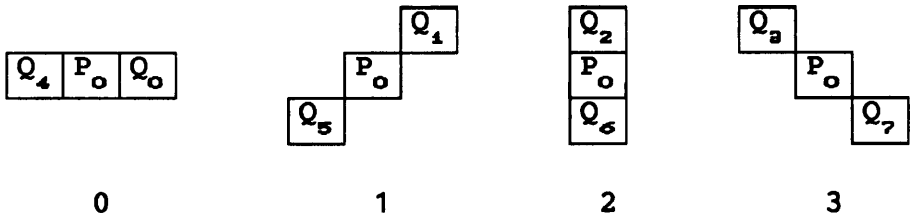

(a) Dynamically Defined Thinning Vectors;

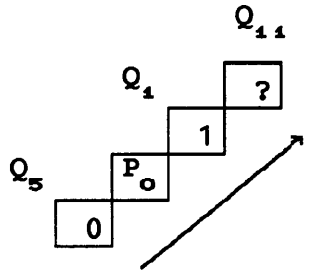

(b) A Non-Zero Vector;

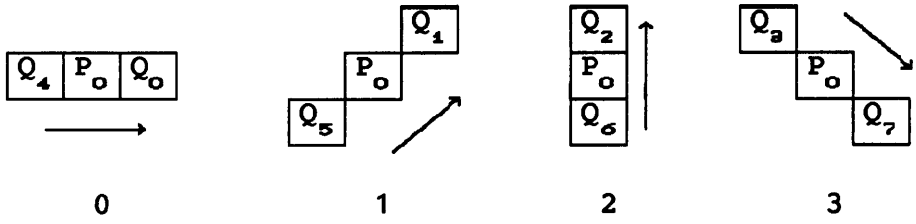

(c) Predefined Thinning Vectors.

Fig8-5 A New Vector-Thinning Algorithm.

pixels (the centre pixel is not considered) from a zero vector with two background pixels, they are denoted by O and B respectively. The value of a vector is defined as 1 if its other two component pixels belong to different subregions, one object and the other background. The direction of a non-zero vector is defined as pointing from the background pixel to the object pixel. Fig8-5b shows an example.

In the first stage of the operation these vectors are tested against the following three combinations of status:

(a). Some vectors are B-zero;

(b). All vectors are O-zero;

(c). Some vectors are non-zero, but no B-zero vectors.

In case (a), the cross section of the object at P_o is only one point thick in the direction (or directions) of the B-zero vector (or vectors) and therefore P_o must not be changed. In case (b), P_o is not an edge pixel which obviously should not be changed. The final case indicates an edge pixel but the object cross section width at P_o needs further checking before P_o can be deleted. This is accomplished by the examination of all those non-zero vectors.

Assuming vector 1 is non-zero (Fig8-5b), and Q_1 is an object

pixel. The pixel outside the 3 by 3 neighbourhood of P_o and located in front of vector 1, Q_{11}, is checked. If this pixel is an background pixel then the cross section of the object is two pixel thick. According to the operation rule, P_o should not be changed. If this pixel is an object pixel, the object is at least three pixels thick in this direction. The result is stored and another non-zero vector is examined in the same way. This procedure continues until all the non-zero vectors have been examined. If all the non-zero vectors indicate the object has a cross section of at least three pixels at P_o, P_o will be deleted under a further condition that its deletion does not destroy the connectivity of the image. However, since the operation is carried out in parallel, two connected pixels may be deleted in one operation. Although the deletion of any one of them preserves the connectivity of the image, it is under the condition that no change incurs to the other pixel. Therefore when both of the pixels are deleted the connectivity of the image may be destroyed. This connectivity breakdown is most likely to occur at places where the thickness of an object undergoes a sharp change, such as where a thin spiky branch joins the thick main branch of an object. It is by this mechanism that spiky branches are broken off from the main skeletons. This is shown in Fig8-6 where the original object is the same as in Fig8-4. It is also because of this operational parallelism that the operation has to be carried out in two stages to preserve the connectivity of the majority of the main branches.

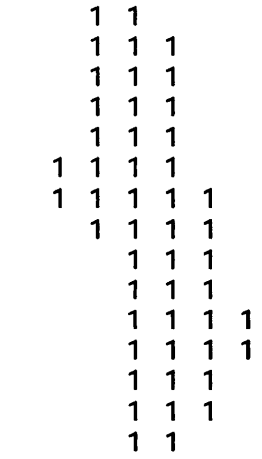

(a)

An Object;

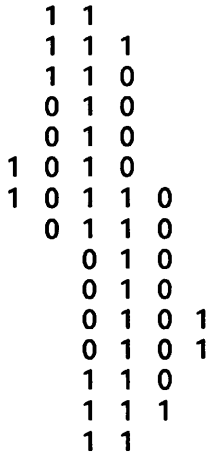

(b)

First Stage Thinning;

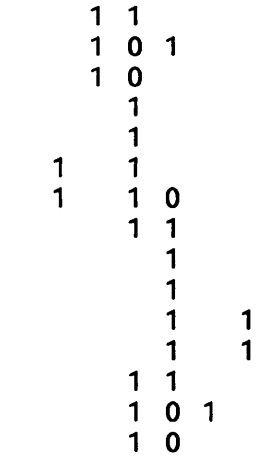

(c)

Second Stage Thinning;

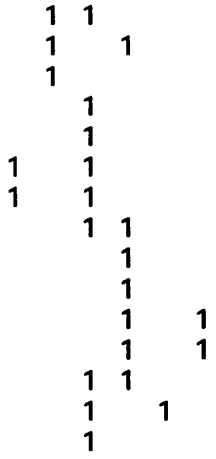

(d)

The Final Skeloton.

Fig8-6 Connectivity Breakdown by the New Vector-Thinning Algorithm.

(the Object Is the Same As in Fig8-4)

The first stage operation may need to be applied to the image several times to reduce the cross sections of all objects to 2 pixels or less. The actual number of operations required depends on the maximum original width of objects within the image. A minimum of four such operations has been found necessary for images obtained from microphotographs such as that shown in Fig8-2.

In the second stage, the directions of the four vectors are fixed (Fig8-5c). Since cross sections of all the figures in the image are not more than two pixels wide, all object pixels are edge pixels. In the case of some vectors being B-zero, pixel P_o is left unchanged. But if no B-zero vectors exist, a non-zero vector is checked. As at the first stage there may be more than one non-zero vector, but only one of them is checked in this stage and the checking order is from vector 3 to vector 1. That means if both vector 3 and vector 2 are non-zero vectors, only vector 3 will be checked and the checking is limited within the vector. If the front pixel of the vector is a background pixel, then P_o is deleted; otherwise, P_o is left unchanged. This operation is similar to thinning from south and east simultaneously by the conventional thinning operation. This second stage operation finally produces an image in which all figures are only one pixel in width. Fig8-7 shows the final result skeletonized by the above procedures from Fig8-2.

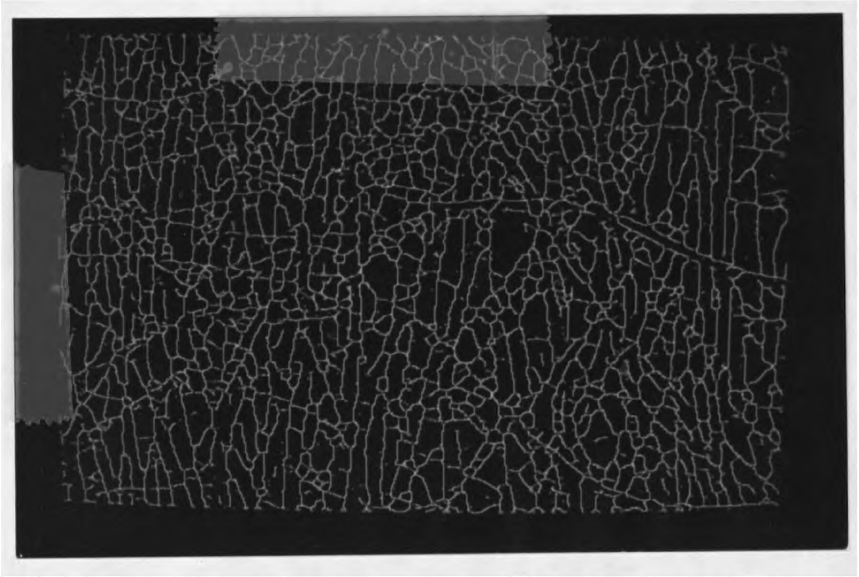

Fig8-7 Skeletonized Image of Fig8-2 by Vector-Thinning.

8.4 The Line Tracer

After thinning, fibres are represented by curves of one pixel cross sectional width. The measurement of fibre orientation distribution becomes the measurement of orientation distribution of these curves. A line tracer is programed to achieve this task. The line tracer traces along these curves and segments them into smaller almost straight parts according to two criteria to be described later. The lengths of these segments are computed and depending on their orientation, these curve segments are divided into 12 or 18 groups with an angular interval of 15° or 10° between -90° and 90°. The machine direction is at 0°. The relative frequency of fibres lying in an angular interval is obtained by summing up all the lengths of segments within the corresponding group and then computing the percentage of the sum in each group over the total length of all segments in the image. It is generally accepted that the mechanical properties of nonwoven fabrics at similar angles on either side of the machine direction do not have any noticeable variation, therefore the frequencies of the negative and positive groups of similar angles are averaged to obtain a histogram symmetric about 0° or the OY axis.

To start the curve tracing process the image is scanned from the upper-left corner to the lower-right corner in columns or in rows. The following discussion assumes that tracing is in columns. It is analogous to tracing in rows.

When an object pixel is found the scanning process is suspended. The coordinates of this pixel is stored for the resumption of the scanning process. Several tests are then made at this pixel. The first test checks whether this pixel is isolated. If it is an isolated pixel, it is deleted and scanning is resumed. If the result is negative, it is then tested as to whether this pixel is at the end of a 8-connective curve. An end pixel in 8-connectivity is a pixel that is connected to only one of its 8 neighbours. If the pixel is found to be an end pixel, tracing will start. TRACING IS DESCRIBED IN THE FOLLOWING PARAGRAPH. If the pixel is not an end pixel, which means it has more than 1 connected neighbours, an end pixel searching process is carried out. The end pixel searching process follows a curve in the same way as the tracing process except it does not segment and delete the curve being followed. It follows the curve until the end pixel of the curve is reached and the tracing process is then initiated from this end pixel. To avoid endless following when the image contains closed curves, the total angle change that has occurred during the searching process is checked. If this total angle change exceeds 540° in either clockwise or

counterclockwise direction, it is assumed that the curve has come to an end. The pixel at which the accumulated angle change reaches the 540° limit is taken as the end pixel of the curve. A total angle change of 360° may indicate a closed curve, but a curve may cause an angle change of 360° or more without being closed, such as a spiral. A 540° limit thus reduces, not eliminates, the possibility of mistaking an open ended curve as a closed curve. But a curve that turns around for one and a half circles without being closed should be rare in the images concerned.

The initial tracing direction is from the end pixel to its connected neighbour. In the case that an open ended curve has been mistaken as a closed curve in the end pixel searching process, the initial tracing direction will be from the false end pixel to the previous pixel (backwards). Fig8-8 shows the tracing algorithm.

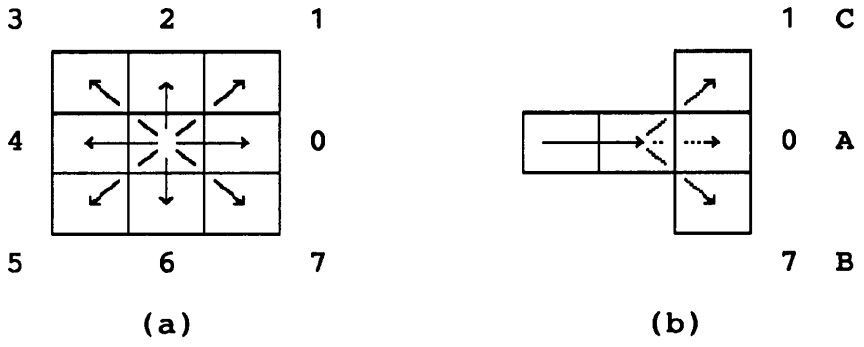

Fig8-8 The Curve Tracing Algorithm.

(a) The 8 Tracing Directions;

(b) An Example.

Denotations in Figure (b):

Solid Arrow = Present Tracing Direction Which Points from the Last Pixel to the Present Pixel;

Dotted Arrows = Possible Next Moves;

A, B, C = Sequence of Checking.

Tracing always proceeds in the present direction which points from the previous pixel to the present pixel. But if the pixel lies in front of the present direction is not an object pixel, the direction is turned by 45° clockwise. If the pixel lying in this direction is an object pixel, tracing proceeds in the new direction. Otherwise the direction is turned 90° counterclockwise (45° counterclockwise in relation to the original direction). If the pixel in this direction is an object pixel, tracing proceeds in this new direction. If the test is again negative it is assumed that the end of the curve has been reached. Curves that contain sharp corners of more than 45° are therefore treated as disconnected at these corners (Fig8-9).

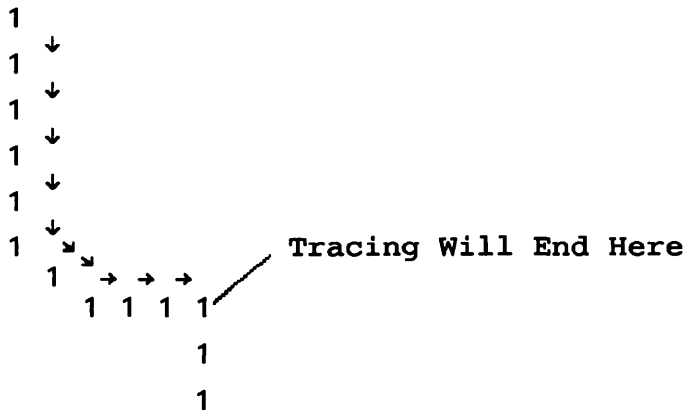

Fig8-9 A Curve Is Disconnected at a Sharp Corner.

Two curve approximation criteria have been used in the curve segmentation process. One is the maximum length of a curve segment (arc length) and the other is the sign of gradient. As the tracing process proceeds, the arc length of the curve being traced is continuously calculated. Since the pixels are rectangles with a width-to-height ratio of 1.5, a vertical step is counted as 1, a horizontal step is counted as 1.5 and a diagonal step as $\sqrt{3.25}$. The arc length is compared with a preset value, the maximum arc length*, after every tracing step. If the arc length reaches the maximum arc length, the orientation of the curve segment having been traced is computed. This orientation is that of the straight line segment connecting the starting pixel and the finishing pixel at which the arc length reaches the maximum arc length. The measured orientation is grouped into either 10° or 15° intervals between -90° and 90°. The interval value is chosen at the beginning of the process. The arc length is added to the corresponding interval decided by the orientation of the curve segment and tracing is restarted from the finishing pixel.

During the tracing process the sign of the gradient of a curve is not allowed to change. Whenever such a change is detected to occur, tracing will be terminated as if the curve has come to an end. This criterion ensures a curve being segmented into relatively straight parts. A curve such as the one shown in

---

* see page 161.

Fig8-10 will therefore be segmented into three parts, $\overset{\frown}{SA}$, $\overset{\frown}{AB}$ and $\overset{\frown}{BE}$, instead of being unfavourably treated as a single segment connecting S and E.

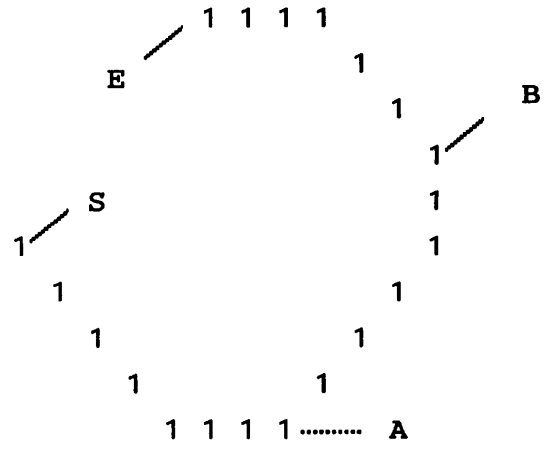

Fig8-10 The Sign of Gradient as a Curve Segmentation Criterion.

Denotations:

S = Starting Pixel; E = End Pixel;

A, B = Last Points Before a Gradient Sign Change.

Whenever tracing is terminated, either because the end of a curve is reached or because the sign of the gradient is to change, the arc length will be compared to a fixed minimum value. If the arc length is less than the minimum value, the curve segment is regarded as noise and is ignored. Otherwise the orientation of the curve segment is computed and the arc length is added to the corresponding interval decided by the computed orientation. Image scanning is then resumed from the pixel at which scanning was suspended. To avoid repetitive tracing of the same curve, all pixels in a curve that has been traced are deleted during the tracing process. The scanning and tracing process are repeated until all curves in the image have been traced and deleted. The sub-total arc lengths of curve segments in all the angular intervals are then summed to obtain the total arc length of curve segments in the whole image. The relative frequency of fibres lying in each angular interval can then be calculated. Fig8-11 is the fibre orientation distribution of the fabric shown in Fig7-1. It was measured from Fig8-7 by the line tracing method. The maximum arc length was 32 vertical pixels.

It is not possible to count the number of fibres within an image by the above described algorithm as tracing may branch from one fibre to another at crossing points and fibres may be broken down in the thinning process. A method of extracting individual fibres from a very thin fibre assembly was developed by Dixon and Taylor[38] for fibre counting. But

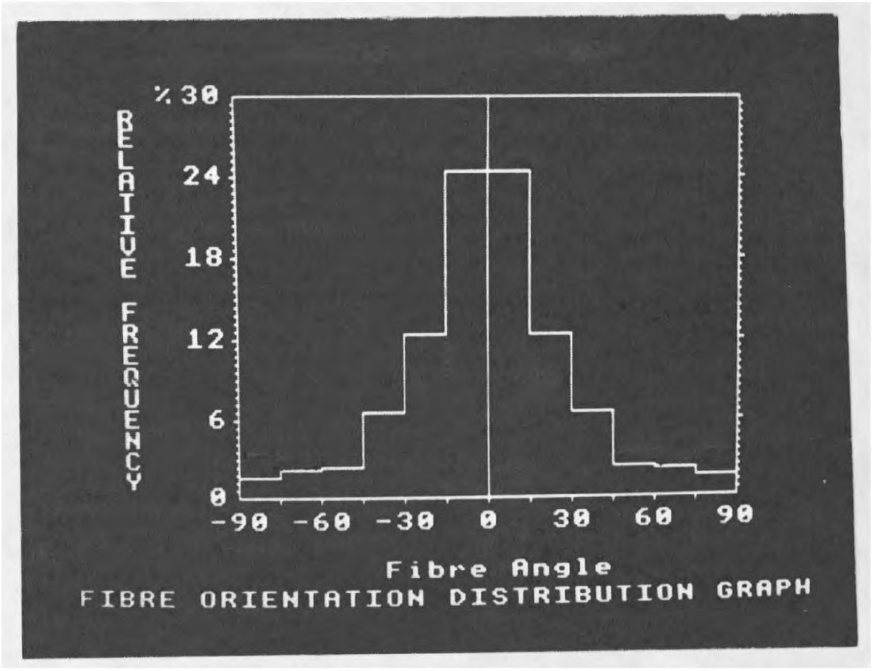

Fig8-11 Fibre Orientation Distribution Measured from Fig7-1.

fibre counting is not the intention of the present work. Also it will be an extremely complicated and time consuming process as the density of the fibre structures concerned is very high.

After obtaining the relative frequency of fibres lying within an angular interval, the total length of fibres contained in that interval per unit fabric area can be calculated by multiplying the corresponding frequency with the total fibre length in the same fabric area. The total fibre length per unit fabric area can be easily calculated from the fabric basic weight (excluding binder and other additives) and the fibre denier.

8.5 Summary

An edge smoothing operator has been described which also clears image noise such as isolated pixels and pinholes. A new vector-thinning algorithm has been developed to achieve further image simplification required before fibre orientation measuring. Fibres are reduced to curves of a cross section of one pixel by the thinning operation. A curve tracing and segmenting algorithm has been implemented to measure the length and orientation of these curves. Discussions of the automatic fibre orientation measuring method are presented in chapter 9.

CHAPTER 9 RESULTS AND DISCUSSION

9.1 SAMPLES

Microscopic photographs of fabric samples were analysed by the automated orientation measuring method. They were taken from a work by Sengupta[82] who investigated the bending rigidities of nonwoven fabrics. The fabrics were made of viscose rayon fibres and were all parallel-laid. Structural details of the five fabric samples selected are listed in Table9-1 and the digitized images are shown in Fig9-1 to Fig9-5. The original photographs were taken through a Scanning Electron Microscope with a magnification of 200 x nominal.

Real fabrics may be analysed directly as the system can provide an adequate magnification. The visual magnification rate of the system is difficult to specify because it varies with the size of the display monitor. At the highest magnification, the objective field size is 1.24 by 1.86mm, equivalent to a resolution of 3.64μm per pixel, and a visual

magnification rate of approximately 120 can be obtained when the image is displayed on a 12' monitor. But at the present time a proper illumination equipment is not available and the images obtained directly from fabric samples do not have sufficient contrast. A proper illumination equipment should provide sufficiently strong and diffused illumination without any bias towards fibres oriented at any particular direction.

Sample No.	Fabric Type	Basic Weight (g/m^2)	Fabric Thickness (mm)
1	PS.LMF.	24	0.30
2	PS.CF.	75	0.39
3	PP.CF.	46	0.39
4	PP.CF.	52	0.39
5	PP.CF	83	0.60

Denotations:

PS = Parallel Laid, Saturating-bonded;
PP = Parallel Laid, Printing Bonded;
LMF = Laboratory Made Fabric;
CF = Commercial Fabric.

Table 9-1 Specifications of Fabric Samples[32].

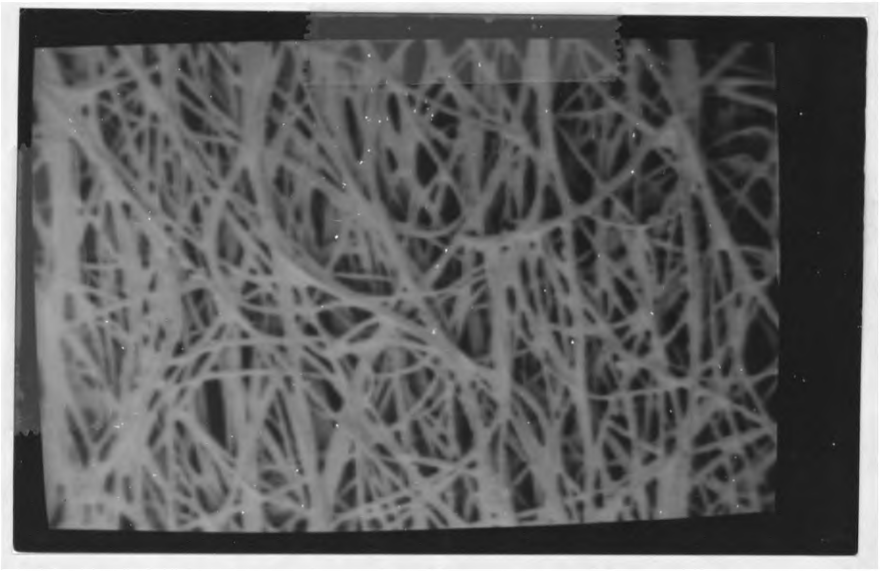

Fig9-1 Digitized Image of Fabric Sample No.1.

Fig9-2 Digitized Image of Fabric Sample No.2.

Fig9-3 Digitized Image of Fabric Sample No.3.

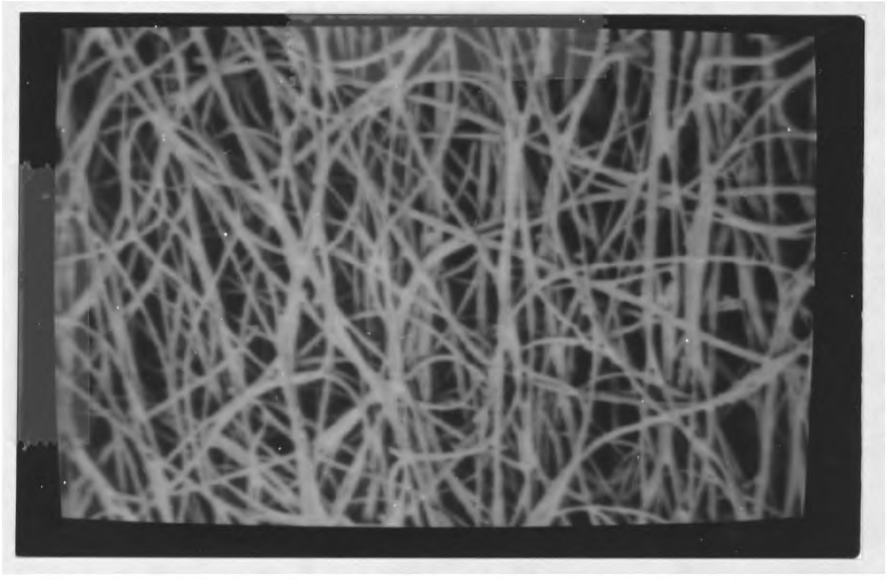

Fig9-4 Digitized Image of Fabric Sample No.4.

Fig9-5 Digitized Image of Fabric Sample No.5.

9.2 Results

Both manual and automated measurements were carried out on the five photographic samples. The results, together with those given by Sengupta, are presented in Table 9-2. The manual and automatic measured results are also compared in Fig9-6 to Fig9-10.

The manual measurements were carried out on the display monitor after photographs were input into the frame store. Fibres were traced manually on the screen with the help of a software defined cursor. As the cursor was moved along the centre of a fibre, it left behind a trail so that the traced and to be traced fibres could be easily distinguished. The length and orientation of fibre segments were calculated at a regular interval equal to 32 vertical steps to make the measurements comparable with the automatic measurements. All the calculations, including fibre length and orientation and the final orientation distribution were carried out by the computer. Even so, manual tracing of fibres remained a very time consuming and tedious work.

Sample No.	Measuring Method	Fibre Angular Interval					
		0 → ±15°	±15° → ±30°	±30° → ±45°	±45° → ±60°	±60° → ±75°	±75° → ±90°
1	A	33.4	26.1	16.2	9.4	10.3	4.7
	M	36.7	18.6	21.5	9.6	7.6	6.1
	S	40.0	24.0	15.8	9.1	6.7	4.3
2	A	33.3	21.5	16.1	12.0	8.8	8.3
	M	38.7	14.2	15.4	10.5	9.5	11.7
	S	28.0	23.5	18.0	13.5	10.0	7.0
3	A	36.2	33.8	13.6	6.6	6.4	3.4
	M	37.0	22.1	16.1	11.0	6.5	7.2
	S	32.0	24.5	19.0	14.5	8.0	2.0
4	A	35.0	26.2	15.7	10.1	8.5	4.5
	M	36.8	18.5	15.7	12.1	8.7	8.0
	S	33.0	24.8	19.0	13.2	7.0	3.0
5	A	48.9	24.9	13.3	4.8	4.7	3.4
	M	49.1	18.7	13.2	7.0	5.2	6.8
	S	33.5	26.5	17.0	13.5	7.0	2.5

Denotations:

A = Automatic Measuring by Image Analysis;
M = Manual Measuring;
S = Results by Sengupta[32];
0° = Machine Direction; ±90° = Cross Direction.

Table 9-2 Fibre Orientation Distribution Data (%).

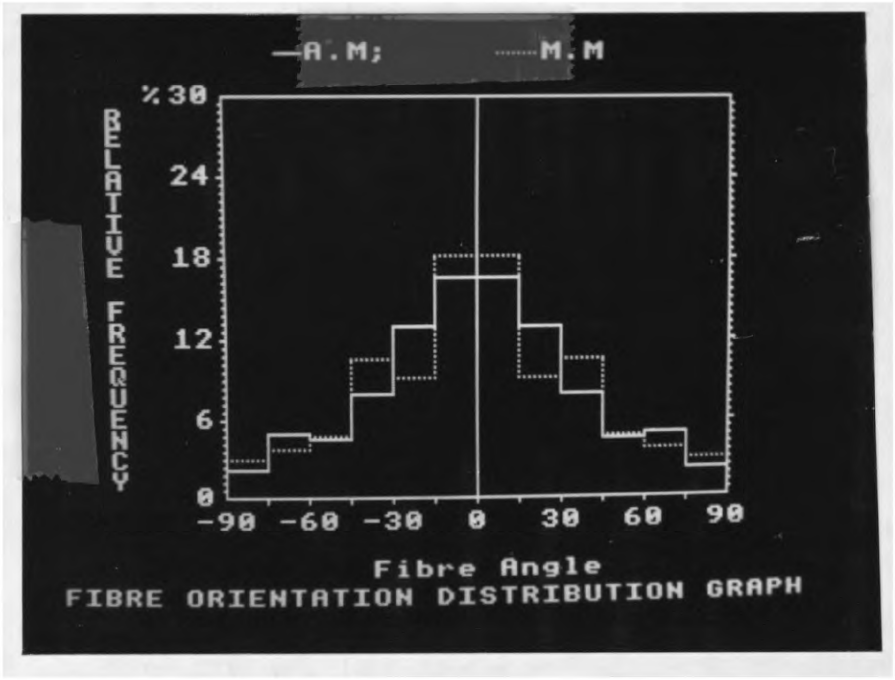

Denotations:

A.M. = Automatic Measuring;

M.M. = Manual Measuring;

0° = Machine Direction;

$\pm 90^{\circ}$ = Cross Direction.

Fig9-6 Fibre Orientation Distribution of Fabric No.1.

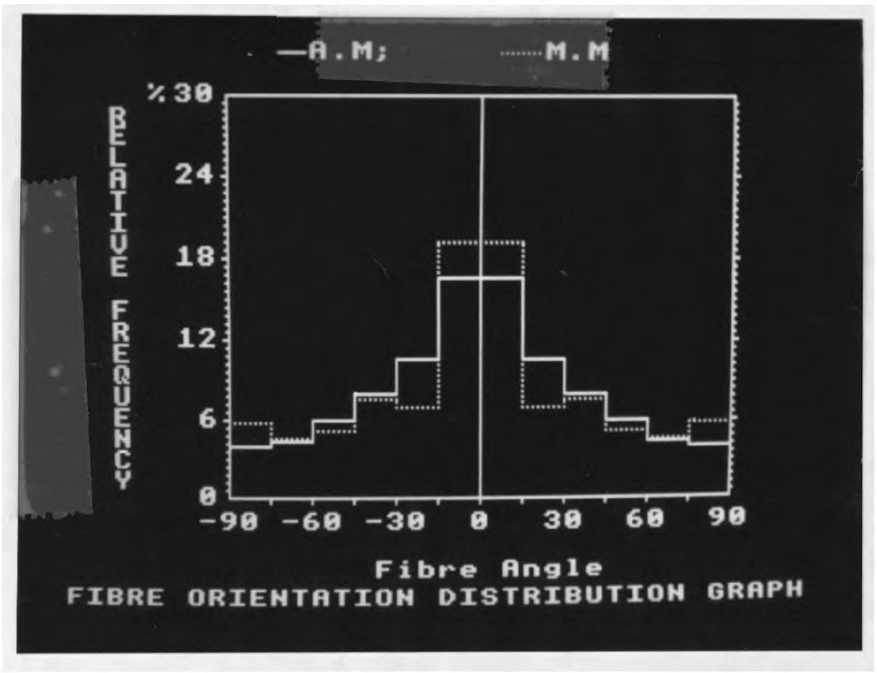

Denotations:

A.M. = Automatic Measuring;

M.M. = Manual Measuring;

0° = Machine Direction;

$\pm 90^{\circ}$ = Cross Direction.

Fig9-7 Fibre Orientation Distribution of Fabric No.2.

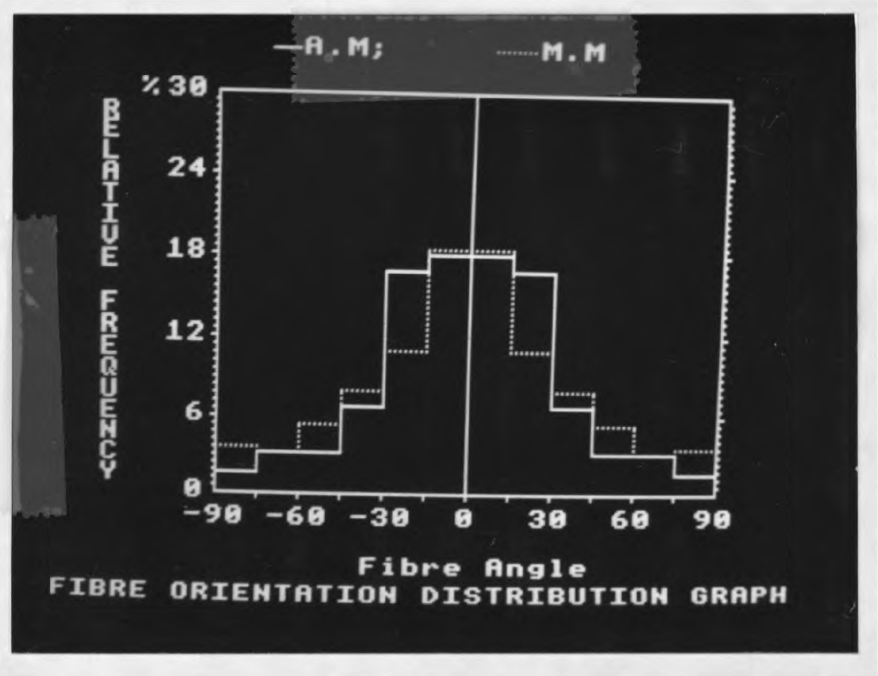

Denotations:

A.M. = Automatic Measuring;

M.M. = Manual Measuring;

0° = Machine Direction;

$\pm 90^{\circ}$ = Cross Direction.

Fig9-8 Fibre Orientation Distribution of Fabric No.3.

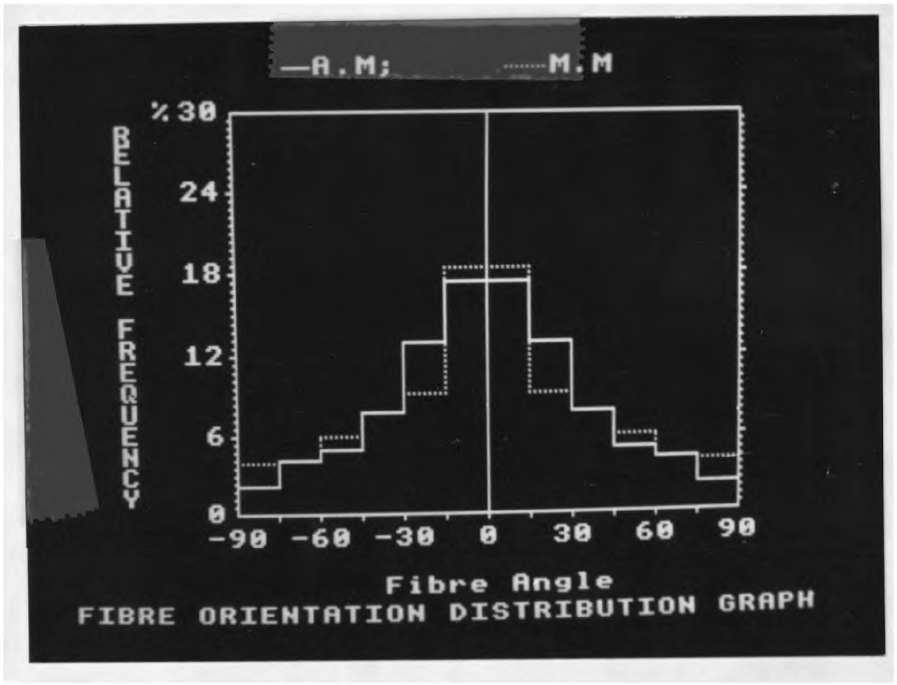

Denotations:

A.M. = Automatic Measuring;

M.M. = Manual Measuring;

0° = Machine Direction;

$\pm 90^{\circ}$ = Cross Direction.

Fig9-9 Fibre Orientation Distribution of Fabric No.4.

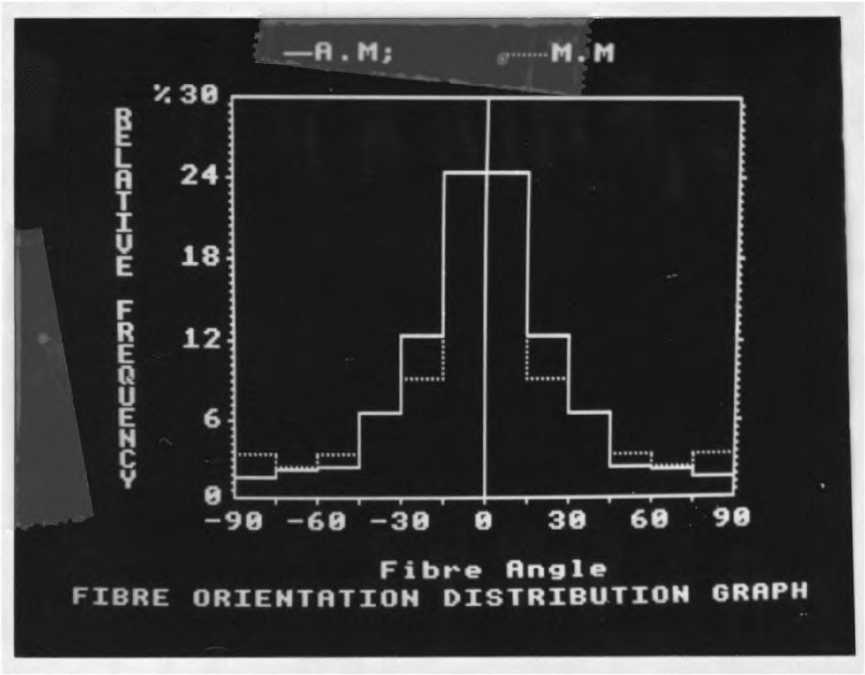

Denotations:

A.M. = Automatic Measuring;

M.M. = Manual Measuring;

0° = Machine Direction;

$\pm 90^{\circ}$ = Cross Direction.

Fig9-10 Fibre Orientation Distribution of Fabric No.5.

The automatic measurements were carried out in the steps as described in chapter 7 and chapter 8. The maximum arc length was fixed at that represented by a straight vertical line of 32 pixels. Two measurements were taken for each sample using different scanning patterns, row by row and column by column. The results given in Table 9-2 for each of the fabrics are the average of the two measurements.

From Fig9-6 to Fig9-10, it can be seen that results obtained automatically and manually agree with each other satisfactorily. The disparities between the results obtained manually in this work and those given by Sengupta (Table 9-2) are mainly due to the fact that his results were not directly obtained on the exact photographs presented in his work. Those photographs were intended just to show the categories of fabrics which he examined.

9.3 Discussion

9.3.1 Scanning Direction

Before a curve can be traced, a starting point has to found. This is achieved by scanning the image systematically, either line by line (horizontally) or row by row (vertically). However different results will be obtained for the same image when scanning directions are different (Table9-3). This is inherent to the tracing algorithm as can be shown by Fig9-11.

Scanning Direction	Fibre Angular Interval					
	$0^\circ \rightarrow \pm 15^\circ$	$\pm 15^\circ \rightarrow \pm 30^\circ$	$\pm 30^\circ \rightarrow \pm 45^\circ$	$\pm 45^\circ \rightarrow \pm 60^\circ$	$\pm 60^\circ \rightarrow \pm 75^\circ$	$\pm 75^\circ \rightarrow \pm 90^\circ$
Horizontal	49.7	26.0	12.5	4.4	4.6	2.9
Vertical	48.1	23.9	14.2	5.3	4.7	3.8

0° = Machine Direction; $\pm 90^\circ$ = Cross Direction.

Table 9-3 Comparison Between Scanning Directions. (Measured from Fig8-7)

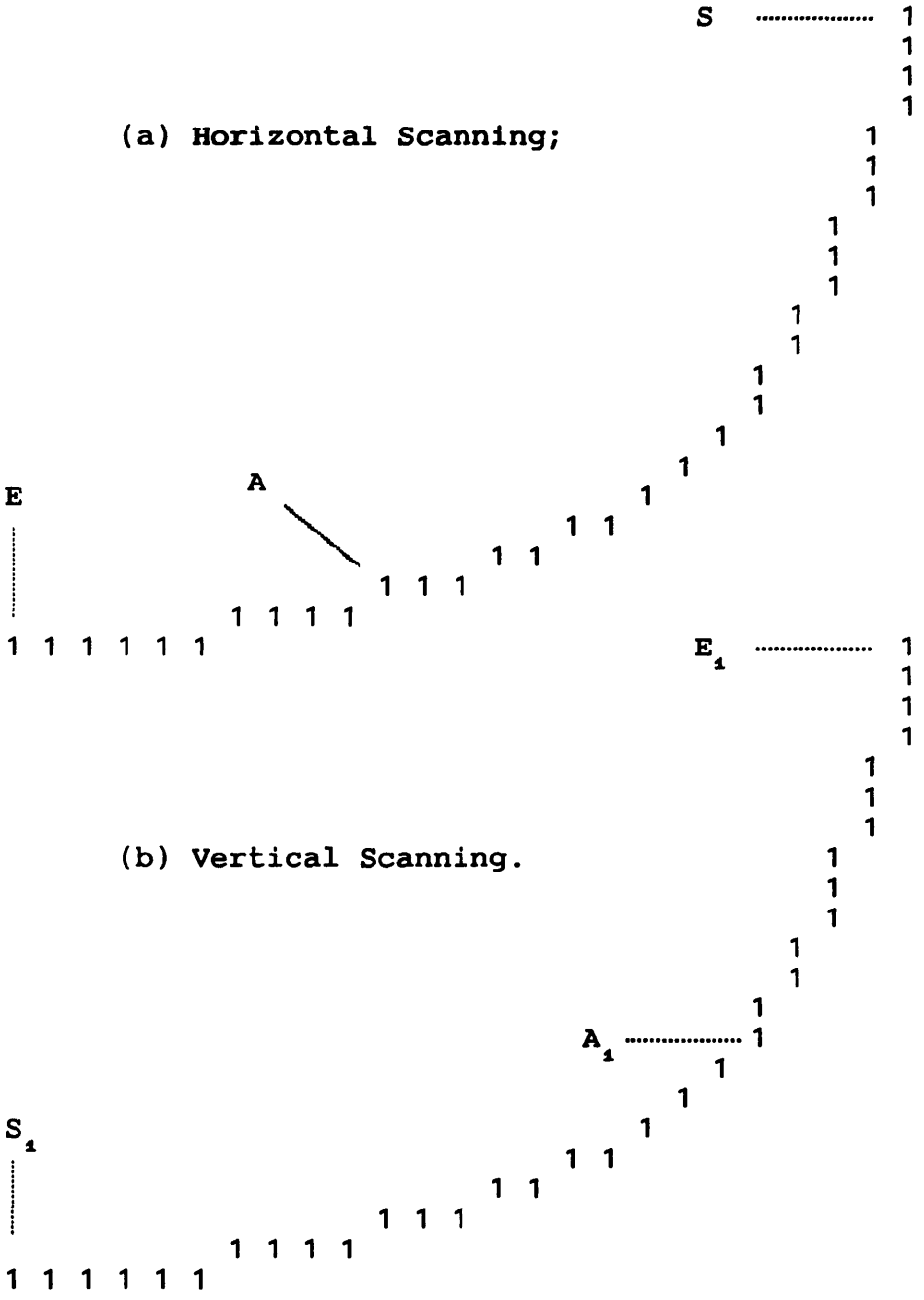

Denotations:

S, S_1 = Starting Pixel; E, E_1 = End Pixel;

$\overset{\frown}{SA} \backsimeq \overset{\frown}{S_1A_1} \backsimeq$ Max. Arc Length = 32 Vertical Steps.

Fig9-11 Comparison between Scanning Directions.

When a curve is traced the length of the curve having been traced is calculated. Whenever this length (arc length) reaches a given value (the maximum arc length), the traced part of a curve is segmented. The curve shown in Fig9-11 will be segmented in different ways when scanning directions differ. When scanning is horizontal it will be segmented into $\widehat{SA}$ and $\widehat{AE}$ while if scanning is vertical it will become $\widehat{S_1A_1}$ and $\widehat{A_1B_1}$. The measured orientations obviously differ from each other for the same curve. A compromise can be made by measuring the same image twice, once performing the scanning horizontally and once vertically. The two measurements can then be averaged to give the final result.

9.3.2 Maximum Arc Length

The maximum arc length also has an effect on the final result. This is illustrated in Fig9-12. The ideal maximum arc length would be the average bond distance within the fabric, because it is the fibre segments between bonding points that play the key role in all the physical property predicting theories of nonwoven fabrics reviewed in chapter 5. This value is however very difficult to estimate and is likely to vary greatly from fabric to fabric. Table9-4 shows the orientation information measured from Fig8-7 with 6 different maximum arc lengths

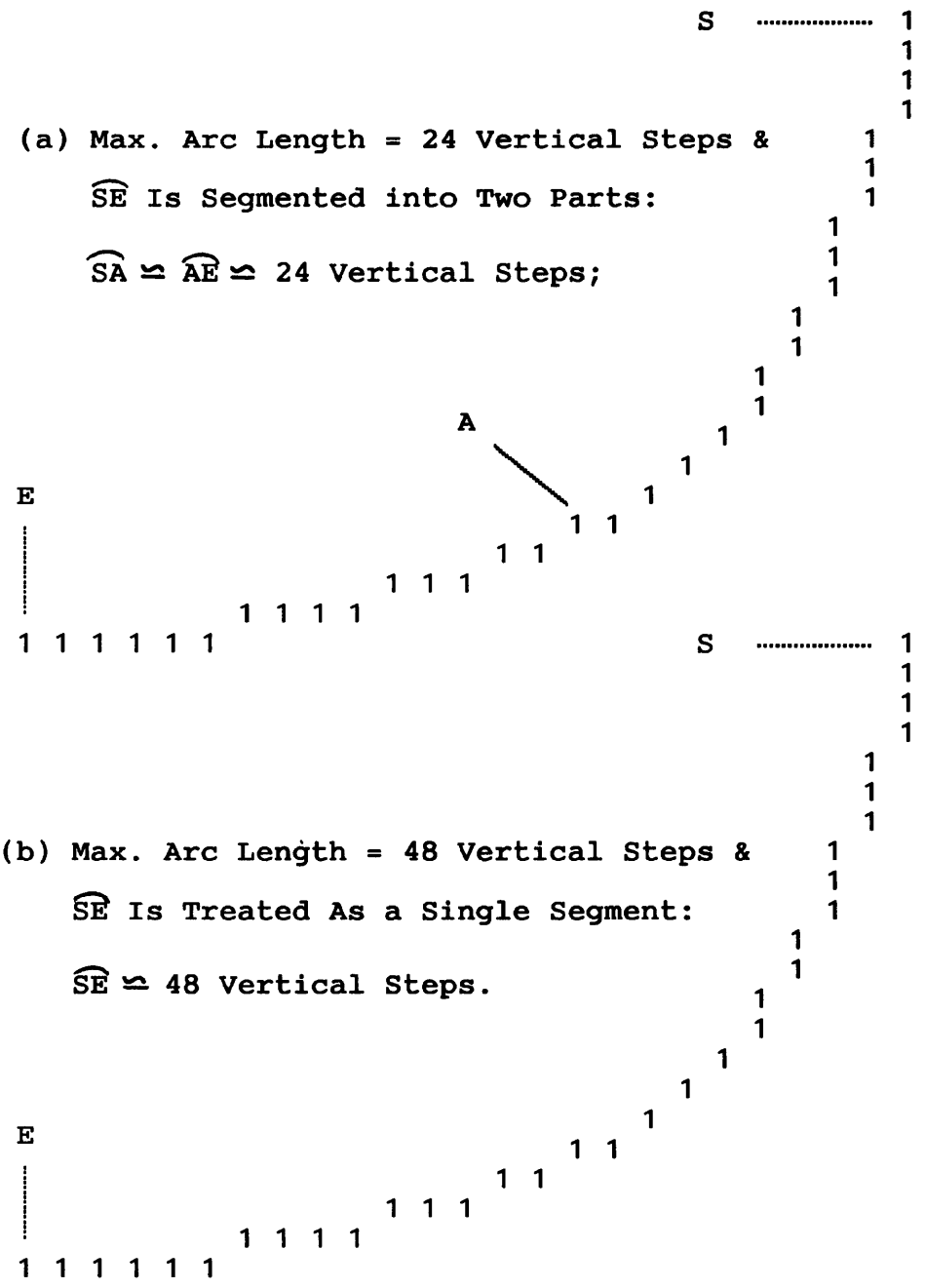

Fig9-12 Effects of Maximum Arc Length

[The Orientation of $\widehat{SE}$ Is Measured Differently in (a) & (b)
As $\overline{SA}$ and $\overline{AE}$ are Clearly Different from $\overline{SE}$ in Orientation]

Maximum Arc Length (Vertical Steps)	Fibre Angular Interval					
	$0^\circ \rightarrow \pm 15^\circ$	$\pm 15^\circ \rightarrow \pm 30^\circ$	$\pm 30^\circ \rightarrow \pm 45^\circ$	$\pm 45^\circ \rightarrow \pm 60^\circ$	$\pm 60^\circ \rightarrow \pm 75^\circ$	$\pm 75^\circ \rightarrow \pm 90^\circ$
8	42.1	14.2	11.8	9.1	12.8	10.0
16	46.1	19.0	12.9	8.5	7.6	5.9
24	50.6	23.0	12.0	5.9	4.0	4.5
32	48.9	24.9	13.3	4.8	4.7	3.4
48	49.2	25.0	13.5	5.8	3.3	3.3
60	48.2	25.5	13.8	6.6	2.7	3.2

0° = Machine Direction; $\pm 90^\circ$ = Cross Direction.

Table 9-4 Comparison Between Maximum Arc Lengths.
(Measured from Fig7-7)

ranging from 8 to 60 vertical steps. It is evident from the figures in Table 9-4 that very small maximum arc lengths tend to produce a more randomized distribution. This point is explained by considering the following simple fact: if a circle is divided into a number of equal segments, the orientation distribution of these segments will generally be more randomized when the number of segments increases. (To be more precise, odd and even numbers should be considered separately as when the number is even there will be parallel pairs of segments, but it is unimportant here.) Also, those short, noise branches in the skeletonized image will have a greater influence on the measurement when the maximum arc length is smaller. These noise branches are more likely to be rejected when the maximum arc length increases. However, the measurements quickly stabilize when the maximum arc length is increased. In fact, it can be seen from Table 9-4 that the difference between the measurements becomes negligible when the maximum arc length is longer than 24 vertical steps. The maximum arc length has therefore been set at 32 vertical steps in the present work. In general, the difference between measurements obtained with different maximum arc lengths will be proportional to the curvature of fibres in the fabric being analysed. For most nonwoven fabrics, however, the curvature of fibres is very small[23] and need not to be taken into account.

9.3.3 Fabric Thickness

The image analysing method is most useful for the measurement of fibre orientation distribution of thin fabrics. When dealing with thick fabrics, only those fibres lying in the top layer can be measured readily. Theoretically fibres lying underneath the top layer can be measured by focusing through the thickness of the fabric. But this is hindered by the blocking of light by fibres lying in the upper layer. Removal of top layer fibers is also very difficult because of the 3-D entanglement of fibres in the fabric. One possible approach is to fix the fabric in a resin and slice the resin block into layers. It will then be possible to analyse these slices to reveal the orientation of fibers within different layers of the fabric. However, research results by Stevenson on binder bonded fabrics showed that for a single ply fabric there is no significant difference between the surface fibre orientation and that of inner layer fibres[23]. It is therefore considered reasonable to use the orientation distribution of top layer fibres to represent that of the fabric. But application of this method to needle-punched fabrics is not appropriate because the needling process changes the web structure, and this change of structure from layer to layer is usually of more interest.

9.4 Theoretical Modelling of Fibre Orientation Distribution

The measured fibre orientation distribution only indicates fibre frequencies in an angular interval of either 15° or 10°. In the theoretical calculation of fabric mechanical properties the fibre frequency at an angular interval of 1° is often required. It is also desirable that the fibre frequency in an angular interval between any two angles can be obtained once the fibre orientation distribution is given. Interpolation is the simplest solution to these problems but it offers very limited accuracy. The best approach is to model the measured distribution data with a theoretical function which will then enable the calculation of fibre frequency at any direction.

A trigonometric function used by Ozsanlav[25] has been found explaining the experimental data satisfactorily. The function has a form of Equation 9-1, where Y and X represent fibre frequency and fibre orientation respectively and a, b, and n are constants to be estimated from the measured data $[X_i, Y_i]$, $i = 1,\ldots,m$.

$$Y = a+bCos^{n}(X) \quad \text{.....} \quad (9-1)$$

Direct estimation of the optimal values of a, b and n from Equation 9-1 is difficult and a transformation is subsequently

applied to it first. Let

$$Z = \mathrm{Cos}^{n}(X) \quad \cdots\cdots (9\text{-}2),$$

Equation 9-1 will become a linear function

$$Y = a + bZ \quad \cdots\cdots (9\text{-}3).$$

The values of a and b can then be optimized for a fixed value of n by using standard linear regression techniques[30] :

$$b = \left[\sum_{i=1}^{m}(X_i-\bar{X})(Y_i-\bar{Y})\right] \Big/ \left[\sum_{i=1}^{m}(X_i-\bar{X})^2\right] \quad \cdots\cdots (9\text{-}4);$$

$$a = \bar{Y}-b\bar{X} \quad \cdots\cdots (9\text{-}5).$$

Where

$$\bar{X} = \left[\sum_{i=1}^{m}X_i\right] \Big/ m \quad \text{and}$$

$$\bar{Y} = \left[\sum_{i=1}^{m}Y_i\right] \Big/ m.$$

The multiple correlation coefficient (M.C.C.) between the theoretical values $\hat{Y}$ and experimental values Y is expressed as

$$r = \sqrt{\left[\sum_{i=1}^{m}(\hat{Y}_i-\bar{Y})^2\right] \Big/ \left[\sum_{i=1}^{m}(Y_i-\bar{Y})^2\right]} \quad \cdots\cdots (9\text{-}6).$$

Where

$$\hat{Y}_i = a + bX_i .$$

A larger r (closer to 1) indicates a better fit of a theoretical model to the experimental data. A computer program has been written to search the optimal values of a, b and n. The procedures can be summarized as following:

(a). Compute the experimental data $[X_i, Y_i]$, i = 1,...,6. The X_i values represent mid-points of the 6 angular intervals between 0° and 90°, that is $X_1 = 7.5^\circ$, $X_2 = 22.5^\circ$, etc. The corresponding Y_i values are obtained by dividing the relative fibre frequencies in the 6 angular intervals by the interval size, 15°.

(b). Given an estimated range of n, $[n_1, n_2]$.

(c). Vary the value of n by a fixed step, s, between the estimated range $[n_1, n_2]$. For every n, compute the corresponding b, a and r according to Equations 9-4 to 9-6 respectively.

(d). The n that gives the maximum r defines the

best model within the estimated $[n_1, n_2]$.

(e). Compare the optimal n with n_1 and n_2. If it is equal to n_1 (or n_2), the original range of n may have been incorrectly estimated. A new estimation of the range of n should be made. n_1 (or n_2) should be contained within this new range. Steps (c), (d) and (e) are then repeated. If the optimal n is away from n_1 and n_2, the theoretical model that is defined by the optimal n and the corresponding a and b is taken as the best model.

Naturally, varying n by a smaller step will produce a model that fits the data more closely and, with the help of a computer there is virtually no restriction to the values of s that can be used. For the present application, however, using only integer values for s (and n) is sufficient.

The theoretical models for all five samples analysed are plotted against the corresponding experimental data in Fig9-13 to Fig9-17. The multiple correlation coefficient (M.C.C.) values are all greater than 95%, which demonstrates the correctness of the theoretical model. For a given value of X, the Y value computed from any of the functions as indicated in Fig9-13 to Fig9-17 represents the fibre frequency within an angular interval of 1° centred at the given X.

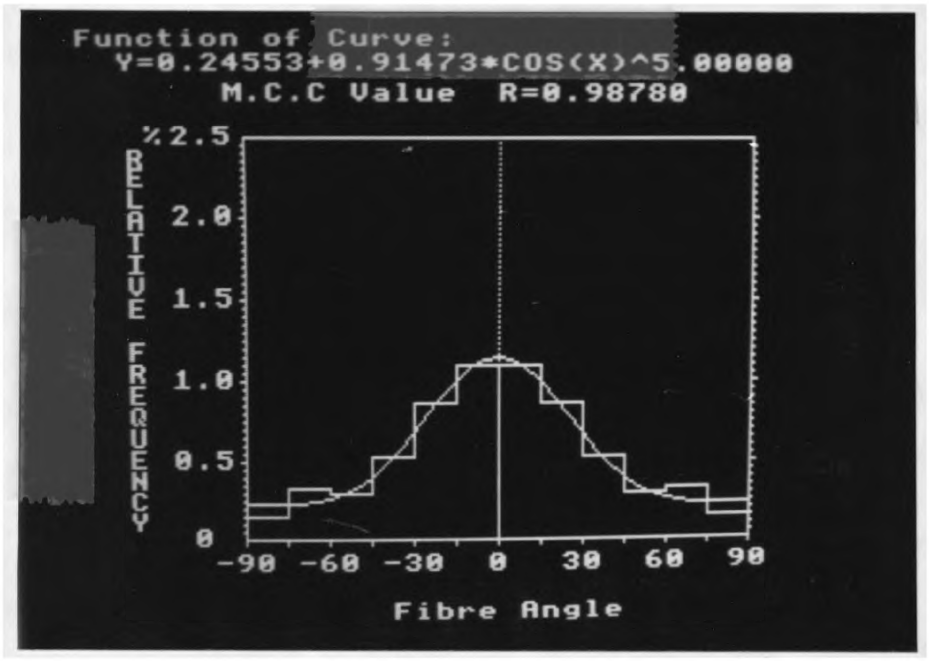

Fig9-13 Theoretical Curve of Fibre Orientation Distribution of Fabric Sample No.1.

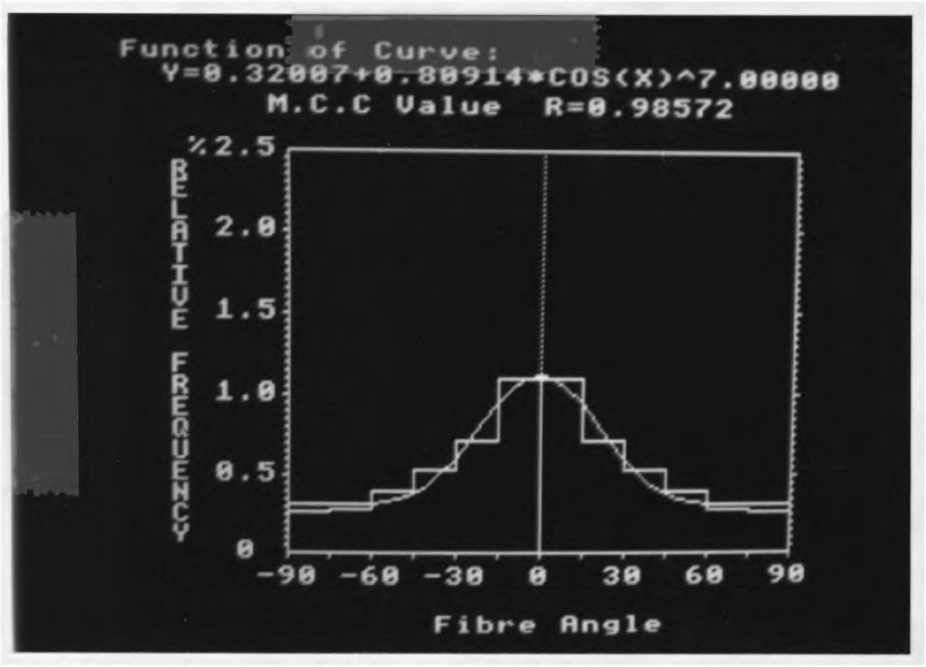

Fig9-14 Theoretical Curve of Fibre Orientation Distribution of Fabric Sample No.2.

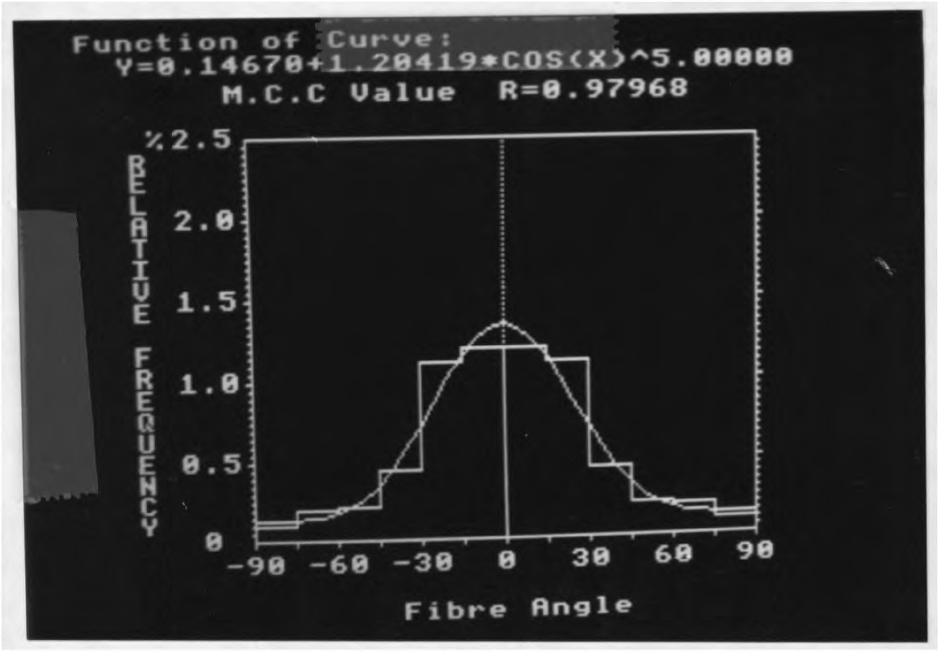

Fig9-15 Theoretical Curve of Fibre Orientation Distribution of Fabric Sample No.3.

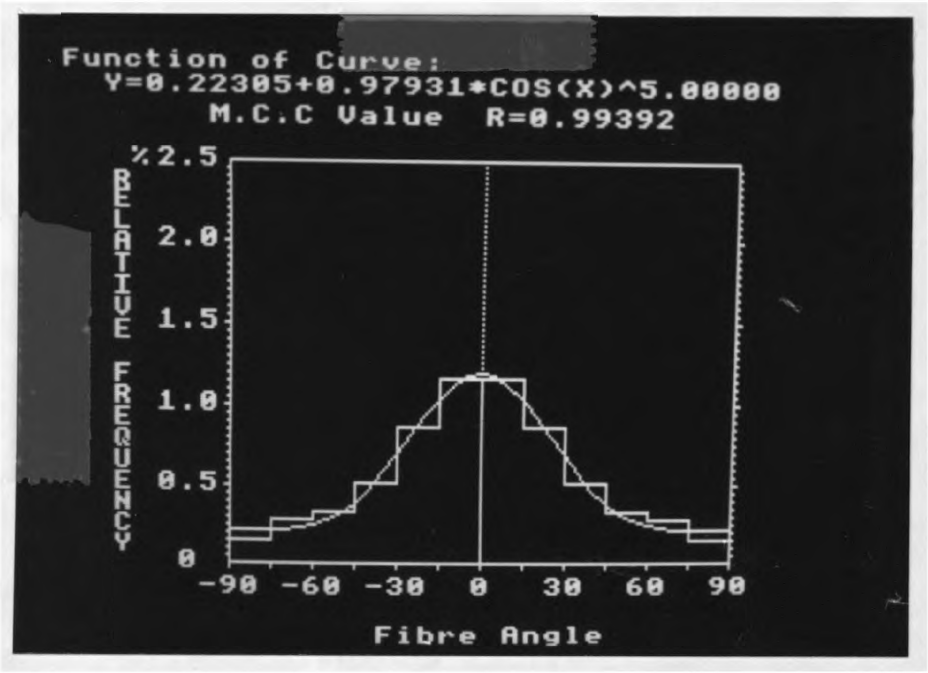

Fig9-16 Theoretical Curve of Fibre Orientation Distribution of Fabric Sample No.4.

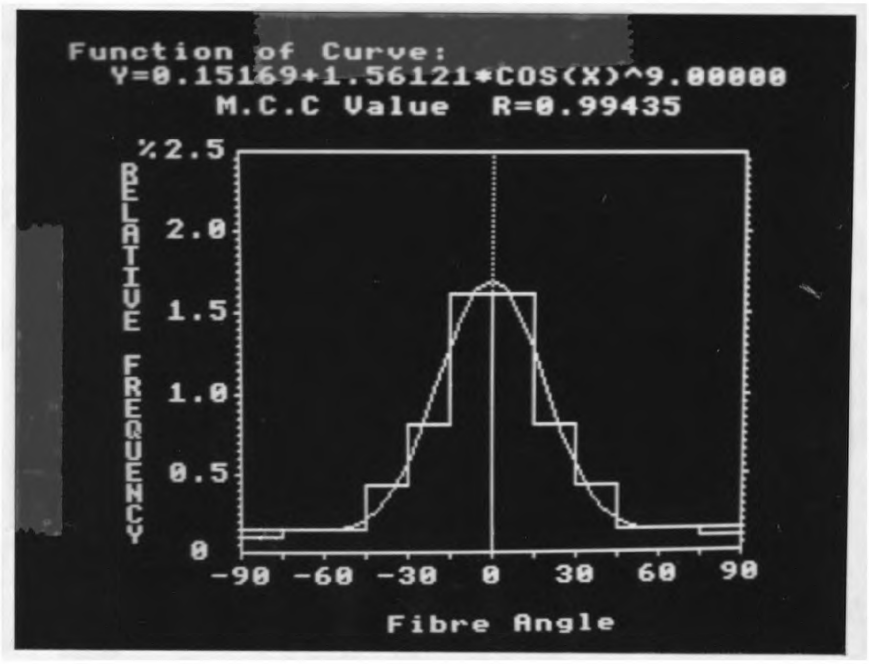

Fig9-17 Theoretical Curve of Fibre Orientation Distribution of Fabric Sample No.5.

9.5 Summary

Five microscopic photograph samples have been examined both manually and automatically. The automatic measurements show good agreement with the manual measurements. The automatic measurement for each sample was obtained by averaging two measurements carried out with vertical and horizontal scanning methods respectively. This is to offset the preferences by the two scanning methods for different fibre orientations. One of the curve segmentation criteria, the maximum arc length, also has some influence on the measurement, but this influence is generally insignificant.

The automatic measuring method is based on the analysing of the top view of a fabric, thus only the surface layer of a thick fabric may be examined readily. But it is believed that for a single ply web there is no significant differences in fibre orientation between the inner part of the web and its surfaces.

A trigonometric function has been proved a suitable model for the theoretical treatment of the experimental fibre orientation distribution data. Fitting a theoretical model to the experimental data enables the calculation of fibre frequency within any angular interval. This approach offers greater reliability than the simple interpolation technique.

PART IV CONCLUSION

CHAPTER 10 CONCLUSION

10.1 Summary of Algorithms

The procedures of measuring pore size and fibre orientation are summarized in Fig10-1 and Fig10-2. As in most image analysing applications, the ultimate goal has been achieved progressively in several stages, image segmentation, noise filtration and object segmentation and property measurement.

The software required in the pore size measurement and the fibre orientation measurement is filed separately and listed in Appendix 2 and Appendix 3 respectively.

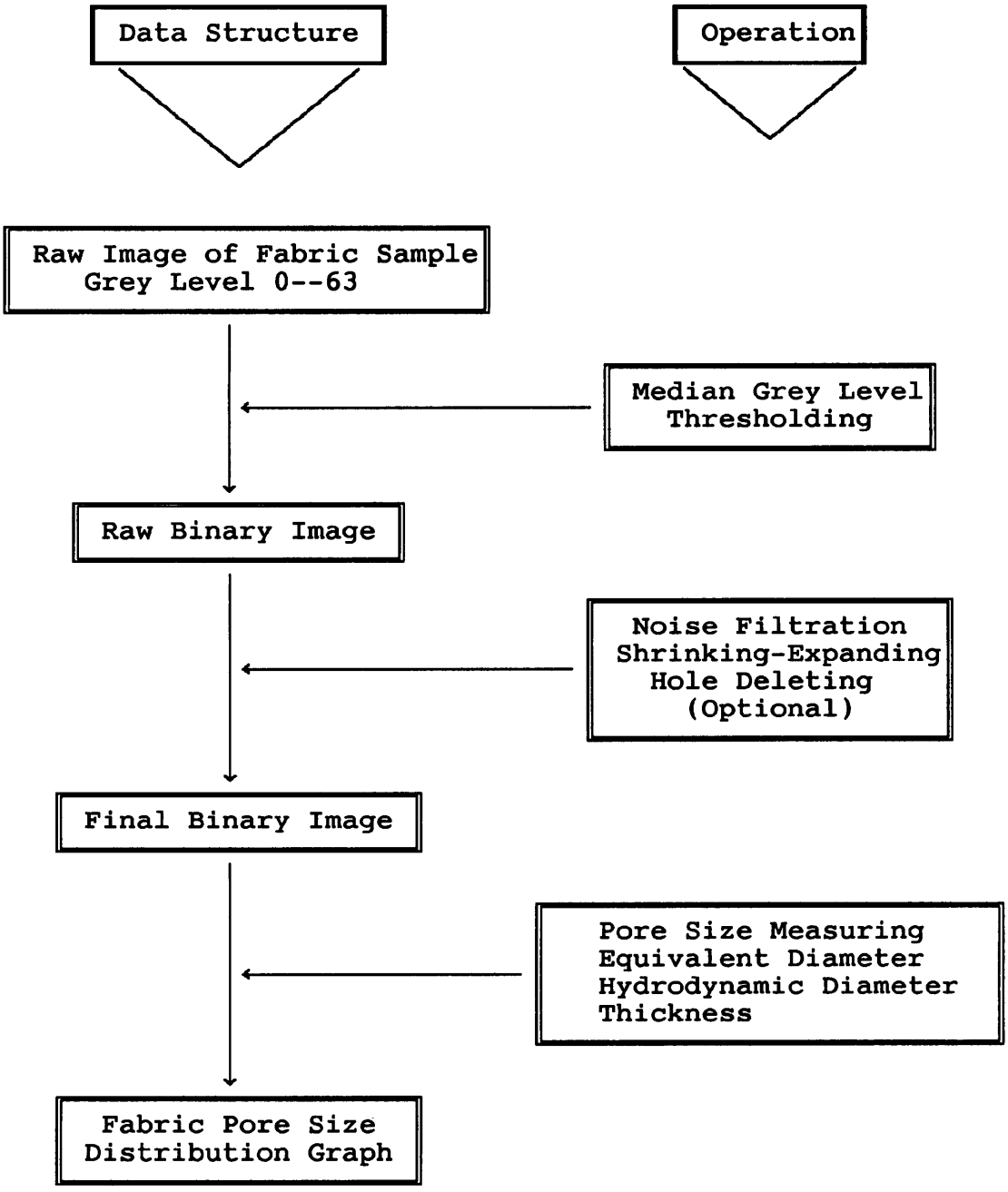

Fig10-1 Summary of Pore Size Measurement Algorithm

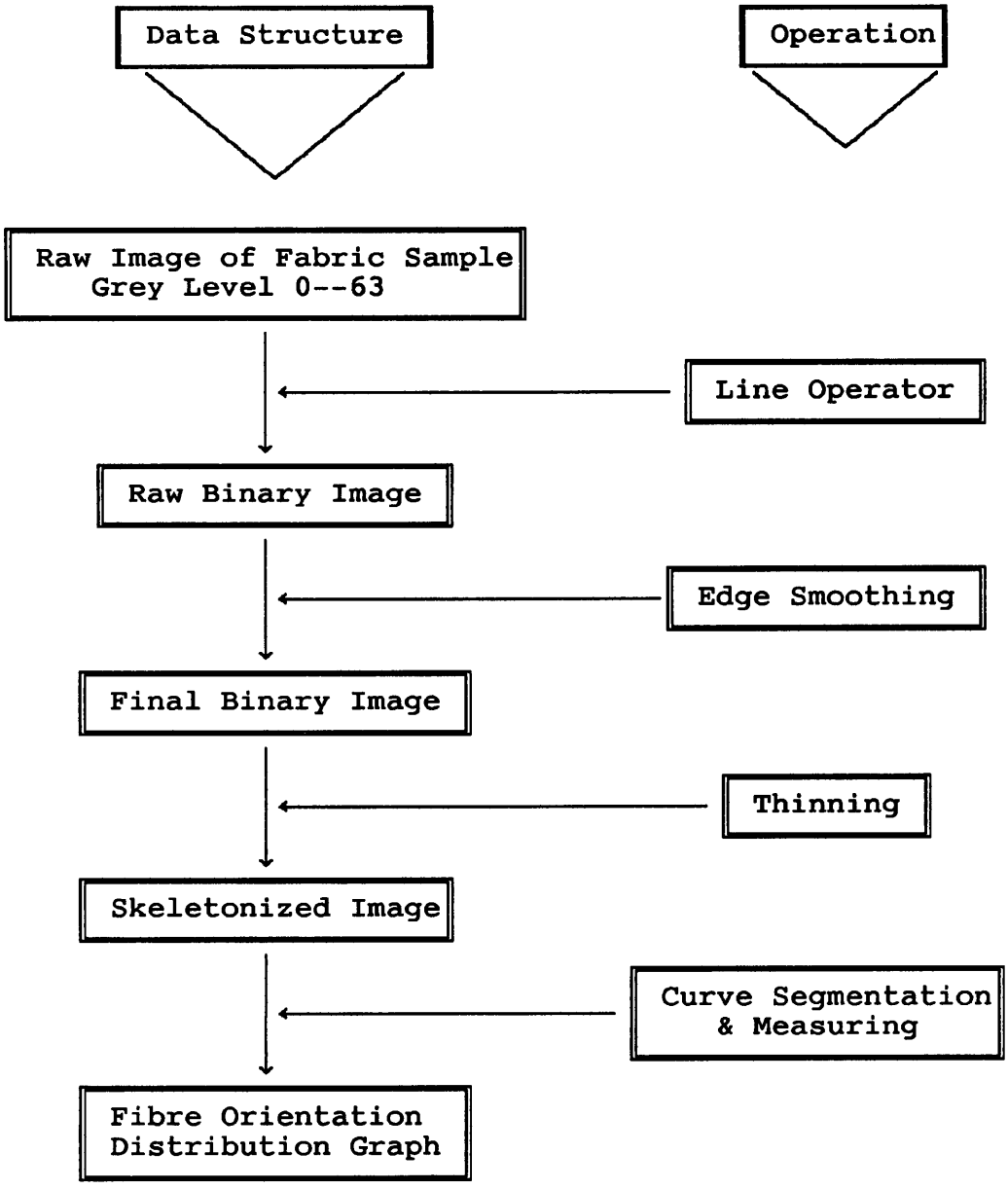

Fig10-2 Summary of Fibre Orientation Measurement Algorithm

10.2 Conclusions

10.2.1 Pore Size Measurement

Global grey level thresholding has been chosen as the means of image segmentation for its simplicity. But the quality of the raw image governs the selection of the optimal threshold which in its turn decides the accuracy of measurement. A mean grey level thresholding algorithm which operates automatically and thus offers operator independent image segmentation has been implemented for images with a good contrast. Such images have been obtained from dark coloured fabric samples under transmitted illumination. For uncoloured fabric samples, because fibres are highly transparent, images taken through transmitted illumination showed a very poor contrast. The selection of a satisfactory threshold for images as such was difficult and the segmenting result was prone to be subjective. Reflected illumination may be used alternatively, but the level of noise will be considerably higher because of the variation of optical properties, both of different parts of a fibre and of different fibres, and the local variation of illumination. The selection of a "satisfactory" threshold will

also be difficult and subjective. It is therefore considered necessary to dye uncoloured fabric samples to a dark colour before analysing. The dyeing process has to conducted in such a way that the structure of the fabric is not altered and the dye has an uniform distribution over all areas of the sample and over all parts of individual fibres.

It is almost universal that image segmentation will produce a noisy result unless the raw image has an exceptionally high signal/noise ratio. The most common form of noise is pinholes, both within objects and background areas. Object edges are often very finely zigzagged. Noise reduction operations are therefore generally required before object property measurement. An amended shrinking-expanding operation has been found having satisfactory effects both in cleaning pinholes and smoothing edges. This operation should be applied to the image for improved measurement accuracy. A special hole filling operation has been developed to fill large holes within objects (pores) which sometimes occur due to poorer raw image quality. But this is an optional operation and whether to apply it will depend on the nature of the image.

Algorithms for measuring three pore size properties have been developed. The thickness approach is considered most suitable for filtration applications. It has been confirmed that both pore size distribution and the specific fabric opening area are important parameters that characterize opening properties

of a fabric. It is therefore suggested both of these parameters should be considered in the designing of an application involving geotextiles. The fabric specific opening area can be easily measured by the image analysis techniques described in this thesis. The Hydrodynamic diameter approach should be more suited to applications where fabric permeability is important, such as in drainage systems.

The measurement of structural properties of nonwoven fabrics should be taken on a sufficiently large sample. But the objective area of one measurement is severely limited by the high magnification rate required in the analysis of a typical fabric. Contradicting the intuitive feeling that a large number of measurements are required to produce a reliable result, preliminary tests on two nonwoven fabric samples indicated that less than ten measurements randomly taken at different areas of a fabric can provide the pore size distribution property of the fabric with sufficient reliance. A quick assessment of the pore size distribution property of a fabric could even be achieved by a single measurement. But the measurement of fabric specific opening area requires a much larger sample since the number of pores per field was found to vary greatly from place to place. For a woven fabric, as was expected, no more than five measurements were found necessary to obtain both its pore size distribution and specific opening area.

The surface image analysing method is only applicable to thin and/or compacted fabrics. Cross sectional analysing techniques are necessary to assess the characteristics of openings in thick and porous structures.

10.2.2 Fibre Orientation Measurement

In the measurement of fibre orientation distribution, surface images of fabrics are analysed. But segmenting images of the surface view of a fabric is more difficult than segmenting images obtained with transmitted illumination from a dark coloured fabric. The simple grey level thresholding approach is inadequate because the high noise level makes it impossible to select a proper threshold, and a more sophisticated approach, the line operator, has been used. The line operator operates on a local basis and utilizes the linear spatial correlation along individual fibres. It is therefore insensitive to noise incurred by local variations of illumination and the variation of optical properties of fibres. A modification to the original line operator defined by Dixon[87] was made. The square region sampling element was removed from the operator and the diagonal region sampling element was used to compute the local average of grey levels for all the 8 line sampling elements.

A noise clearing operation is also necessary and a template matching technique has been used. It deletes pinhole noise and smooths object edges, but unlike the shrinking-expanding technique used in pore size measurement, it preserves thin lines.

The cross section of fibres has to be reduced to a single point before measurement can be taken. This has been achieved by a series of thinning operations that take away successive edge pixels from objects. A curve tracing algorithm has been implemented to segment these thin curves into relatively straight parts, to measure the length and orientation of these segments and finally, to produce the fibre orientation distribution curve.

Five microscopic photograph samples have been examined both manually and automatically. The automatic measurements show reasonable agreement with the manual measurements. The automatic measurement for each sample was obtained by averaging two measurements carried out with vertical and horizontal image scanning directions respectively. This is to offset the preferences by the two scanning methods for different fibre orientations.

Two criteria of equal priority were used in the curve segmentation process. One is the sign of gradient and the other is the maximum arc length. Using a different maximum arc

length will produce a different orientation distribution for the same image. But in the present work, it was found the difference in the results caused by the difference in the maximum arc length is insignificant after the maximum arc length reaches a minimum threshold of approximately 24 vertical pixels. The maximum arc length was therefore fixed at 32 vertical pixels

The automatic measuring method is restricted to the surface layer of a fabric. But it is believed that for a single ply web there is no significant differences in fibre orientation between the inner part and its surfaces, providing the web is not needle-punched or spunlaced.

The experimental fibre orientation distribution was successfully modelled by a trigonometric function which enables the calculation of fibre frequency within any angular interval. This approach offers greater reliability than the simple interpolation technique.

10.2.3 The Advantages and Disadvantages

The speed and economic advantages of the measurement methods described in this thesis are overwhelming over their traditional counterparts. The system is not dedicated to any

particular application and therefore highly flexible. It can be programmed to perform numerous other tasks. But clearly, only properties that can be expressed pictorially can be measured, apart from the hardware limitations discussed in section 2.1.

10.3 Suggestions for Further Research

The emphasis has been placed on the development of measurement algorithms for pore sizes and fibre orientation. More experimental work is required to exploit fully the commercial potentials of the measurement techniques.

While the correlation between the automatic pore size measuring method and the existing sieving techniques can be revealed by more experimental comparisons, a study into the application of the automatically measured pore size distribution in the prediction of fabric permeability and in the evaluation of fabric performance may be more valuable.

The pore size distribution of the two nonwoven fabrics analysed indicated that a similar fabric structure may have a similar pore size distribution. But due to the limitation in the number and variety of fabrics analysed, this finding is

not conclusive. Examination of more fabrics of various types is needed to verify whether this relationship between fabric structure and pore size distribution can be established for a wider range of fabric structures.

The testing of the automatic fibre orientation measurement method has been limited to microscopic photographs. But this is not a limitation imposed by the algorithm but by the lack of an appropriate illumination equipment. By simply adding such an equipment to the present system, direct measurements of real fabric samples should be possible.

The microscopic photographs were all taken from parallel-laid fabrics. It is therefore proposed that the automatic measurement techniques be tested on other types of fabrics.

The system employed is a general purpose image analyser and therefore can be used to solve other problems. The pursuit of measuring properties other than pore size and fibre orientation provides perhaps the greatest area for future work. These properties should not be limited to those of nonwoven structures, other types of structures such as yarn, woven fabrics should also be considered. Fibre properties, such as fibre curl, may also be analysed.

The pore size measurement algorithms can be readily used to measure the size of particles, such as that of sand, which is

traditionally measured by the laborious sieving techniques.

Although some general purpose software has been developed, it is unlikely to be adequate for a particular new application. Software development has to follow the advent of new problems, but the system has the flexibility of being fully programmable and thus allows individual problem solutions.

APPENDIX I IMAGE PROCESSING OPERATIONS

(A) MAIN MENU

IMAGE PROCESSING MENU 1

Refresh	frame store
Histogram	of image
Intensity	curve of one line or column
Threshold	image with operator selected threshold
Shrink	image by a factor of 2
Enlarge	image by a factor of 2 (interpolating)
Enlarge#	image by a factor of 2 (multiplying)
Average	grey levels in a 2×2 neighbourhood
Enhance	image contrast by expanding grey level range of image
Reverse	image contract
Shift	image grey level range (up/down)
More Menu	(menu 2)

Image Processing Menu 2

Rotate ..... image by 90° counterclockwise

Line Operator ..... (with 5×5 diagonal region sampling element)

Edge ..... extraction in binary images (4/8-connective)

Analysis ..... of image (see sub-menu)

Filter ..... (deleting pixels which are 4/8-connected to less than a selected number of neighbours)

Clear ..... part/whole of frame store

Thin (Standard) ..... from North/South/East/West

V-Thin-1 ..... (vector-thinning stage 1)

V-Thin-2 ..... (vector-thinning stage 2)

Mean Sgmnt ..... (mean grey level image segmentation)

Smooth ..... edges of objects by template matching

More Menu ..... (menu 3)

Previous Menu ..... (menu 1)

Image Processing Menu 3

Draw Fabric ..... in frame store

Orientation ..... measurement (see sub-menu)

Erode ..... objects by edge deletion

Expand ..... objects by edge addition

Count ..... number of objects

Fill ..... holes within objects

Size ..... measurement (see sub-menu)

More Menu ..... (menu 4)

Previous Menu ..... (menu 2)

Image Processing Menu 4

Pseudo Colour ..... display of an image window

Store Image ..... to disk

Load Image ..... from disk

Store Window ..... of image to disk

Load Window ..... of image from disk

Print Image ..... after thresholding

Catalogue ..... of files on disk

More Menu ..... (menu 1)

Previous Menu ..... (menu 3)

EXIT ..... menu

(B) Sub-menus

Image Analysis Menu

Dimension ..... of objects (manual measuring)

Angle ..... between two lines (manual measuring)

Area ..... of objects in a window

Count ..... number of objects manually

Draw ..... dots/lines

Refresh ..... frame store

Magnification ..... selection

Main Menu

Orientation Measurement Menu

Column6 ..... (scanning in columns, 6 angular intervals between $\pm 90^{\circ}$ — 0°)

Column9 ..... (scanning in columns, 9 angular intervals between $\pm 90^{\circ}$ — 0°)

Row6 ..... (scanning in rows, 6 angular intervals between $\pm 90^{\circ}$ — 0°)

Row9 ..... (scanning in rows, 9 angular intervals between $\pm 90^{\circ}$ — 0°)

Main Menu

Size Measurement Menu

Equivalent ..... diameters of objects

Hydrodynamic ..... diameters of objects

Thickness ..... of objects

Result ..... of measurement

Reset ..... data file of object sizes

Main Menu

(C) Operation Instructions

The programs listed in (A) and (B) are contained in one double sided, 80 track, $5\frac{1}{4}$ inch floppy disk. To initiate the Microsight II Image Analyser, this system disk should be inserted in DRIVE0 of the dual disk driver, then press SHIFT and BREAK simultaneously. Individual programs can be operated simply by following the on-screen instructions.

The same operating procedure applies to programs listed in Appendix II and Appendix III which are filed separately on two disks.

APPENDIX II PORE SIZE MEASUREMENT MENU

Refresh ..... *

Automatic ..... measurement of pore size distribution **

Histogram

Intensity

Threshold

Mean Sgmnt

Shrink-Expand ..... (noise cleaning and edge smoothing by shrinking and expanding)

Fill

Size

Save Image

Load Image

Enlarge#

Restore ..... an image after taking an measurement

EXIT

Note:

* Refer to Appendix I for comments of operations not commented here.

** When the Automatic pore size measuring operation is selected, the following operations will be executed consecutively and automatically:

Mean Sgmnt ⟶ Shrink-Expand ⟶ Size <Thickness>.

APPENDIX III FIBRE ORIENTATION MEASUREMENT MENU

Refresh ..... *

Reverse

Automatic ..... measurement of fibre orientation distribution **

Line Operator

Smooth

Clear

V-Thin-1

V-thin-2

Orientation

Save Image

Load Image

Shrink

Restore ..... an image after taking a measurement

EXIT

Note:

* Refer to Appendix I for comments of operations not commented here.

** When the Automatic fibre orientation measuring operation is selected, the following operations will be executed consecutively and automatically:

Line Operator ⟶ Smooth ⟶ V-Thin-1 <4 times> ⟶ V-Thin-2 ⟶ Orientation <Row6>.

REFERENCES

1. William, B.G., Digital Image Processing: A System Approach. Van Nostrand Reinhold Company. New York, 1983.
2. Rosenfeld, A. & Kak, A.C., Digital Image Processing, 2nd Edt., Vol.1 & Vol.2. Academic Press, London, 1982.
3. Ballard, D.H., & Brown, C.M., Computer Vision. Prentice-Hall Inc., New Jersey, 1982.
4. William, K.P., Digital Image Processing. John, Wiley & Sons, USA, 1978.
5. "World News Network", Textiles Horizon, Vol.8, No.9, Sep. 1988, pp10.
6. Fernando, G.M.X. & Monro, D.M., "A Localized Image Segmentation Algorithm". Proceedings of 2nd International Conference on Image Processing and Its Applications, (Imperial College, London, June, 1986), pp.68-71. Conference Publications No.165, IEE, 1986.

7. Ronce, C., & Devijver, P.A., Connected Components in Binary Images: The Detection Problem. Research Studies Press, England, 1984.
8. John, N.W.M., "Some Design Criteria for Geotextile Filters". UMIST Nonwovens Conference Papers, June, 1988, pp.301-316.
9. Raumann, G., "Geotextiles: Construction Materials in Evolution". Proceedings of 2nd International Conference on Geotextiles, Las Vegas, USA, 1982, Vol.4, pp.10-15, Industrial Fabrics Association International, 1983.
10. Tan, H.H., et al., "Hydraulic Function and Performance of Various Geotextiles in Drainage and Related Applications". Proceedings of 2nd International Conference on Geotextiles, Vol.1, pp.155-160.
11. Hoare, D.J., "Geotextiles in the U.K.". Ground Engineering, Nov. 1983, Vol.16, No.5, pp.30-38.
12. Murray, R.T. & McGown,A., "The selection of Testing Procedures for the Specification of Geotextiles". Proceedings of 2nd International Conference on Geotextiles, Vol.2, pp.291-196.3
13. Ball, J., "Development of Test Methods by ASTM". Proceedings of 2nd International Conference on Geotextiles, Vol.2, pp.331-333.
14. Du Pont, Designing Drainage Systems with Typar Spunbonded Polypropylene.

15. ICI, A Guide to Test Procedures Used in the Evaluation of Civil Engineering Fabrics, Nov. 1981.
16. Cooke, T.F., "Geotextiles: Main Types and Uses". Textile Month, Oct. 1988, pp.42-46.
17. Masounave, J., Desin, R. & Rollin, A.L., "Prediction of Hydraulic Properties of Synthetic Nonwoven Fabrics Used in Geotechnical Work". Can.Geotech.J., 1980, Vol.17, pp.517-525.
18. Rosin, P.L. & West, G.A.W., "Detection of Circular Arcs In Images". Proceedings of the Fourth Alvey Vision Conference, University of Manchester, Sept. 1988, pp259-263.
19. Wittmann, L., "Soil Filtration Phenomena of Geotextiles". Proceedings of 2nd International Conference on Geotextiles, Vol.1, pp.79-83.
20. Giroud, J.P., "Filter Criteria for Geotextiles". Proceedings of 2nd International Conference on Geotextiles, Vol.1, pp.103-108.
21. Petterson, D.R. & Backer, S., "Some Principles of Nonwoven Fabrics". Text. Res. J., Sep. 1960. pp704-711.
22. Petterson, D.R. & Backer, S., "Relationships between the Structural Geometry of a Fabric and its Physical Properties". Text. Res. J., Oct. 1963. pp809-816.
23. Stevenson, P.J., Ph.D. Thesis, UMIST, Oct. 1962.
24. Newton, A., Ph.D. Thesis, UMIST, Oct. 1965.

25. Ozsanlav, V., Ph.D. Thesis, UMIST, Feb. 1971.
26. Chun, K.W., M.Sc. Dissertation, UMIST, Jan. 1974.
27. Britton, P.N. & Sampson, A.J., "Computer Simulation of the Mechanical Properties of Nonwoven Fabrics, Part 1: The Method". Text. Res. J., June 1983, Vol.53, pp363-367.
28. Britton, P.N. & Sampson, A.J., "Computer Simulation of the Mechanical Properties of Nonwoven Fabrics, Part 2: Bond Breaking". Text. Res. J., Jan. 1983, Vol.54, pp1-5.
29. Britton, P.N. & Sampson, A.J., "Computer Simulation of the Mechanical Properties of Nonwoven Fabrics, Part 3: Fabric Failure". Text. Res. J., June 1984, Vol.54, pp425-428.
30. Grindstaff, T.H. & Hanson, S.M., "Computer Model for Predicting Point-Bonded Nonwoven Fabric Strength, Part 1". Text. Res. J., June 1986, Vol.56, pp383-388.
31. Barker, R.L. & Scheininger, M.M., "Predicting the Hand of Nonwoven fabrics from Simple Laboratory Measurements". Text. Res. J., Oct. 1982, Vol.52, pp615-620.
32. Sengupta, S., M.Sc. Dissertation, UMIST, Jan. 1975.
33. Chaudhray, M.M., M.Sc. Dissertation, UMIST, 1972.
34. Judge, S.M., M.Sc. Dissertation, UMIST, 1973.
35. Orchard, G.A.J., "The measurement of Fibre Orientation in Card Webs". J. Text. Institute, 1953, Vol.44, T380-385.

36. Chudleigh, P.W., "Image Formation by Fibres and Fibre Assemblies". Text. Res. J., Dec. 1984, Vol.54, pp813-820.

37. Dixon, R.N., Ph.D. Thesis, University of Manchester, Oct. 1980.

38. Dixon, R.N. & Taylor, C.J., "Automated Asbestos Fibre Counting". Inst. Phys. Conf. Ser. No.44, Chapter4, pp178-185.

39. Brook, R.J. & Arnold, G.C., Applied Regression Analysis and Experimental Design. Marcel Dekker, Inc. New York, 1985